ABSTRACT

Title of dissertation:	THERMODYNAMIC AND TRANSPORT PROPERTIES OF AVIATION TURBINE FUEL: PREDICTIVE APPROACHES USING ENTROPY SCALING GUIDED MACHINE LEARNING WITH EXPERIMENTAL VALIDATION
	William Anthony Malatesta, Doctor of Philosophy, 2021
Dissertation directed by:	Professor, Bao Yang, Department of Mechanical Engineering

With issues such as increasing power generation densities, design restrictions on heat rejection, and finite heat sink capacity, fighter aircraft face significant thermal management challenges which are driving research from component to system level technology regimes. As aviation turbine fuel often represents half of the take-off weight of aircraft, it is an integral piece of the thermal management puzzle and generally regarded as the primary internal heat sink for fighter aircraft. Though typical thermal performance analysis requires temperature dependent transport and thermodynamic properties of fuel, the variation in properties associated with the fact that fuels are mixtures with varying composition is not well understood. As such, the present work aimed to define bounds of density, viscosity, thermal conductivity, and specific heat of aviation turbine fuel as functions of composition and temperature by developing numerical models which were validated against test data. Data collected

for this work included 96 samples with measured composition and viscosity at a single temperature (54 F-24, 26 JP-8, 11 Jet A, 5 Jet A-1), and four samples (3 JP-5 and 1 F-24) which underwent compositional and temperature dependent property testing. The novel modeling approaches to predict viscosity and thermal conductivity of jet fuels employed pseudo component entropy scaling techniques with artificial neural networks occupying an intermediate step in the overall model. Simple hyper-parameter optimization techniques were developed to promote model stability, computational efficiency, and long-term repeatability of the approach. Additionally, a model for predicting temperature dependent isobaric specific heats of liquids based on atomic density was developed for well-defined hydrocarbon mixtures. Model performance against test data showed average deviations of 0.1%, 1%, and -2% for viscosity, thermal conductivity, and specific heat respectively. Utilizing the compositional data collected, the models were then used to estimate bounds of these properties. Analysis of Prandtl numbers calculated using the modeled property ranges suggests that the observed variation in properties should be considered during a thorough aircraft thermal management design or performance analysis effort.

THERMODYNAMIC AND TRANSPORT PROPERTIES OF AVIATION TURBINE FUEL: PREDICTIVE APPROACHES USING ENTROPY SCALING GUIDED MACHINE LEARNING WITH EXPERIMENTAL VALIDATION

by

William Anthony Malatesta

Dissertation submitted to the Faculty of the Graduate School of the
University of Maryland, College Park, in partial fulfillment
of the requirements for the degree of
Doctor of Philosophy
2021

Advisory Committee:
Dr. Bao Yang, Chair
Dr. Ashwani K. Gupta
Dr. Patrick McCluskey
Dr. Michael Azarian
Dr. Peter Sunderland (Dean's Representative)

Dedication

To my endlessly supportive wife and wonderful children: thank you for always helping me to find a quiet place.

To all of my amazing parental units: thank you for laying the foundation of curiosity and knowledge that enabled me to be me.

To all of my extended family and friends: given that I am a certified member of the "luckiest people on the planet" club, there are too many of you to name but my character has been greatly shaped by your love and support.

To all of my teachers, especially Dr. Bao Yang, Dr. Richard Widdess, Dr. Richard Beers, Erode Nagaraj, Jamey Haddad, Mohamed Kalifa Kamara, Cheryl Blockland, and Alex Jaffurs: my life is infinitely enriched by your generous contributions and guidance.

Acknowledgements

Sincere gratitude goes to my team and chain of command within the Naval Air Systems Command, especially Nathan Kumbar, Marilyn Cullivan, Dr. Michael Peretich, Dave Rawlinson, and Jordan Wedderburn. Additional appreciation goes to the Navy Fuels and Lubricants Team at NAS Patuxent River, particularly Rick Kamin, Andy McDaniel, Dr. Alison Metz and Olivia Sarver for their support providing resources to procure and test the fuel samples used in the study. Finally, it should be noted that the conclusions contained herein are those of the author and should not be interpreted necessarily representing endorsements of those of NAVAIR.

I would also like to acknowledge the support of the staff within the University of Maryland Department of Mechanical Engineering Graduate Office, especially Kerri, Megan, and Marta who patiently answered many questions over several years.

Table of Contents

List of Figures

List of Tables

1. Introduction

Aircraft power plants and the systems harnessing the energy outputs to provide propulsion and power represent not only the highest operational cost items for air vehicles [1] but they also provide, from a thermodynamic perspective, the essential functions to complete missions: they store, manage, transport, and convert energy required to fly and utilize payloads. The present work is motivated not only by the inherent importance of these systems but also the relevant trends, system architectures, physical constraints, and safety considerations which have combined to drive research in technology for improving reliability and increasing efficiency to both fielded systems and those of the coming generations. Of these challenges, the present work is chiefly concerned with addressing how the thermodynamic and transport properties of aviation turbine fuel influence how aircraft manage heat at the sub-system and system level, the discipline of aircraft thermal management. More specifically, with the knowledge that the composition of aviation turbine fuel is variable batch to batch, this work aims to establish a practical working range of fuel properties relevant to its performance as a cooling medium.

For the reader who is unfamiliar with aircraft thermal management architectures, sections **1.1 Motivation** and **1.2 Active Research** aim to give sufficient background for the reader to appreciate the complexity of aircraft thermal management systems, the relevance of fuel transport and thermodynamic properties to these systems, and areas of application for the present work. With this knowledge in hand, section **1.3 Objectives** describes the aim of the present work: to establish the

practical bounds of aviation turbine fuel thermodynamic and transport properties relevant to aircraft thermal management. From there, section **2 Literature Review** reviews the current body of work on the aviation turbine fuel properties of interest using both experimental and numerical techniques, as well as machine learning modeling techniques for predicting properties of fluid mixtures. Gaps noted in the research and the resulting strategy toward achieving the objectives of **1.3** is then outlined in **2.4 Approach.** Test data collected for the present effort that was not previously presented in the literature is described in **3 Fuel Property Testing** before novel computational models for predicting viscosity, thermal conductivity, and specific heat of jet fuels are presented in section **4 Entropy Scaling Guided Neural Network Thermal Conductivity Model,** section **5 Entropy Scaling Guided Neural Network Viscosity Model**, and section **6 Specific Heat Model.** Finally, ranges of prediction for the properties of interest informed by the compositional range of fuels sampled for this effort are presented in **7 Predicted Ranges of Fuel Thermodynamic and Transport Properties**

Prior to progressing into details specific to aviation turbine fuel thermal management, the author would like to point out that even though the primary inspiration for and focus of the present work comes from fighter aircraft (U.S. Tri-service designation "F"), the trend of continuously increasing power demand, density, and resulting integration challenges is a reality driving research in energy system technology across many domains of scale and application. It is the hope of the author that the study of relatively power dense, temporally dynamic, and highly integrated energy systems such as those found on fighter aircraft may provide useful insight to

researchers working to further diversification of the terrestrial energy system portfolio.

1.1 Motivation

The primary focus of this work is to support further quantification of the role that aviation turbine fuel plays in fighter aircraft thermal management design and operation. To establish a basic foundation for this understanding, an appreciation of the relevant trends affecting design and operation of these aircraft (**1.1.1**) as well as the basic design features of fighter aircraft thermal management systems (**1.1.2**) is required. Alongside this, an understanding of aviation turbine fuel performance requirements and composition (**1.1.3**), will be useful before proceeding. All of these items have conspired to motivate the present study and enable the coordination of resources from both the U. S. Naval Air Warfare Center Aircraft Division and the University of Maryland to address the identified gap.

1.1.1 Power and Thermal Trends in Military Aviation

Over the course of human history, technology advancement has regularly been driven by a desire for military dominance. In the case of modern military aircraft, growth of performance and capability to gain or maintain air superiority typically requires the expansion of flight envelopes (higher speeds, longer range, more extreme maneuvers), the addition of payloads (more weapons systems, more sensors), or

growth for existing payloads (expansion of radar range) all of which require suitable energy resources to be utilized or themselves expanded. As a result, there has been a consistent trend toward increasing the density of electrical power onboard U. S. fighter aircraft (**Figure 1**).

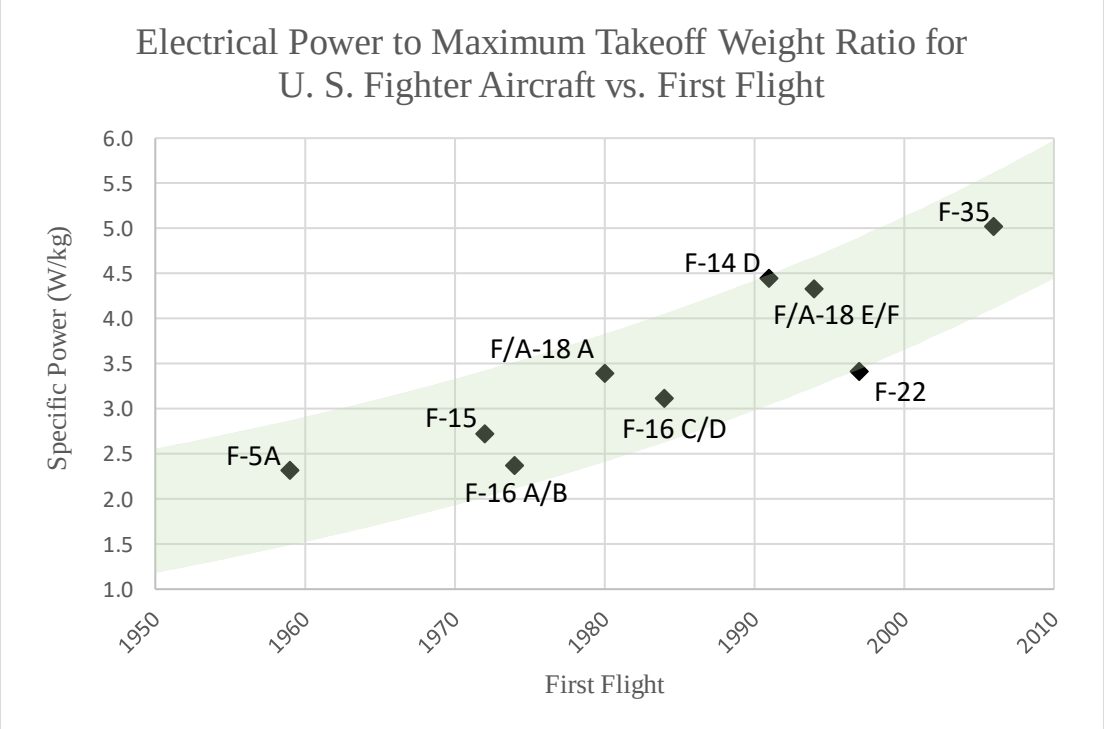

Figure 1: Growth in Specific Electrical Power (W/kg) of U. S. fighter aircraft. Developed from U. S. Navy internal repositories and included with permission of the Naval Air Systems Command.

As fighter aircraft have essentially maintained the same volume throughout their history from World War I to the present, the doubling in specific electrical power (W/kg) observed over a roughly thirty year period (1975-2005) has directly led to

increased interaction between subsystems to a point where managing subsystem waste heat at the system level has evolved to be seen as a critical technology gap for next generation aircraft [1] - [2].

While capability expansion continues to drive specific power growth on these aircraft, there are a few broad performance requirements which are increasing the thermal resistance between the aircraft internal systems and the ambient, further complicating the design task and reducing thermal margins [3] [4] [5] [6] [7]. The first area of concern competing with the task of thermal management designers is increased performance with respect to speed. As requirements drive improvements in engine thrust and airframe designs from an aerodynamic perspective, the portions of the flight envelope that fighter aircraft are able to operate at supersonic speeds also increases. From the thermal perspective this creates a situation where heat rejection from convection is challenging or impossible due to the stagnation temperature of the ambient air increasing near or above the temperature of working fluids within the aircraft [3] [4] [7]. Though this phenomenon directly effects heat exchanger performance, the effects are further exacerbated by the use of composite aircraft skins which have replaced what were previously reasonably high thermal conductivity materials such as steel and aluminum at the largest surface area interface between the aircraft and the ambient. This directly affects large thermal masses in contact with the skin internally, such as fuel within the wings, and decreases the rate at which heat can be rejected to the ambient from any given portion of the aircraft [4] [6].

Finally, one of most challenging aspects for thermal management designers is the incorporation of low-observability requirements to meet the demand for stealth

operation. These requirements impose limitations on aircraft infrared signatures and directly limit aircraft skin temperatures, increasing both convective and radiative thermal resistance to the ambient [4] [5] [2].

To the best knowledge of the author, these overall trends are expected to continue, bringing aircraft thermal management to forefront of the design process for sixth generation fighter aircraft. As reported by the Congressional Research Service in October of 2020 [2], the next generation fighters will likely require new stealth technology and directed energy weapons which will demand "tremendous amounts of electrical power" and variable cycle engines integrated with advanced techniques to manage generated heat.

1.1.2 Thermal Management Architecture in Fighter Aircraft

To further elucidate the purpose of the present study, a basic understanding of fighter aircraft thermal management architecture is required. From the system perspective, the result of the trends cited in sections **1.1.1** is the development of energy dense aircraft containing several subsystems with differing and sometimes competing thermal requirements. These are individually complex systems which are similarly trending toward increased design influence over each other due to interaction required by the second law of thermodynamics. This section will not be an exhaustive look at thermal management architectures and technology, but will rather focus on presenting enough technical detail to enable an appreciation for the primary subsystem interactions present in typical fighter aircraft. Several

technologies have been studied and in some cases deployed to address aircraft thermal management challenges including air cycle machines, vapor compression cycles, thermal energy storage devices, and variable displacement pumping. Still, the problem of thermal management persists and has evolved to the point given the discussions in the previous section that rather than continuously attempting to reject heat, a significant portion of the solution must involve utilizing the thermal mass within the aircraft itself. This brings us to first key aspect of the architecture: *fuel*.

Fuel often represents on the order of half of the mass of an aircraft when at maximum take-off weight [8]. Additionally, in order to maximize range, fighter aircraft have been designed to take advantage of nearly every bit of available space within the airframe. As such, fuel can be found throughout the fuselage, wings, and even vertical stabilizers connected with piping, valves, and pumps to allow a pilot to use either automated or manual control procedures to adjust the center of gravity, a parameter which generally changes as fuel is utilized during the course of a mission [8]. Lastly, fuel is able to safely have its temperature increased within reasonable limits, even in the presence oxygen, and indeed it is required to do so prior to combustion to facilitate maximum utilization of its stored energy. So to a point, it is advantageous to heat fuel prior to entering the combustion section of an engine [8]. Given all of these points: (1) fuel is a large portion of the total aircraft mass, (2) it is distributed throughout the aircraft, (3) and it is able to absorb thermal energy, it has become a central piece of the thermal management puzzle.

After answering the basic question of *why* use fuel as a heat sink, the next piece of this discussion centers on *what* is cooled by the fuel. In essence, it is safe to

say that potentially any heat producing payload on these aircraft is cooled directly or indirectly by fuel [5]. Meaning, a payload such as a power supply or an avionic system has fuel flowing through a heat exchanger within its packaging or a fluid within another circuit such as air, oil, hydraulic fluid, or polyalphaolefin (PAO) [9] directly cools the equipment before flowing through a secondary heat exchanger to then supplying heat to the fuel [4] [5]. Generally speaking, these other fluid systems do not have significant reservoirs (thermal mass) and their operating temperatures do not vary significantly throughout the course of a mission. Given the cited trends and these general considerations, it should be clear why fuel has come to be regarded as the primary heat sink for these types of vehicles [7].

An additional interesting piece of thermal management architecture in fighter aircraft that is relevant to the present study is the method of cooling electrical generators. The standard design practice in these types of aircraft can be pieced together by looking at several figures from the flight manual for the U. S. Air Force F-16 A/B variant [10] and is nearly identical to the relevant architecture of the U. S. Navy F/A-18 E/F variant [11].

As discussed in F-16 A/B flight manual [10], the engine and accessory drive gearboxes where shaft power from the engine is supplied to gearboxes which then distribute work to many of the systems distributed throughout the aircraft which subsequently interact (thermally) with one another in other locations. Some of the relevant accessories are the main electrical generator, main fuel pump, and hydraulic system pumps.

Not only are the primary points of energy distribution collocated for these systems but they also directly interact here as well. **Figure 2: Simplified Fuel Thermal Management Schematic Adapted from** gives a partial view of a typical fuel system schematic which includes relevant items just upstream of the engine: hydraulics, accessory gearbox, and generators. After cooling these units, this fuel may flow to the engine for combustion or be returned to the main fuel tanks to mix with what fuel remains [10].

The act of returning some portion of the heated engine feed fuel to the main fuel tanks highlights a final point about this type of architecture relevant to the present effort: not only is flowing fuel used to absorb thermal energy, the fuel stored within the fuel tank structure is heated throughout the course of a mission. The result of this is that the bulk temperature of the fuel in the various reservoirs is not static and is influenced by the temporally dynamic states of: engine operation, electrical loads, hydraulic loads (such as flight control surface actuators), mechanical loads from gearbox accessories, environmental control system demands, electrical power generation, and aircraft external boundary conditions. The temperature is further impacted by the simple fact that the mass of the fuel within the aircraft is constantly decreasing as it is combusted and its products expelled over the course of a mission, resulting in a general increase in the rate of temperature rise at later stages of a mission.

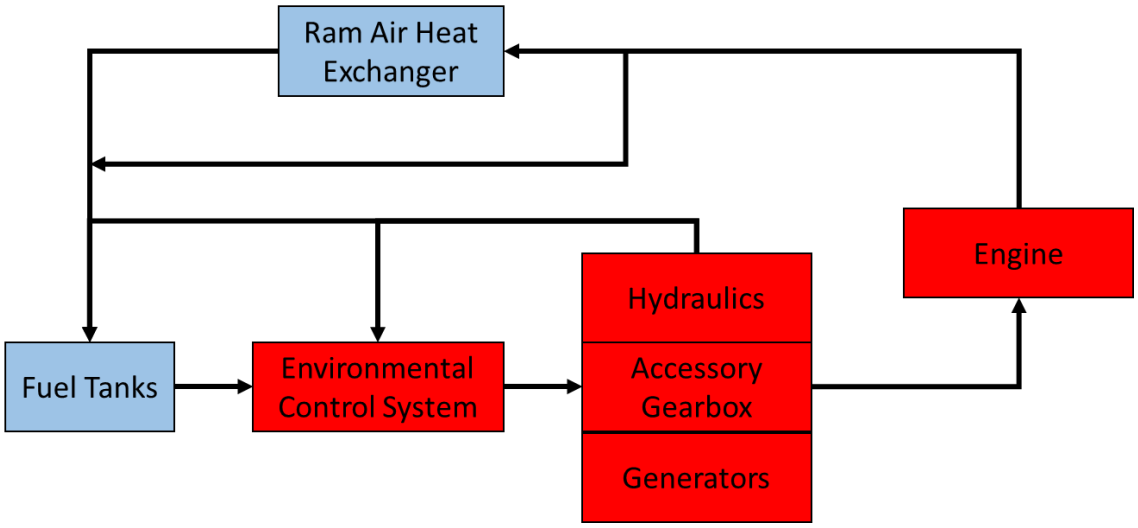

Figure 2: Simplified Fuel Thermal Management Schematic Adapted from *[12]*. Red blocks represent heat added to the fuel while blue blocks are heat removed from the fuel.

It is worth mentioning that fuel does indeed have practical limitations which give upper bounds to how hot it can safely operate. Beyond the obvious issue of the presence of air in fuel tanks and the risk of combustion at elevated temperatures [8], fuel which experiences excessive thermal stress through elevated temperatures begins to undergo chemical reactions which result in the precipitation of solids in a process generally referred to as coking [7] [13] [14]. These solids can deposit throughout a fuel system and severely degrade its operation, cause significant engine damage, or catastrophic engine failure through clogging of engine combustor nozzles [7] [13] [14].

In summary, the concepts of fighter aircraft thermal management architecture relevant to this discussion are as follows:

- Fuel is used as a heat sink

- Fuel directly/indirectly cools:
    - Mechanical loads
    - Electrical loads
    - Electrical generation systems
- Fuel temperatures vary throughout a mission

1.1.3 Aviation Turbine Fuel: Composition and Performance Requirements

With the relevant trends in military aviation of increasing power density and decreasing ability to reject heat to the environment, as well as a basic understanding of the relevant thermal management architecture highlighting the fact that many sub-systems interact via thermal energy exchange and that fuel has become the dominant means to balance their competing requirements, it will now be useful to develop a basic description of fuel composition to establish awareness as to why there are unanswered questions worth exploring in the present work. This section will cover that topic and will then briefly give attention to some of the basic system constraints which further underscore the importance of fuel in aircraft thermal management.

Aviation turbine fuels, also known as jet fuels, are mixtures comprised of hundreds of chemical compounds designed to meet a range of performance requirements which are traditionally focused on engine performance [15]. The composition of the fuels is dominated by hydrocarbon compounds including n-paraffins, iso-paraffins, monocycloparaffins, dicycloparaffins, tricycloparaffins,

alkylbenzenes, cycloaromatics, diaromatics, triaromatics, and light types of hydrocarbons as well as trace elements of several types [15]. Though a large proportion of typical jet fuel may be composed of C_{10} through C_{16} paraffins, the distillation process inevitably leads to the inclusion of a large amount of hydrocarbons outside of this band, with the final content depending on a number of factors including the source of the crude oil input. This means that just as every sample of crude oil has a unique composition depending on where and when it was harvested, each batch of aviation turbine fuel has a unique composition and a resulting unique range of properties [16]. Risk for performance impacts as a result of fuel variation are mitigated by ensuring that typical aviation fuels used in fighter aircraft such as JP-5, JP-8, F-24, Jet A, and Jet A-1 meet the requirements specified by MIL-DTL-5624W [16], MIL-DTL-83133J [17], NATO AFLP–3747 [18] , and ASTM D1655 [19] (Jet A and Jet A-1) respectively. Typical requirements within these specifications include those shown in **Table 1**.

Table 1: Sample of aviation turbine fuel specification points *[16] [17] [19] [18]*

Property	Minimum	Maximum
Volume Percent Aromatics	-	25.0 (JP-5, JP-8, F-24, Jet A) 26.5 (Jet A-1)
Density at 15 ℃ (kg/L)	0.788 (JP-5) 0.775 (JP-8, F-24, Jet A, Jet A-1)	0.845 (JP-5) 0.840 (JP-8, F-24, Jet A, Jet A-1)
Viscosity at -20 ℃ (mm^2/s)	-	7.0 (JP-5) 8.0 (JP-8, F-24, Jet A, Jet A-1)
Freeze Point (℃)	-	-46 (JP-5) -40 (F-24, Jet A) -47 (JP-8, Jet A-1)

Net Heat of Combustion MJ/kg	42.6 (JP-5) 42.8 (JP-8, F-24, Jet A, Jet A-1)	-
Flash Point (°C)	60 (JP-5) 38 (JP-8, F-24, Jet A, Jet A-1)	-

Though these requirements are certainly not exhaustive of those contained within the specifications, the table does contain all of the thermodynamic and transport properties directly controlled by the specification as well as the complete range explicitly described by them. Certainly the limits on heat of combustion, flash point, and aromatic content must bound the distribution of the previously cited hydrocarbon groups within the fuels, and these in turn must affect the thermodynamic and transport properties of the fuels. However, the specifications do not provide insight into what the working distributions of hydrocarbon constituents are, their connection to the properties cited in the specifications, or additional properties of interest to thermal performance such as constant pressure specific heat and thermal conductivity and their respective temperature dependence.

1.2 Active Research

In order to address the challenges of designing, maintaining, and upgrading the highly integrated power and thermal systems described in **1.1**, several areas of research have developed which consistently contribute to relevant bodies of peer

reviewed technical literature. The following section will briefly review efforts aimed at improving aircraft thermal management, including detailed modeling efforts to quantify subsystem interactions and performance, adoption of advanced control systems, and modification of fuel chemistry.

The discipline of modeling known as "tip to tail" modeling of aircraft systems is an active field which aims to develop accurate transient power and thermal models of aircraft systems, allowing understating of the operating temperatures of critical systems throughout the course of a given mission. Validated models of this type may be used for design, mission planning, or reliability studies, making them a powerful and versatile addition to the traditional engineering toolset available to support these aircraft during their entire lifecycle.

From the aircraft subsystems perspective, tip to tail modeling generally includes fuel systems, environmental control systems, electrical power systems, hydraulic and propulsion systems, and relevant boundary conditions such as ambient temperature and altitude, and Mach number to capture all of the significant thermal exchanges over the course of a given flight profile. One of the larger research groups supporting this discipline is geographically centered upon the United States Air Force Research Laboratory (AFRL) at Wright-Patterson Air Force Base near Dayton, Ohio and includes authors from the University of Dayton, Wright-State University, Purdue University, the engineering firm Paul C. Krauss and Associates (PCKA), and the AFRL internally.

In 2008 the AFRL established the Integrated Vehicle Energy Technology (INVENT) program to address "thermal management challenges in modern

survivable military aircraft, from a vehicle energy perspective, through new system integration and optimization approaches" [20]. "INVENT Modeling, Simulation, Analysis and Optimization" 2010 [20] describes how the INVENT program has been striving for standardization in the tip to tail field to address some of the recurring challenges faced in this field such as appropriate model fidelity, software, and data structure. Standardizations described include practices for selection of numerical methods for particular subsystem models and time steps, all of which is required as the general approach to these types of efforts involves different subsystem models running at unique time steps and communicating as appropriate with other subsystem models.

In "Generic Aircraft Thermal Tip-to-Tail Modeling and Simulation." 2012 [21], the authors applied a representative flight profile to a modeled notional thermal management system constructed in Simulink. These models are meant to capture the entire flight profile from take-off through landing with missions on the order of hours of real time and as such demand significant computational resources. Of additional interest in [21] is the inclusion of basic thermal management logic which directs how available cooling is distributed throughout the aircraft given the conditions present. Results show larger than 50 °F deviation between fuel set point temperature and modeled temperature, demonstrating the difficulty in balancing cooling demands utilizing the traditionally employed federated approach to thermal management control systems as the avionics cooling air temperature greatly exceeds the set point for a significant portion of this mission.

Oppenheimer et al. 2018 [22] thoroughly describes how mass and energy conservation are applied to model the constituents of an aircraft thermal management system as well as discussing the numerical techniques used prior to discussing the effects different control schemes and fuel pump sizing have on overall thermal management system performance. Results indicate on the order of a 7% increase in thermal endurance by adjusting the size of the engine feed fuel pumps downward.

In "Vehicle Level Transient Aircraft Thermal Management Modeling and Simulation" [23], three separate modeling efforts are described, each of which utilize tip to tail level modeling. The initial effort explored the use of a variable displacement fuel pump as opposed to the traditional centrifugal pump with results showing an increased fuel burn of less than 1% and a drop in main tank bulk fuel temperature of 136 °F. The second effort focused on the addition of a High Energy Pulsed System (directed energy weapon) to the aircraft and discussed the multitude of challenges from the thermal, electrical, space, and weight perspectives that such a system presents. The final effort focused on inclusion of a detailed air cycle system in a tip to tail model of a legacy aircraft and highlights one of the most significant and long term challenges of the tip to tail modeling field: model validation.

In an attempt to migrate away from potentially competing temperature set-point demand signals and adopt a more holistic view of the energy systems at hand, several authors have investigated the use of alternative control schemes. Using more modern control techniques, alternative architectures, or control criteria other than temperature all provide promising results as discussed below.

Pangborn et al. 2017 [24] implemented control for fuel thermal management in both the modeling and experimental domains to explore control approaches and validate modeling efforts. Using a $1/12^{th}$ scale fuel system representation with simulated aircraft heat loads and water as the working fluid, the authors evaluated a purely reactive approach to thermal management control and contrasted it with a scheme which uses knowledge of the mission to prepare for perturbations. The advanced knowledge scheme, a model predictive control (MPC) scheme, was evaluated using varying degrees of advanced knowledge of the event as well as incorrect knowledge of the event. Though in all cases considered it outperforms the purely reactive proportional-integral scheme, the authors caution that much more thorough treatment of the MPC scheme in the setting where the advance knowledge is incorrect must be completed prior to it being considered flight worthy [24].

"Fuel Flow Topology and Control for Extending Aircraft Thermal Endurance" 2018 [25] presents a potential alternate fuel system architecture with an additional reservoir of fuel that does not receive recirculated hot fuel from any system. After deriving the governing equations for the alternate configuration as well as a standard single tank configuration, open and closed loop control schemes are derived which aim to maximize the rate at which heat is rejected from the aircraft. Results suggest that implementation of the proposed closed loop control scheme offers promise of significant reduction fuel temperatures with the two tank configuration offering additional benefit.

Though not applied directly to aircraft systems, it is worth mentioning "Thermodynamics-based Optimization and Control of Integrated Energy Systems"

2013 [26] where the author applied offline static set-point temperature optimization algorithms to minimize exergy destruction in systems where electrical energy production and waste heat are both managed. It was shown through simulation that the minimization of exergy destruction may increase the rate of energy consumption but that this trade-off may prove worthwhile. This balance between exergy and energy illustrates why such work may be useful in the aircraft thermal management field as range and thermal margin are now in competing regimes within the aircraft performance trade space.

In a program starting in 1989, the U. S. Air Force began research into increasing the thermal stability of JP-8 with the primary aim being an increase in the "heat sink capacity" of the fuel by 50% which was defined as raising the maximum operating temperature of the fuel from 163℃ to 218℃ [14]. "JP-8+100: The Development of High-Thermal-Stability Jet Fuel" 1996 [14]outlines several items which were key to achieving this goal: additional knowledge required to better understand the distinction between thermal and oxidative stability, improving thermal stability test methods, developing chemistry based modeling methods to predict additive improvements, development of an additive package, and demonstration on aircraft.

With JP-8+100 developed, trade studies were conducted including "Thermal Benefits of Advanced Integrated Fuel System Using JP-8+100 Fuel" [13] where the authors used low fidelity Tip-to-Tail modeling to predict the additional thermal margin for various platforms, including U. S. Navy F/A-18C/D and F/A-18E/F models. The results of the modeling efforts suggested increased air cooling thermal

margin on the order of 4%-31% depending on mission segment. Though results looked promising and the Navy supported research to the point of demonstrations on F404 engines [27] (legacy F/A-18 engine), the requirement for high flashpoint fuel (JP-5) onboard air capable ships [14] and significant logistical issues with modifying a well-established supply chain have and will continue to prevent regular use of JP-8+100.

1.3 Objectives

> *"Increasingly stringent requirements for aerospace propulsion system performance, reliability, and operability motivate quantitative connections between fuel composition, physical characteristics, and system performance."*
>
> - Berrier et al. 2020 [28]

The success of the efforts cited in the previous section rely upon not only properly defined and implemented interfaces to establish mass and energy conservation, but accurate representation of the physical dimensions and material properties to enable accurate prediction of system level thermal performance. As highlighted by the 2016 Small Business Innovative Research (SBIR) topic titled "Probabilistic Design of Fuel Thermal Management Systems" [29] published by the AFRL and awarded to PCKA, the material properties relevant to aircraft thermal performance are generally well known, other than those of jet fuel. Citing previous investigations conducted by the AFRL, the SBIR discusses the variability in

thermodynamic and transport fuel properties between batches and points out that while it is known that specific heat may vary by 15% for samples of Jet-A fuel, no published study has explored the effects of all of the fuel properties relevant to aircraft thermal management.

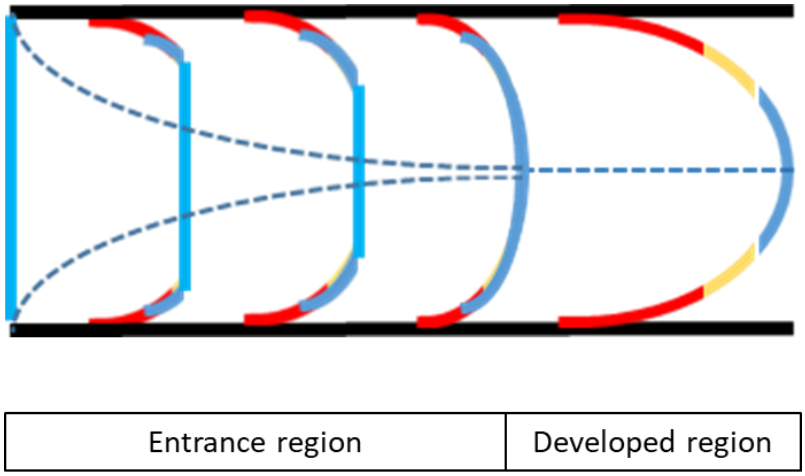

Figure 3: Thermal (color) and velocity (shape) boundary development regions for generic internal flow convective heat transfer

Reviewing the basic relationships relevant to convection in closed ducts (the dominate mode of heat transfer for aviation turbine fuel in fighter aircraft thermal management systems) reveals a strong dependence on properties not well defined by the fuel specifications discussed in section **1.1.3 Aviation Turbine Fuel: Composition and Performance Requirements**. This generic heat transfer configuration is depicted in **Figure** 3 which considers both entrance and fully developed flow regions. Whether considering a fixed temperature or a constant heat flux boundary condition, the heat transferred to a given single phase fluid in a heat

exchanger can be expressed in the well-known form shown in **equation (1)** which balances the rate of thermal energy transfer Q across the wall of the duct with the rate of change of energy within the fluid [30].

$$Q = \dot{m} c_p (T_{outlet} - T_{inlet}) \tag{1}$$

A slightly different but equivalent view of this process involves consideration of the thermodynamic and transport properties which can be utilized to formulate the convective heat transfer coefficient h shown in **equation (2)** [30]. When used in the appropriate differential form, this expression can enable quantification of spatial temperature gradients.

$$Q = h A_s (T_{outlet} - T_{inlet}) \tag{2}$$

Where:

$$h = \frac{Nu\ k}{d_h} \tag{3}$$

$$Nu = f(Re, Pr) \tag{4}$$

$$Re\ = f(\rho, \mu)\ \ Pr = f\left(c_p, k, \mu\right)$$

As can be seen from the definition of h in **equation (3)**, its value is not only dependent upon the geometric constraint of hydraulic diameter d_h, but also the fluid specific properties of Nusselt number Nu and thermal conductivity k. The Nusselt

number is in turn a function of the Reynolds number and Prandtl number meaning that the heat transferred to a fluid in a generic internal flow heat exchange setting is a function of the density, viscosity, specific heat, and thermal conductivity of the fluid. Specific empirical correlations for the Nusselt number have been developed which must be appropriately selected based upon the degree of turbulence encountered, or the temperature dependence of fluid properties such as viscosity [31]. Given the large range of flow rates, temperatures, and heat fluxes encountered for fuel in a typical aircraft thermal management architecture, it should follow that temperature dependent properties should be employed when performing detailed aircraft thermal management design and analysis.

With the fundamental background motivating the present work now established, the objective of the effort can be stated as follows: define temperature and compositional dependent bounds of thermodynamic and transport properties for aviation turbine fuel relevant to aviation thermal management performance, specifically:

- Density $\rho(T, w_{1..i})$
- Viscosity $\eta(T, w_{1..i})$
- Specific heat $c_p(T, w_{1..i})$
- Thermal conductivity $\lambda(T, w_{1..i})$
- Prandtl Number $Pr\ (T, w_{1..i})$

Where

$$T = \text{Temperature}$$
$$w_{1..i} = \text{hydrocarbon composition}$$

Hopefully, the motivation for addressing this gap within the field of aircraft thermal management is now clear to the reader. In summary, the most important points to be considered are: (1) aircraft thermal management has evolved to become a thriving technical discipline with typical architectures being heavily reliant upon using aviation turbine fuel as a heat sink (2) aviation turbine fuels are complex mixtures which vary batch to batch (3) the resulting fuel transport and thermodynamic property variation which influences aircraft thermal performance is not clearly understood within the research community.

2. Literature Review

To address the objective of defining the density, viscosity, specific heat, thermal conductivity, and Prandtl number of aviation turbine fuel as a function of composition and temperature, a literature review was conducted which covered three primary areas. To immediately address the issue and avoid an unnecessarily deep dive on the topic, the first approach (**2.1 Aviation Turbine Fuel Experimental Compositional, Thermodynamic, and Transport Data**) aimed to derive sufficient data from the literature on within the chemical transport property data to establish bounds on compositional, thermodynamic, and transport properties with available test data. The second focus area within the literature (**2.2 Hydrocarbon Mixture Thermodynamic and Transport Properties: Numerical Approaches**) sought to supplement any test data uncovered with numerical models capable of utilizing compositional data to predict thermodynamic and transport properties of complex hydrocarbon mixtures. The final area of review (**2.3 Machine Learning Models of Fluid Properties**) centered on finding models derived using machine learning which are capable of accomplishing the same task as its preceding section, or perhaps supporting it.

2.1 Aviation Turbine Fuel Experimental Compositional, Thermodynamic, and Transport Data

The goal of this particular section of the review was to identify the body of test data existing within the literature which could help establish the appropriate bounds of composition and properties of interest for the present study.

"Properties of a 50/50 Mixture of Jet-A + S-8" 2007 [32] analyzed the composition and thermophysical properties of a 50/50 (vol/vol) blend of a sample of Jet-A and the Fischer Tropsch process derived synthetic S-8 fuel. Compositional analysis was performed using gas chromatography–mass spectrometry. Distillation curves, speed of sound, density, compressed liquid density, and viscosity measurements were also taken at a range of temperatures before establishing correlations for the properties of density, viscosity, and speed of sound using polynomial and exponential models without compositional information. Hydrocarbon type analysis provided by ASTM D-2789 is given in Table 2.

Table 2: Composition (Vol%) of Fuel Samples as reported in *[32]*

	Paraffins	Monocyclo-paraffins	Dicycloparaffins	Akyl-aromatics	Indanes and Tetralins	Naphthalenes
Jet A-4658	46.5	22.5	5.4	18.4	4.5	2.4
S 8-4734	80	17.3	0.9	0.1	0	1.9

"Surrogate Mixture Models for the Thermophysical Properties of Aviation Fuel Jet-A" 2010 [33] modeled the volatility, density, speed of sound, viscosity, thermal conductivity, and cetane number for two samples of Jet-A fuel using the surrogate technique informed by compositional information collected using gas-chromatography-mass spectrometry. One sample used, Jet-A-4658, was a mixture in equal aliquots of five samples of Jet-A and as such was deemed "representative of Jet-A" by the authors. The other sample, Jet-A-3638 was noted for is exceptionally low aromatic content. Modeling of the properties of the two fluids was accomplished by using equations of state with unique parameters for each potential surrogate component, viscosity and thermal conductivity surfaces, and a mixture model to combine the properties of the pure components appropriately. Surrogate components were selected from the measured compositional data for each fuel, but represent only on the order of 10% of the constituents. The models were tuned by varying relative amounts of surrogate components within the modeled mixtures to minimize error, resulting in non-physical and non-generalizable models.

The authors of "Thermodynamic, Transport, and Chemical Properties of "Reference" JP-8" 2010 [34] used gas chromatography-mass spectrometry to determine compositional information on five samples of fuels (JP-8-3773, Jet-A-3602, Jet-A-3638, Jet-A-4658, S-8) and two molecular fluids chosen to represent cyclic branched alkanes: methylcyclohexane and propylcyclohexane. Additional testing on all samples was done to establish distillation curves and thermophysical properties as a function of temperature (density, viscosity, specific heat, and thermal

conductivity) using gas chromatography mass spectroscopy, where the authors note the following limitation:

> *"The chemical analysis typically allows the identification of between 40 and 60 percent (by mass) of the fluid components. There are usually numerous minor components that cannot be identified because of their low concentrations, and other cases in which chromatographic peak overlap prevents reliable identification of even the more abundant components."*
>
> -Bruno et al. 2010 [34]

Finally, empirical models built using this compositional information were established to represent each sample of jet fuel, though each model was adjusted to minimize error by adjusting the weighting of the constituents and including methlycyclohexane and propylcyclohexane in the formulation, as their properties were established during testing. The result of this approach are models of the thermophysical properties of these jet fuels which only apply to these individual samples and are not broadly applicable to hydrocarbon mixtures or jet fuels.

"Effect of composition on freezing points of model hydrocarbon fuels" 1984 [35] studied the effect of composition on freeze point of jet fuel type mixtures using mixtures of higher n-alkanes (C_{12} – C_{17}) in solution with various solvents and noted interaction between certain molecules which influenced the result.

"Preliminary Surrogate Mixture Models for the Thermophysical Properties of Rocket Propellants RP-1 and RP-2" [36] 2009 developed surrogate models of density, viscosity, speed of sound, and thermal conductivity as functions of temperature for the reduced sulfur formulation of RP-1 and the ultra-low sulfur RP-2 kerosene fuels

and informed the compositional basis for the surrogates with gas chromatography-mass spectrometry. The modeling procedure used was similar to that of [33].

"Density and Speed of Sound Measurements of Jet A and S-8 Aviation Turbine Fuels" 2009 [37] Presents measured data of the density and speed of sound as a function of temperature of three Jet-A samples and one Fischer-Tropsch process derived synthetic hydrocarbon fuel (S-8) alongside data from the Coordinated Research Council World Fuel Sampling Program CRC Report 663 [38]. The Jet-A samples chosen for [37] were selected to cover what was thought to be the range of properties, while the data from [38] is averaged in an effort to show the central behavior. A key takeaway from comparing the two sources, as demonstrated within [37], is that one of these two sets of data does not in fact accurately capture the center of properties such as speed of sound.

The apparent discrepancy of the true center of the speed of sound shown in [37] is contrasted in "Comparison of Jet Fuels by Measurements of Density and Speed of Sound of a Flightline JP-8" 2010 [39] by the density measurement and comparison with data from [38] where both sources of data seem to describe the same central tendency. Given that density is controlled by the specifications of aviation turbine fuels, this central tendency is likely better understood.

Outcalt and Fortin 2011 [40], noted that instability in supply of petroleum derived sources of aviation fuels was and continues to drive demand for alternative sources of these fuels. As such, they measured the density and speed of sound of two synthetic isoparaffinic kerosenes (SPKs), one derived from coal and one from natural gas. Measurements were made over the temperature and pressure ranges of 270-

470K and 0.083-50 MPa respectively. A modified Tait equation using empirically derived parameters for each sample provided a correlation to the measured data yielding absolute average deviations within the uncertainty of the test data but not a generalizable model. Comparison between the measured values of density and speed of sound against literature data showed significant deviation from Jet A samples but similar values to S-8, also synthetically derived. Though a discussion on composition of the fuels is provided, only the four most prominent constituents of each fuel were reported which combined totaled on the order of 45% of area for the natural gas derived sample, and 14% for the coal derived sample.

Building on their work from 2011, Outcalt and Fortin 2012 [41] measured the densities and speeds of sound of four biomass-derived fuels. The feed stocks of the four fuels were as follows: (1) camelina, (2) castor seed, (3) plant isoprenoid, and (4) reclaimed waste fats and grease. For the experimental portion of the work, the temperature and pressure ranges were the same as those investigated for the SPK fuels and a similar procedure was utilized to derive non-generalizable equations for density. Comparison against a petroleum derived Jet A sample shows that only the plant isoprenoid derived sample has a comparable density. Hydrocarbon compositional data were reported for these samples in the earlier work of Bruno and Baiborine [42] though only the CSK fuel reported sufficient area percentages via the gas chromatography mass spectrometry methods used to account for more than 75% of the composition.

Continuing with the investigation into densities and speeds of sound of alternative jet fuels, Outcalt 2014 [43] repeated the procedures applied in the two

previously reported works on three more alternative fuels. One fuel was derived from hydroprocessed chicken fat, one from dimerized components of crude turpentine, and a third utilized a Fischer-Tropsch process to synthesize a jet fuel from natural gas. Once again, an empirically derived model was used to describe each individual fuel and compositional information was supplied by Gough and Bruno [44] but without sufficient detail to represent the entire body of hydrocarbon constituents.

"Convective Heat Transfer Characterization of Aviation Turbine Fuel-Metal Oxide Nanofluids" 2012 [45] investigated heat transfer performance enhancement given to unnamed type of aviation turbine fuel of unnamed composition and relates improvement to increases in Prandtl number and subsequently Nusselt number.

Motivated by a desire to increase the utility of chemometrics (using chemical compositional information to inform property models of substances), Berrier et al. 2020 [28] applied a comprehensive two-dimensional gas chromatography with time-of-flight mass spectrometry (GC x GC-TOFMS) to a chemically diverse set of 74 distillate and multicomponent aerospace fuels and correlated the resulting compositional information with measured viscosity, density, heat of combustion, hydrogen content. While 18 ATF samples are presented with measured density at three temperatures ($15℃, 45℃, 85℃$), viscosity is presented only at one temperature and the empirically derived model has mean squared error of 6.01% which is significantly higher than the test uncertainty of 0.1% typical of viscosity measurements. Additionally, though chromatograms are presented in the supporting information, sample compositions were not quantitatively reported.

Coetzer et al. 2018 [46] provided experimental data for surrogate mixtures used to explore the effect of n- and iso-paraffin mixture composition on freeze point and low temperature viscosity of jet fuels. Empirical models were developed to correlate the relative compositions of individual carbon bins for both paraffin groups to the respective properties.

The primary findings from the body of test data reviewed on this topic show that most of focus for property measurement centered upon specification properties, and not those of interest for the present study. Four samples of fuel were repeatedly presented throughout the literature (JP-8-3773, Jet A-3602, Jet A-3638, Jet A-4658) and from the data collected, the density, viscosity, specific heat, and thermal conductivity across a range of temperatures can be pieced together and Prandtl numbers derived. However, as noted by the authors, the compositional information reported used techniques which leave a large amount of the hydrocarbon compositional data incomplete. Additionally, the four samples presented are certainly not statistically sufficient to establish a range of the desired properties.

2.2 Hydrocarbon Mixture Thermodynamic and Transport Properties: Numerical Approaches

Within this portion of the review, the focus shifts from test data to predictive approaches quantify the properties of interest. Aside from jet fuel specific works, models for hydrocarbon or related organic substances were investigated with the most relevant literature presented below.

Lötgering-Lin and Gross 2015 [47] established models for predicting viscosities of 12 chemical families including non-polar, polar, and hydrogen bonding self-associating components are considered. The authors built upon entropy scaling approaches established by Rosenfeld [48] by utilizing group contribution methods informed by the perturbed chain polar statistical associating fluid theory (PCP-SAFT) equation of state (EoS). Viscosity is scaled in terms of a third order polynomial which uses the residual entropy provided by the PCP-SAFT EoS. Mean absolute deviations for the 110 pure substances considered are on the order of 5% except for alkanes, alcohols, and aldehydes which are closer to 10%. Lötgering-Lin et al. 2018 [49] then expanded on this effort to develop a model suitable for mixtures, evaluating 566 mixtures containing either non-polar substances, or at least one polar substance. Relative mean deviations on the order of 5% were reported as well as model limitations in cases where hydrogen bonding was present.

"Thermal Conductivity of Hydrocarbon Mixtures: A Perturbation Approach" 1993 [50] presents a method for predicting the thermal conductivity of hydrocarbon mixtures using a continuous mixture model which is informed with empirical correlations developed from tests of pure substances and validated against binary and ternary hydrocarbon mixtures. The model contains no reference to fundamental physical relationships driving the behavior.

Hopp and Gross 2017 [51] built upon the work of Lötgering-Lin and Gross [47] by applying the same entropy scaling concept to thermal conductivity, with particular focus on strongly non-spherical species, such as long chain hydrocarbons. The authors demonstrate that a reference thermal conductivity based on the residual

entropy itself is required to enable a monovariate relationship between the thermal conductivity and residual entropy. The residual entropy was calculated using the PCP-SAFT EoS and performance of the entire model was evaluated over 147 substances. Two general approaches were applied: one where model parameters were calculated from empirically fitted equations, and one where some of the model parameters were fitted for individual substances. The latter approach provided an average relative deviation across the substances considered of 4.2%.

Hopp and Gross then expanded on the 2017 work [51] in 2019 with [52], refining the group contribution method, expanding the substances covered to 231, and producing an absolute average error across all substances of 6.17% using fitted parameters for each substance.

Naef 2019 [53] developed a method to predict the isobaric heat capacity of molecular liquids and solids at a single temperature $(298.15\ \mathrm{K})$ by establishing empirical correlations between theoretical molecular volumes and experimentally measured isobaric heat capacities. 1303 liquid compounds were considered, including paraffins, cycloparaffins, and aromatics. Separate linear correlations were developed based on the number of hydroxyl groups present in any given molecule. Mixtures of hydrocarbons were not considered in this work.

Dadgostar and Shaw 2012 [54] developed a predictive correlation for constant pressure liquid heat capacity which can be applied to both pure organic compounds and "ill-defined" mixtures over a temperature range of several hundred Kelvin. The correlation is based off of a similarity parameter (α) which is proportional to the number of atoms per unit mass of a given substance. The model was developed using

150 experimental heat capacity values representing 19 liquids to fit model coefficients and was then evaluated against 111 data points representing 12 organic liquids and 3 molten polymers where average deviations were found to be on the order of 3%.

In the most comprehensive work to date on the properties and substances relevant to the present study, Rokni et al. 2019 [55], Rokni et al. 2019 [56], and Rokni et al. 2019 [57] utilized entropy scaling using the PC-SAFT equation of state to predict the density, isothermal compressibility, volumetric thermal expansion coefficient, viscosity, and thermal conductivity of hydrocarbon mixtures, diesel, and jet fuels. To address the difficulty in capturing interactions between large numbers of molecules, a pseudo-component technique was developed which treated the mixtures as homogenous substances comprised of single chain hydrocarbon molecules and utilized the ratio of carbon atoms to hydrogen atoms to inform the appropriate amount of aromatic behavior in the resulting model. (A detailed description of the pseudo-component entropy scaling model parameters used in the PC-SAFT EoS is provided in 4.1 Pseudo Component Entropy Scaling) To link the residual entropy calculated from the PC-SAFT EoS to the transport properties of viscosity and thermal conductivity, the coefficients of a third order polynomial (as shown below in equation (5)) are calculated from surfaces generated from fits of experimental data.

$$\ln(\lambda^*) = A + Bs^* + Cs^{*2} + Ds^{*3} \quad (5)$$

Tracing the development of this polynomial through the research preceding that of Rokni et al., this model seems to have developed out of mathematical convenience rather as opposed to being driven by physical considerations [47] [51] [58], a point which will be of central importance to the approaches applied in subsequent sections of the present study. Rokni et al. did address jet fuels in their works, however, the error for the models which did not utilize test data to fit parameters of individual mixture samples was typically one order of magnitude (density, thermal conductivity) to two orders of magnitude (viscosity) above the uncertainty of the associated test data.

In summary, the literature reviewed for this section produced promising results from the perspective of functional models containing physical understanding. These models lay a strong foundation to expand upon provided that sufficient compositional information can be collected to inform models and that reasonable enhancements to fidelity can be made to facilitate having the model error approach the uncertainty in the associated test data.

2.3 Machine Learning Models of Fluid Properties

> *"By using machine learning approaches, we seek to elucidate underlying universal characteristics of fluids and fluid mixtures that enable property prediction. Namely, thermodynamic properties of these systems which play a significant role in applications ranging from medicine to industrial manufacturing. A deeper understanding is expected to facilitate improved pharmaceutical development, cheaper chemical separations, and lower energy alternatives to chemical processes."*

- National Institute of Standards and Technology (NIST) 2020 [59]

The sentiments of the final area of focus are well captured by the above from "Machine Learning Fluid Equations of State" which is an ongoing NIST project. For the present work, the aim was to look for consistently applied approaches within the machine learning literature on fluid properties. Of chief concern was the selection of model hyper-parameters, which are the parameters used to determine the structure of a particular machine learning architecture and then train it, but are generally not used once the model has been deployed. Additionally, as pointed out by Piccione et al. 2020 [60], rather than consistently utilizing raw data as inputs to train and deploy machine learning models, if physical information is known or suspected about a system it can be included to process data both on input to our output from a model. This approach can lead to additional understanding of the system or potentially refinement of physical models. As such, the literature considered for the present review was evaluated with this additional consideration in mind.

Joss et al. 2019 [61] demonstrated the basic power of an artificial neural network as compared to linear and multivariate linear correlation approaches where assumptions about the underlying behavior of the model must be made. The example used to illustrate the improvement focuses on prediction of boiling point of pure substances using the molecular weight and acentric factor as inputs to the neural network and multivariate models, and just molecular weight for the basic linear model. Though several relevant hyper-parameters such as the number of hidden

layers and the number of neurons per layer are discussed, guidance on selecting those parameters is not provided beyond noting that there are trade-offs.

Atashrouz et al. [62] utilized a hybrid group method of data handling (GMDH) neural network model to predict the activity in water (a_w) in aqueous binary solutions of glycols and polyethylene glycols. Measured values of temperature, molecular weight of the polymer and mass fraction of water were used as input variables to the network which then directly predicted a_w. Results were compared to a standard neural network but discussion on hyper-parameters was limited.

Lashkarbolooki et al. [63] used an artificial neural network to predict the heat capacities of binary ionic liquids. Inputs were experimentally measured molecular weight, melting temperature, temperature, and mass fraction with the network directly providing specific heat as an output. A single hidden layer was used with the number of neurons (16) optimized to find minimum absolute average relative deviation, though additional discussion on hyper-parameters is not given.

Dargahi-Zarandi et al. [64] Applied a GMDH neural network to predict dynamic viscosities of gas mixtures of hydrocarbons and various impurities. Inputs were experimentally measured molecular weight, and density as well as derived inputs of reduced temperature and pressure. The model directly provided viscosity as an output.

Wole-Osho et al. 2020 [65] investigated the thermal conductivity of hybrid nano-fluids both experimentally and numerically using three separate approaches: a polynomial correlation model, an adaptive neuro-fuzzy inference system model, and

an artificial neural network. Model inputs were temperature, mixture ratio of the two nano-particles (aluminum oxide and zinc oxide), and volume concentration within the base fluid (distilled water). The models all provided thermal conductivity as a direct output. Figure 4: Flow Chart of Artificial Neural Network, provides a good example of a typical approach to machine learning model construction where a thorough system for dealing with model hyper-parameters is not employed.

Goussard et al. 2020 [66] used three separate methods to predict viscosities of pure liquids at 25 ℃: a group contribution method, an artificial neural network, and a graph based machine. Inputs to the neural network were first passed through the Conductor-like Screening Model for Real Solvents (COSMO-RS) which uses quantum chemistry and statistical thermodynamics to estimate chemical potential of solutes in liquid phase. Viscosity at 25 ℃ was the direct output of the machine learning models investigated, and no specific discussion of hyper-parameter selection was provided.

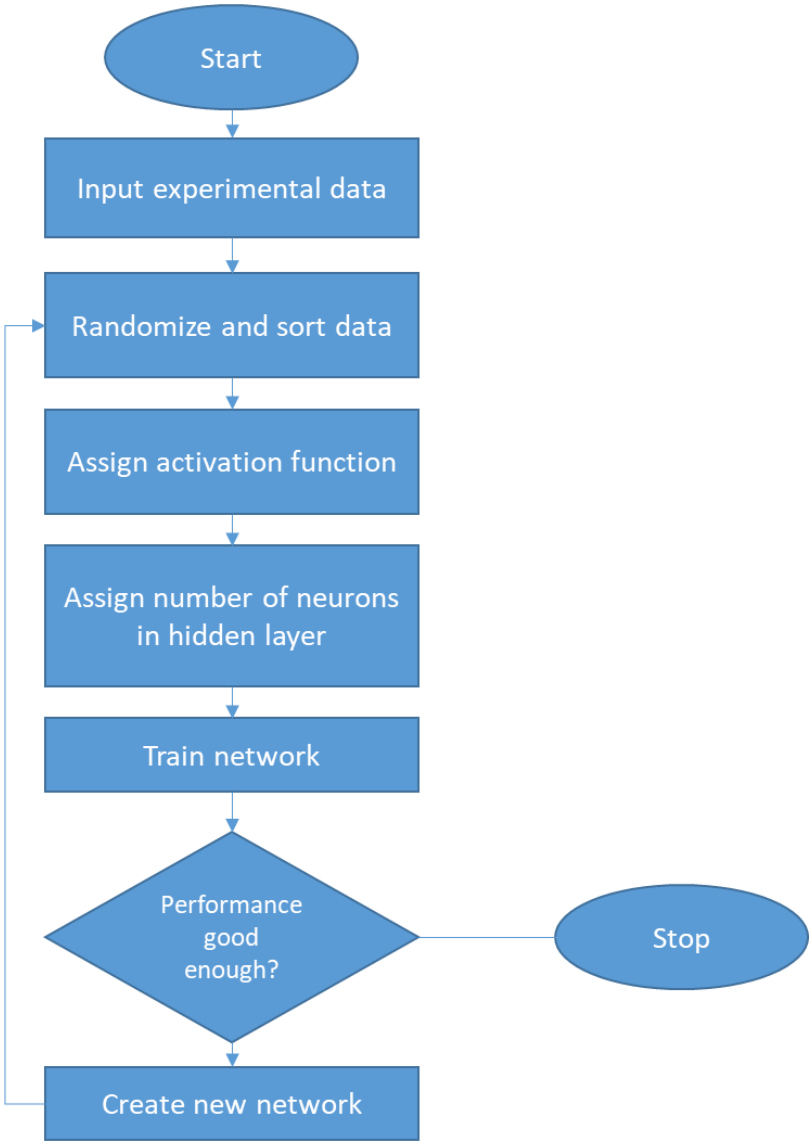

Figure 4: Flow Chart of Artificial Neural Network Modeling redrawn from Wole-Osho et al. 2020 *[65]*

In "Machine Learning to Predict Thermodynamic Properties of Pure Fluids and their Mixtures" Liu et al. 2019 [67] used support vector regression to develop an equation of state model which provides the pressure given inputs of volume, temperature, and $n-1$ molar fractions of the substances within the mixtures

considered, which in this case was water, carbon dioxide, and molecular hydrogen. The support vector model directly provided pressure as an output without additional computation. The authors optimized hyper-parameters essential for establishing model complexity and error by utilizing a grid search method applied to the two parameters of interest and finding the minimum average error resulting from a k-fold cross validation technique.

Gong et al. 2018 [68] predicted the density, intermolecular energy, and constant pressure specific heat of alkanes using an artificial neural network trained using data generated from a high-throughput force field simulation procedure. The authors used a relatively complex neural network architecture of three hidden layers with 16, 8, and 4 nodes in the respective layers moving from input towards output. Hyper-parameter discussion was limited to focusing on determining the optimal set of features to be used as inputs to the model.

Craven et al. 2020 [69] predicted the radial distribution functions of a Lennard-Jones fluid using a linear regression with a multivariate function decomposition and the pressure and internal energy of the same fluid using a kernel ridge regression process. Training data was generated using molecular dynamics simulation results from literature data as well as some generated specifically for the study. Extensive use of grid search methods were employed for model hyper-parameter optimization. Though physical models were used to generate the data, none was employed to inform the machine learning models.

Sözen et al. 2009 [70] applied artificial neural networks to predict thermodynamic properties of refrigerant mixtures, such as R407c. Separate models

were developed for saturated liquid-vapor and superheated vapor regions with model inputs of vapor quality and temperature for the former model while temperature and pressure were used for the latter. Both models directly provided enthalpy and entropy outputs, while the superheated vapor model also provided specific volume. Both models used single hidden layers with the number of neurons determined by finding the minimum error over a range of 5 to 11 neurons. No additional discussion of hyper-parameters was provided.

The authors of "Prediction of Flash Points for Fuel Mixtures Using Machine Learning and a Novel Equation" 2013 [71] directly predicted flash points for surrogate mixtures of jet fuels using genetic function approximation and support vector machines. A second method was also applied which first predicted flash points of individual mixture constituents using support vector machines and then applied the "Le Chatelier" mixing to predict surrogate flash point. The authors point to other works for discussion on hyper-parameter optimization.

Jiao et al. 2020 [72] studied the performance of four different machine learning techniques for predicting the lower flammability limit of hydrocarbon mixtures. Eleven different mixture weighted averaged molecular descriptors are used as inputs to each of the models developed which are (1) k-nearest neighbor, (2) support vector machines, (3) random forest, and (4) boosting tree which each provide the lower flammability limit as a direct output. Hyper-parameters used for each approach are provided but the logic guiding their selection was omitted.

Faundez et al. 2020 [73] presented objective criticism of common approaches to employing neural networks for prediction of fluid properties including

inconsistency in selecting the number of hidden layers and neurons of neural networks, not presenting or discussing training data, not presenting or discussing the tuned parameters (weights and biases) of trained networks, and not presenting performance of the trained network outside of the training set. The authors then presented a study where they employed their prescribed process improvements to develop a model to predict the solubility of diflouromethane (R-32) in seventeen ionic liquids. Model inputs were temperature, pressure, and ionic liquid specific properties of critical temperature, critical pressure, mass connectivity index, acentric factor, cation mass, and anion mass.

Overall, the body of work capturing machine learning approaches for predicting the thermodynamic and transport properties of fluid mixtures does lack consistency in approach to selection of model hyper-parameters and was found to lack depth in application of derived information between test data and model input. Save for one example (Saldana et al. 2013 [71]), post processing of data or employment of physical understanding after model output was not used. Certainly no single study was found which encompassed all of these desired attributes.

2.4 Approach

The preceding sections of the literature review have established some key points that guide the work in the remainder of the present study. Succinctly put, the points are as follows:

1. There is insufficient published test data to estimate the practical bounds of aviation turbine fuel composition, density, viscosity, specific heat, and thermal conductivity.

2. Physics based models, such as those using entropy scaling, are able to predict transport and thermodynamic properties of hydrocarbon mixtures using compositional information. These approaches yield consistent results yet have room to improve from the perspective of accuracy.

3. Machine learning approaches applied to prediction of fluid mixture properties tend to yield accurate results of ranges of training data but generalization outside of the training range may be improved through more consistent use of physics based knowledge. Additionally, more rigor is desired when selecting model hyper-parameters.

Using these considerations, the gaps identified between the published body of literature and the objective defined in section 1.3 will be addressed in the following sections by realizing the following steps:

1. Collect a statistically significant number of samples of aviation turbine fuel compositional information.

2. Expand the data set of temperature dependent thermodynamic and transport property data for aviation turbine fuels.

3. Improve the accuracy of viscosity and thermal conductivity entropy scaling models described by Rokni et al. 2019 [56] [57] by employing using a hybrid machine learning approach generically described by Piccione et al. [60].

4. Expand the specific heat model described by Dadgostar and Shaw 2012 [54] to apply to well-defined hydrocarbon mixtures.

5. Validate the approaches of steps 3 and 4 using data collected from the literature and supplemented by step 2.

6. Predict practical ranges of density, viscosity, specific heat, thermal conductivity, and Prandtl number using the compositional data

collected in step 1, models developed in steps 3 and 4 (Density will utilize the Rokni et al. model).

Realization of these steps will supply future efforts with well-informed estimates of practical working ranges of aviation turbine fuel properties relevant to thermal management studies and simultaneously outline a process of combining physics based information with machine learning techniques in a repeatable and logical manner.

3. Fuel Property Testing

As the range of known combinations of hydrocarbon fuel composition and properties presented in the literature was limited, an expansion of this data set was deemed critical to successfully predicting the range of aviation turbine fuel density, viscosity, specific heat, thermal conductivity, and Prandtl numbers. The following chapter provides an overview of the test methods utilized and relevant results. Complete datasets are provided in appendices as referenced throughout the chapter.

In coordination with the Fuels and Lubricants group within the Naval Air Warfare Center Aircraft Division at Patuxent River, Maryland, three samples of JP-5 and one sample of F-24 aviation turbine fuel were identified to undergo hydrocarbon compositional characterization as well as density, viscosity, and thermal conductivity testing under atmospheric pressure and temperatures between -20 ℃ and 100 ℃, and specific heat testing at atmospheric pressure and temperatures between 10 ℃ and 130 ℃. An additional data set was shared which contained hydrocarbon composition and specification viscosity $(0.1\ \text{MPa}, -20\ ℃)$ for 96 samples of varying grades of fuel (54 F-24, 26 JP-8, 11 Jet A, 5 Jet A-1).

3.1 Methods

To characterize the five parameters of interest to the present effort required 4 separate methods: ASTM D7042 for density and viscosity, ASTM E1269 for specific heat, ASTM D7896 for thermal conductivity, 2 dimensional gas chromatography (GCxGC) with configurations as described by Metz et al. [74].

In the case of density and viscosity measurements, ASTM D7042 requires the use of a Stabinger Viscometer which utilizes concentric rotating cylinders separated by the sample and known magnetically induced torque to establish different steady state rotational speeds between the cylinders. This difference allows for direct measurement of the sample dynamic viscosity. A standard Stabinger Viscometer such as the Anton Paar SVM 3000, is capable of providing sample temperature control between -20 ℃ and 100 ℃, directly measure density, and provide measurements of viscosity and density with uncertainty of 0.1% [75].

ASTM E1269 describes measuring specific heat using differential scanning calorimetry. The basic principle of this method is to measure the difference in energy required to increase the temperature a sample of interest and a reference of known heat capacity. The sample and the reference are seated in separate crucibles within an adiabatic chamber which has been instrumented to measure sample and reference temperatures and power or heat flux into the chamber [76]. Typical uncertainty for this type of method is on the order of 1.5% [77].

The method for thermal conductivity measurement described by ASTM D7986 utilizes the well-known transient hot wire approach. Here a platinum wire with a known relationship of temperature and resistance runs vertically through a fluid sample of interest. A known amount of power is dissipated through the wire for a short amount of time (on the order of a second or less) while the resistance of the wire is measured, thus providing its temperature. Utilizing the relationship between power, time and temperature change, the thermal conductivity of the sample can be

determined [78]. Based on typical heated wire diameters (<0.3mm) used in this method for fluids, typical uncertainty for this method is on the order of 3% [79].

For measurement of hydrocarbon composition, the GCxGC method with hardware configurations described by Metz et al. was applied. The basic principles of gas chromatography involve using a carrier fluid accelerating a mixture of interest through a column of known dimension with a detector at the exit with different compounds in the mixture arriving at the detector at different times based on relative masses [80]. The residence time of each constituent of the mixture compared to the overall sum of residence times allows for calculation of the relative concentrations of constituents while the addition of an additional technology such as flame ionization detection allows chemical identification of constituents, particularly in the case of hydrocarbons [80]. For mixtures such as aviation turbine fuel which have many constituents with similar carbon number, standard gas chromatography is insufficient in resolving all of the various compounds [74]. To overcome this, two dimensional gas chromatography has been adopted by the U. S. DoD to more accurately characterize fuel composition. The primary principles are the same however a second column is included within the hardware setup that has different dimensions and different conditions such as flow velocity, temperature, or surface polarity that influence the relative rate of constituent migration through the column. This essentially allows increased resolution in different molecular regimes between the two columns. **Table 3: Hydrocarbon Bins for Fuel Composition Considered in the Present Study** provides a listing of the hydrocarbon tiers and associated bins

which are able to be resolved with the method which has demonstrated reproducibility of no more than 3.2% across each tier considered.

Table 3: Hydrocarbon Bins for Fuel Composition Considered in the Present Study

Hydrocarbon Type	H Atoms per Molecule	Range of Carbon Atoms per Individual Molecules	Range of Carbon Atoms for Averaged Molecules	Total Bins
n-paraffin	2C+2	7-30	-	24
isoparaffins	2C+2	7-23	24-31	18
monocycloparaffins	2C	8-21	6-7, 22-26	16
dicycloparaffins	2(C-1)	8-18	19-25	12
tricycloparaffins	2(C-2)	10-20	-	11
alkylbenzenes	2C-6	6-19	20-24	15
cycloaromatics	2C-8	9-16	17-21	9
diaromatics	2C-12	10-16	17-20	8
triaromatics	2C-18	-	14-16	1
light hydrocarbons	2C+2	-	1-6	1
TOTAL	-	-	-	**115**

3.2 Results

Mass percent for each bin for each sample to undergo the full suite of property tests is given in **APPENDIX A**: **GCxGC COMPOSITION OF FULL PROPERTY SUITE SAMPLES** while the associated property data is reported in **APPENDIX B: DENSTIY, VISCOSITY, SPECIFIC HEAT, AND THERMAL CONDUCTIVITY OF FULL PROPERTY SUITE SAMPLES AT 0.1 MPa**.

Plots of the measured property data for the 4 full property suite samples including

values from the CRC World Fuel Sampling Program [38] which is assumed to represent the central tendency, are shown in **Figure 5 (a-d)**. Notable observations when reviewing this data include (1) the central tendency of JP-5 reported in [38] falls roughly in the middle of the JP-5 samples collected for the properties of density and viscosity but is definitively outside of that group for specific heat and thermal conductivity and (2) the slopes of the approximately linear behaving properties of density, specific heat and thermal conductivity are unique across the data collected and over the ranges considered there is crossing of values observed. Finally, it is also worth noting that (3) the variation in properties observed is larger than the expected uncertainty in test methods, confirming that variation is present.

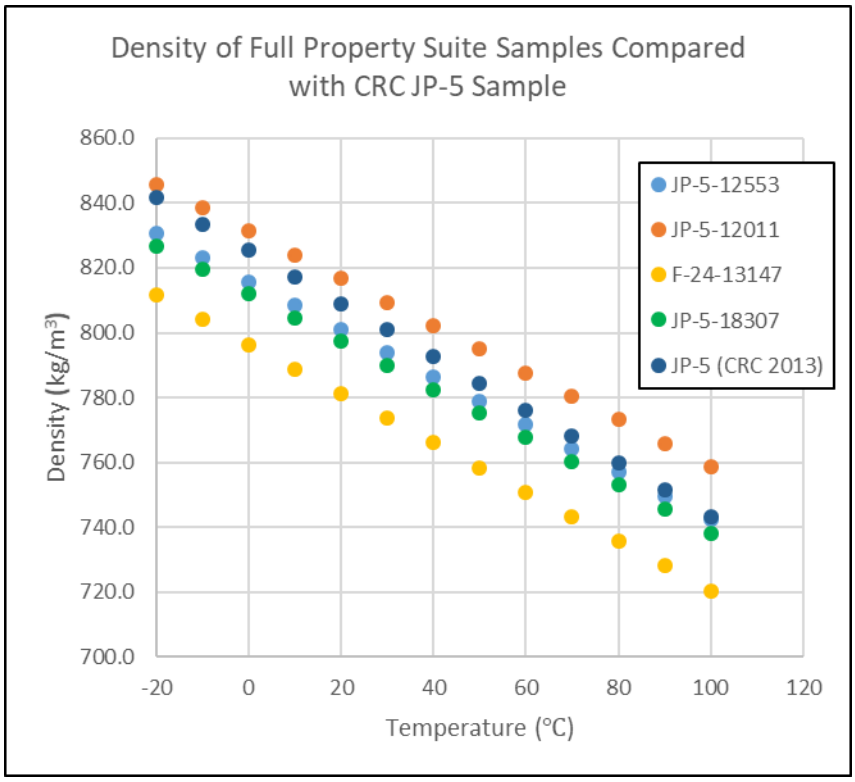

(a) Density vs. temperature

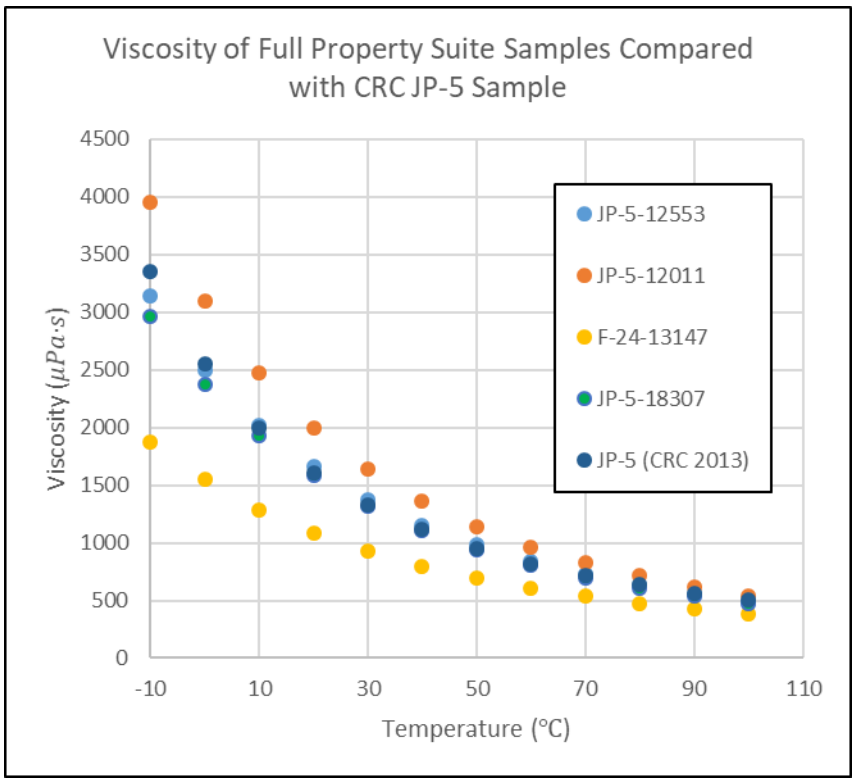

(b) viscosity vs. temperature

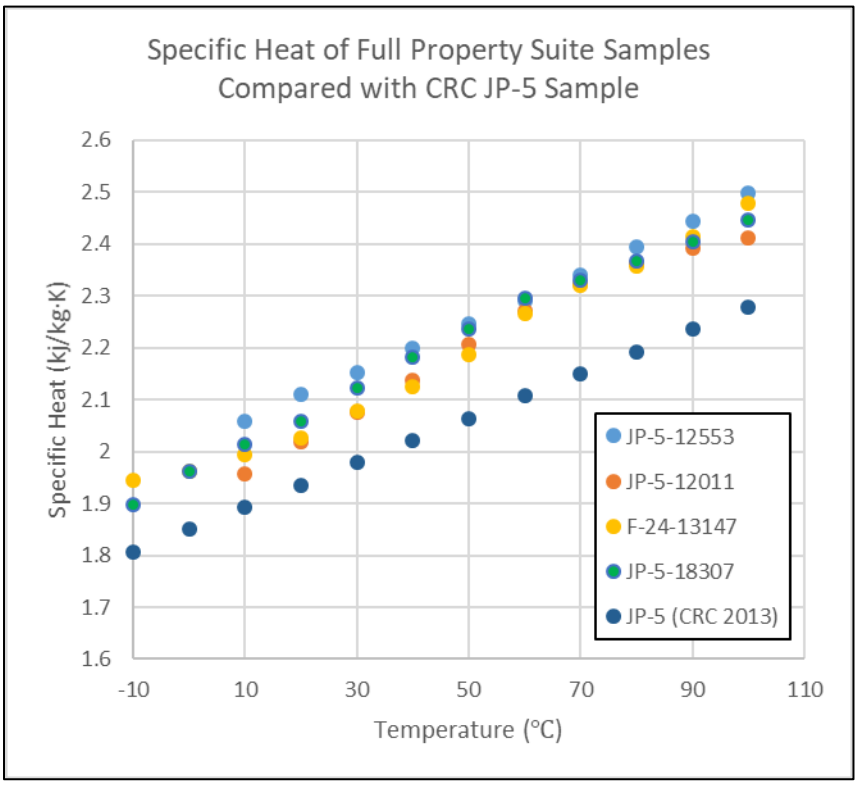

(c) Specific heat vs. temperature

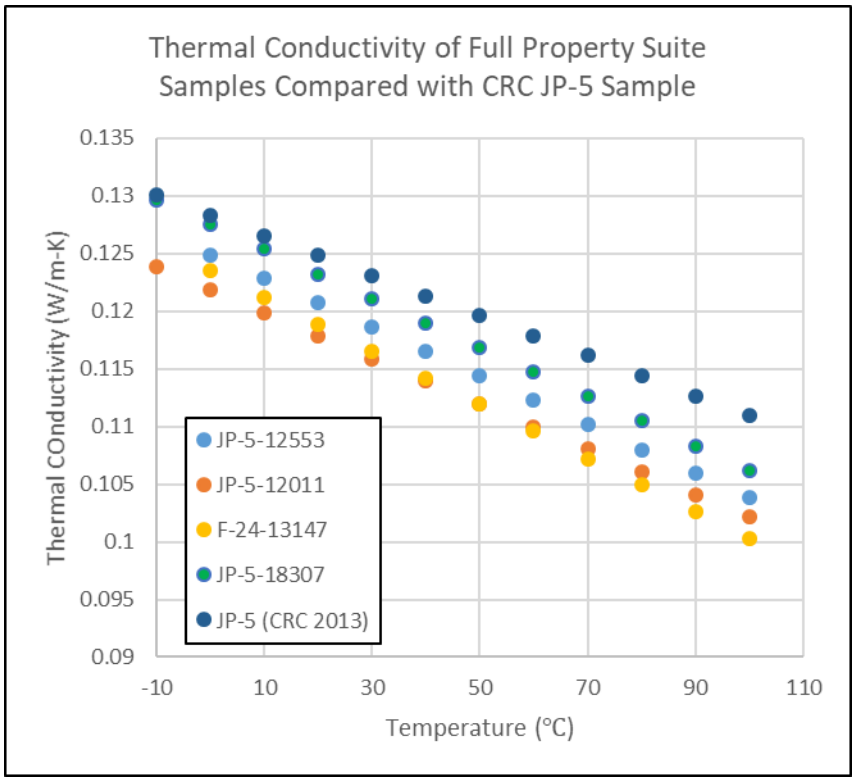

(d) Thermal conductivity vs. temperature

Figure 5: Density (a), viscosity (b), specific heat (c), and thermal conductivity (d) results of the samples which underwent the full suite of property testing along with the assumed central tendency of JP-5 according to *[38]*

To support utilization of the approaches developed by Rokni et al., the detailed compositional information collected for all samples in the present study were used to calculate the parameters described by equations (6) – (8). The mixture averaged molecular weight ($\overline{MW}$) is calculated using all of the bins cited in **Table 3** ($n = 115$). Similarly, the hydrogen number to carbon number ratio $\frac{HN}{CN}$ equation (8), helping to define the relative aromatic content of the mixture is calculated on the basis of the relative mole fraction (x_i) of equation (7) and the number of hydrogen and carbon atoms of the i^{th} molecule considered, $N_{H,i}$ and $C_{N,i}$ respectively.

$$\overline{MW} = \frac{100}{\sum_{i=1}^{n} wt\%_i / MW_i} = \frac{1}{\sum_{i=1}^{n} w_i / MW_i} \quad (6)$$

$$x_i = w_i \frac{\overline{MW}}{MW_i} \quad (7)$$

$$\frac{HN}{CN} = \frac{\sum_{i=1}^{n} x_i N_{H,i}}{\sum_{i=1}^{n} x_i C_{H,i}} \quad (8)$$

Using the expressions above and the data provided in **APPENDIX A: GCxGC COMPOSITION OF FULL PROPERTY SUITE SAMPLES**, the values in shown in **Table 4** were calculated.

Table 4: Calculated Compositional Parameters of Fuel Samples

	JP-5-12011	**JP-5-18307**	**JP-5-12553**	**F-24-13147**
$\overline{MW}$(g/mol)	167.85	161.44	162.96	144.02
HN/CN	1.902	1.927	1.938	1.982

Finally, the GC x GC data collected over the same hydrocarbon 115 bins for the 96 compositional samples was used to calculate $\overline{MW}$ and $\frac{HN}{CN}$ for each sample with results tabulated in **APPENDIX C: COMPOSITIONAL RANGE DATASET**. This data is presented in the histograms of **Figure 6** and **Figure 7** normal distributions developed using the mean and standard deviation of the data are overlaid.

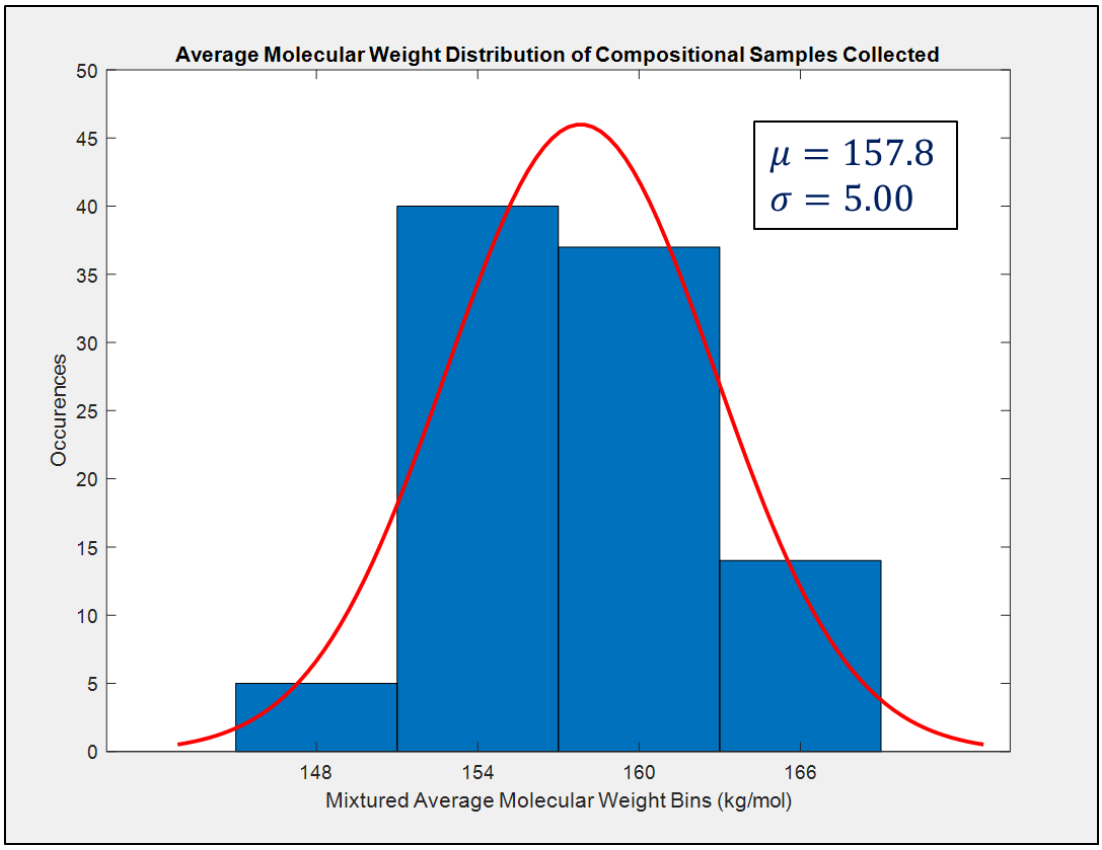

Figure 6: Mixture averaged molecular weight $\overline{MW}$ of the 96 compositional two dimensional gas chromatography samples collected. Assumed to be normally distributed.

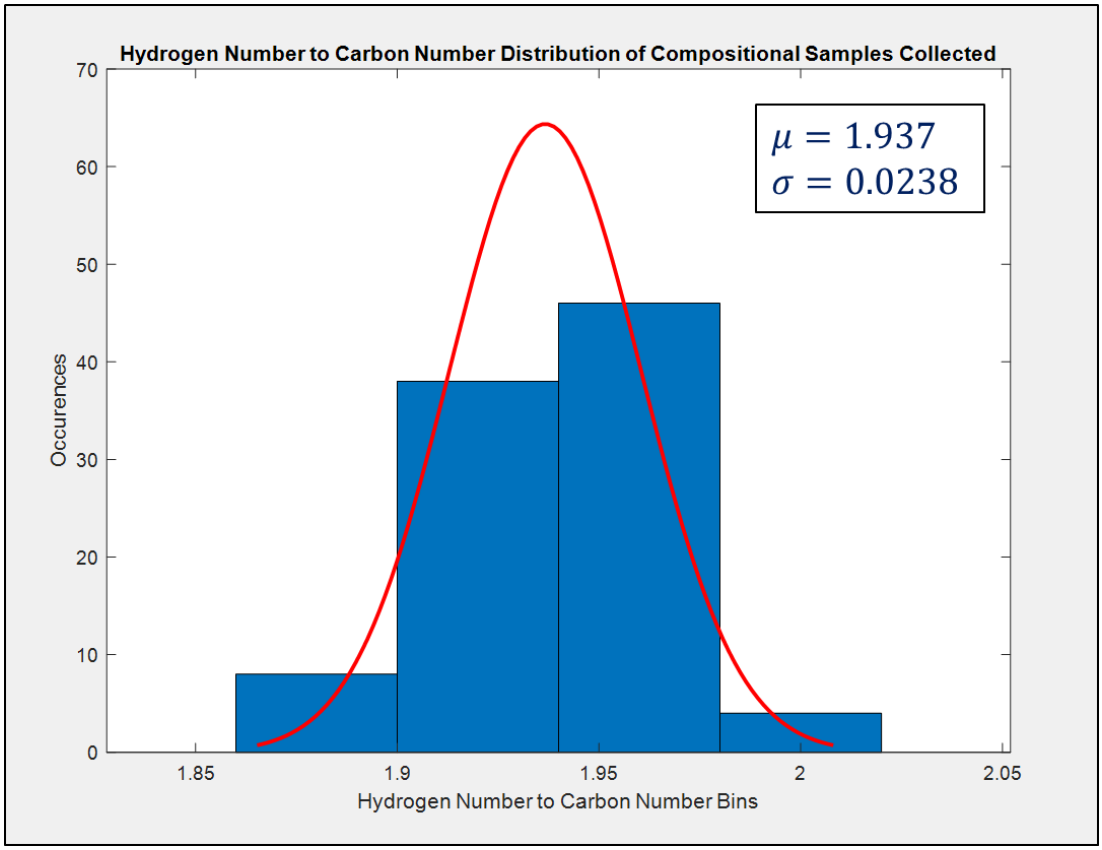

Figure 7: Hydrogen number to Carbon number ration $\frac{HN}{CN}$ of the 96 compositional two dimensional gas chromatography samples collected. Assumed to be normally distributed.

4. Entropy Scaling Guided Neural Network Thermal Conductivity Model

The results of the literature review in section **2** suggested opportunity to improve the model of Rokni et al. 2019 [57] given that the error of the models was typically significantly higher than the uncertainty of the test data for thermal conductivity of liquid hydrocarbons. The following sections describe the steps used to develop a novel predictive model which makes use of physical information about the system of interest to efficiently train and confidently deploy a hybrid entropy scaling guided artificial neural network for predicting the thermal conductivity of well-defined liquid hydrocarbon mixtures.

4.1 Pseudo Component Entropy Scaling

The overall approach to the entropy scaling portion of the present work is well described by Rokni et al. 2019 [81] and is roughly similar to the process described by **Figure 8**. The fundamental concept in the entropy scaling process is that the natural logarithm of reduced transport properties of fluids tends to scale with the reduced residual entropy as originally described by Rosenfeld in 1977 [48]. The following section summarizes steps used in the present work to calculate the reduced dimensionless residual entropy s^*.

The residual entropy s^{res} is defined as the difference between the entropy of the substance of interest and the entropy of an ideal gas at the same temperature and volume [52] or:

$$s^{res}(T, v) = s - s^{ig}(T, v) \tag{9}$$

$$s^{*} = s^{res}/(k\ m) \tag{10}$$

The reduced dimensionless residual entropy (s^{*}) of equation (10) can be found by dividing the residual entropy by the product of Boltzmann's constant (k) and the number of segments per chain (m), shown in equation (11) for the present application. s^{*} can be directly calculated using the PC-SAFT equation of state (EoS) developed by Gross and Sadowski 2001 [82]. For the present work, the PC-SAFT EoS of [82] with correction described in [83] was employed using a Newton-Raphson iterative scheme with packing fraction as a the independent variable and pressure as the dependent variable and using a forward difference scheme to calculate the derivatives used to determine subsequent guess values. In the context of a mixture of more than one hundred hydrocarbon types, such as aviation turbine fuel, the input parameters of the PC-SAFT equation of state relevant to the fluid composition may be calculated using the pseudo component technique developed by Rokni et al. [81] where the mixture is represented as a homogenous substance of a single chain type hydrocarbon

molecule with $m_{pseudo-comp.}$ segments per chain, segment diameter $\sigma_{pseudo-comp.}$, and potential well depth $(\varepsilon/k)_{pseudo-comp.}$ (equations 11-19).

$$m_{pseudo-comp.} = (1-Z)m_{n-alkane} + Zm_{PNA} \quad (11)$$

$$m_{n-alkane} = 0.0325\,\overline{MW} + 0.2463 \quad (12)$$
$$m_{PNA} = 0.0231\,\overline{MW} + 0.7392 \quad (13)$$

$$(m\sigma)_{pseudo-comp.} = (1-Z)(m\sigma)_{n-alkane} + Z(m\sigma)_{PNA} \quad (14)$$

$$(m\sigma)_{n-alkane} = 0.1265\,\overline{MW} + 0.7564 \quad (15)$$
$$(m\sigma)_{PNA} = 0.0874\,\overline{MW} + 2.6366 \quad (16)$$

$$(\varepsilon/k)_{pseudo-comp.} = (1-Z)(\varepsilon/k)_{n-alkane} + Z(\varepsilon/k)_{PNA} \quad (17)$$

$$(\varepsilon/k)_{n-alkane} = e^{(5.4762-1.3302/\overline{MW})} \quad (18)$$
$$(\varepsilon/k)_{PNA} = e^{(5.8137-15.5549/\overline{MW})} \quad (19)$$

Each of these pseudo component parameters is calculated by scaling between the extreme behaviors of the n-alkane and poly-nucleic-aromatic (PNA) bounds by utilizing the average molecular weight $(\overline{MW})$ of the hydrocarbon types and their respective concentrations, the degree of unsaturation (DoU) of the mixture, and the subsequent averaging parameter Z which provides a measure of the aromatic versus alkane content of the substance [81].

$$Z = \begin{cases} \frac{DoU_{pseudo-comp.}}{DoU_{PNA}}, & \overline{MW} < 178\ g/mol \\ \frac{DoU_{pseudo-comp.}}{10}, & \overline{MW} \geq 178\ g/mol \end{cases} \quad (20)$$

$$CN = \frac{\overline{MW}}{120.01 + 1.01(HN/CN)_{pseudo-comp.}} \quad (21)$$

$$DoU_{pseudo-comp.} = \frac{1}{2}(2 \times CN + 2 - HN) \quad (22)$$

$$DoU_{PNA} = 0.05993\overline{MW} - 0.68158 \quad (23)$$

After using these compositional parameters as inputs to the PC-SAFT EoS to calculate s^*, a standard entropy scaling model would then calculate the transport property of interest by utilizing relationships such as those shown in equations (24-25)

$$\ln(\lambda^*) = \ln\left(\frac{\lambda}{\lambda_{ref}}\right) = f(s^*, composition) \quad (24)$$

$$\lambda_{ref} = \frac{5}{16}\frac{\sqrt{\frac{\overline{MW}k_bT}{N_A\pi\, m_{pseudo-comp.}}}}{\Omega^{(2,2)*}\left(\sigma_{pseudo-comp.}\right)^2} \quad (25)$$

As prescribed by Rokni et al., the present study utilized the Chapman-Enskog relationship shown in equation (25) to calculate the reference thermal conductivity (λ_{ref}), with collision integral ($\Omega^{(2,2)*}$) calculated using the method described by [84]. As pointed out by [47], [81], [85], and [86] one of the most critical parts of the entropy scaling process involves definition of the function $f(s^*, composition)$ on the right hand side of equation (24), which enables quantitative description of the relationship between s^* and a transport property of interest and which varies based on substance [47]. However, unlike authors such as [47], [81], [85], and [86] who assumed the behavior of $f(s^*, composition)$ to follow a polynomial relationship with s^* as the independent variable and the coefficients of the polynomial to be empirically derived, the present study attempted to describe this relationship from a perspective of complete ignorance. That is, by recognizing that 1) the mechanisms responsible for distinguishing the functions $f(s^*, composition)$ for individual substances or mixtures (particularly as the number of constituents becomes large) are not well understood or are impractical to model and 2) that existing models tend to produce error that is an order of magnitude larger than the uncertainty of the associated test data [57], one is able to step back and consider supplanting the existing models without assuming the nature of their behavior. As such and since experimental data is available, the process of quantifying $f(s^*, composition)$ is well suited to techniques which are able to model non-linear relationships of variables where no underlying behavior is assumed, such as those covered by the broad class of approaches termed: machine learning. For the present study, this piece of the pseudo

component entropy scaling process was therefore accomplished by utilizing a machine learning method as described in the following sections.

4.2 Hybrid Artificial Neural Network

As stated previously, determining an appropriate function to satisfy the relationship of equation (24) with function inputs of s^* and compositional information of the substance of interest is a problem well posed for machine learning. Given a relatively long history and ease of implementation, a logical choice of machine learning techniques is the Artificial Neural Network. Neural networks can and have been used to model relationships between many types of complex behavior [87] as detailed further in the literature review.

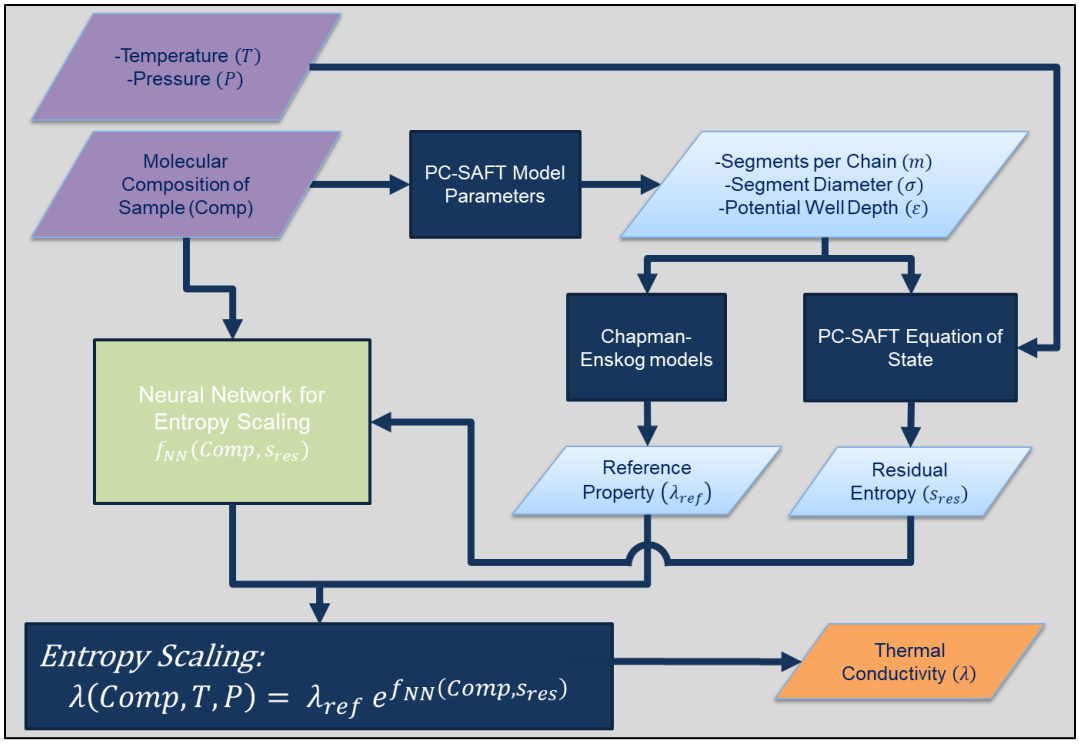

Figure 8: Entropy Scaling Guided Artificial Neural Network Thermal Conductivity Model Architecture

The following sections describe how the present work approached a novel implementation of a neural network in building a predictive model of aviation turbine fuel thermal conductivity (λ) where as shown in **Figure 8**, the network serves as an intermediate step between compositional description of a fuel and the predicted thermal conductivity. This is in contrast to typical machine learning approaches for fluid property prediction such as [59], [61]- [70], [73] , where primarily "black box" machine learning methods were employed and physical information that could have been modeled up or downstream of the machine learning models to reduce the computational load of machine learning was not utilized.

Along with the goal of creating a model that consistently predicts λ with error on the order of the uncertainty in test data, a desire to describe a repeatable process for selection of neural network hyper parameters drove a careful treatment of network sizing and length of training which are further described below.

4.2.1 Network Architecture

The neural network used to calculate $\ln(\lambda^*)$ is a fully connected feedforward neural network with three layers: input, hidden, and output. There are three nodes in the input layer $(s^*, \overline{MW}, HN/CN)$, 5 nodes in the hidden layer, and one single node in the output layer providing $\ln(\lambda^*)$. Each node of the hidden layer utilizes a Sigmoid activation function $S(x)$ given by:

$$S(x) = \frac{1}{1 + e^{-x}} \tag{26}$$

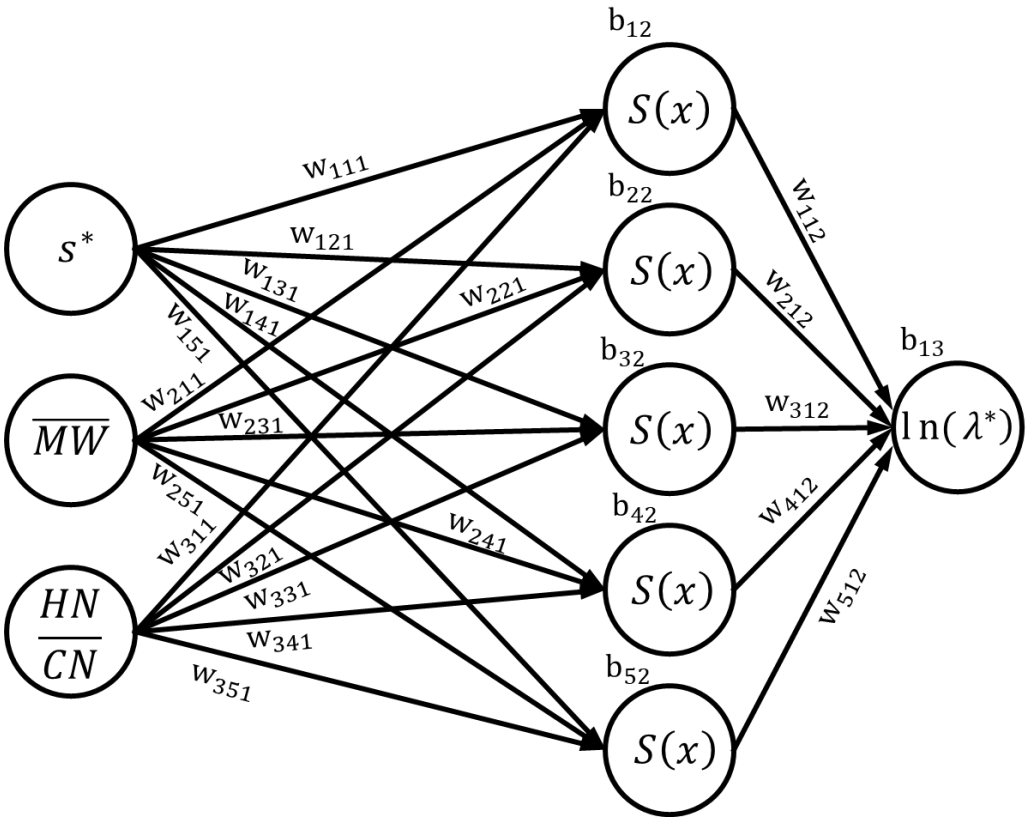

Figure 9: Neural Network Structure for Thermal Conductivity

The number of nodes in the hidden layer was determined utilizing a variation on the basic approach described by Faundez et al. [73] and is detailed in section 4.2.2.3. As is standard for this type of network, the input (x_{jk}) to each node j and layer k after the input layer is the sum of the weighted outputs $(y_{i(k-1)})$from all of the nodes of the previous layer offset by the bias of that node as shown in equation (27).

$$x_{jk} = \sum_{i=1}^{n} w_{ij(k-1)} y_{i(k-1)} + b_{jk} \tag{27}$$

where $x_{i(k-1)}$ is the output of node i of the previous layer $(k-1)$, $w_{ij(k-1)}$ is the weight applied to each x (there is a unique set for each node j of layer k), b_{jk} is the bias for the node of interest, and n is equal to the number of nodes in layer $k-1$. Applying this to a Sigmoid activation function gives the output of each node within the hidden layer as shown in equation (28).

$$y_{jk} = \frac{1}{1 + e^{-(\sum_{i=1}^{n} w_{ij(k-1)} y_{i(k-1)} + b_{jk})}} \tag{28}$$

Given the type of network used, the number of nodes, and a (3, 5, 1) architecture, the number if independent parameters in the network is therefore 26, with unique weights applied to each input variable before being passed to any of the nodes in the hidden layer (15), unique biases for each node in the hidden layer (5), unique weights applied to the output of each node in the hidden layer (5), and a single bias on the output node (1).

4.2.2 Training

To make any Artificial Neural Network (ANN) useful, the weights w_{ijk} and biases b_{jk} need to be adjusted during a training procedure until the outputs of the

network provide an acceptable level of error when compared to a data set with known inputs and outputs. The sections which immediately follow outline a repeatable process which can be employed to establish these weights and biases and to determine the number of neurons for a single hidden layer neural network.

4.2.2.1 Algorithm

For the present study, a supervised learning procedure was utilized where a specific set of training inputs was passed to the network and the outputs of the network were then quantitatively compared against the corresponding training data outputs by calculating the mean squared error $\left(MSE = \frac{1}{n}\sum_{i=1}^{n}\left(y_{i,ANN} - y_{i,train}\right)^2\right)$. When each data point (a given hydrocarbon or hydrocarbon mixture at a given temperature and pressure with a corresponding thermal conductivity) had been passed to the network only one time in random order and the MSE calculated, a milestone referred to as an $epoch$ was met [88]. To facilitate a simple investigation into hyper-parameter selection, training was stopped once a pre-determined number of epochs was reached, as detailed in section 4.2.2.3. This is in contrast to common approaches within the literature where either an acceptable level of error is achieved, an acceptable change in error between epochs is observed, performance on a validation dataset (a set not used to directly adjust weights and biases) consecutively decreases for a prescribed number of iterations, or a maximum clock time interval has passed [89].

After randomly assigning initial values between -1 and 1, weights and biases were updated after each epoch using the Levenberg-Marquardt backpropagation algorithm as described in [89] and briefly outlined below. Equation (29) summarizes the critical information required for the process:

$$\Delta \mathbf{x}_k = -[\mathbf{J}^{\boldsymbol{T}}(\mathbf{x}_k)\mathbf{J}(\mathbf{x}_k) + \mu_k \mathbf{I}]^{-\mathbf{1}} \mathbf{J}^{\boldsymbol{T}}(\mathbf{x}_k)\mathbf{v}(\mathbf{x}_k) \tag{29}$$

where $\Delta \mathbf{x}_k$ is the change to the vector of weights and biases of the neural network being trained $\mathbf{x}_k$ for the $\boldsymbol{k}^{th}$ epoch, $\mathbf{J}(\mathbf{x}_k)$ is the Jacobian matrix comprised of partial derivatives of neural network outputs with respect to weights and biases, μ_k is a scalar which is adjusted as required during each iteration to ensure a decrease in global output error, $\mathbf{I}$ is the identity matrix, $\mathbf{v}(\mathbf{x}_k)$ is a vector of errors. For the present work, μ_k was initialized at 0.001, and increased or decreased an order of magnitude as required based of the performance at the current iteration.

As described previously, the inputs to the ANN used from this training data were the $\overline{MW}$, HN/CN, and s^*. To calculate the MSE and update weights and biases after each epoch, the outputs of the network were evaluated against their respective $\ln(\lambda^*)$ values from the training set, which was calculated for each data point from the values for λ found in the literature by utilizing the Chapman-Enskog relationship described by Rokni et al. [81]. This step enables the utilization of physical knowledge downstream of the ANN and was performed prior to the training procedure in the present study, which allowed for efficient computation of derivatives

used in the Levenberg-Marquardt algorithm. However, it should be strongly noted, that utilization of physical information downstream of a neural network does not preclude this efficient implementation, particularly if analytical derivatives are employed when training using a backpropagation scheme.

4.2.2.2 Training Data

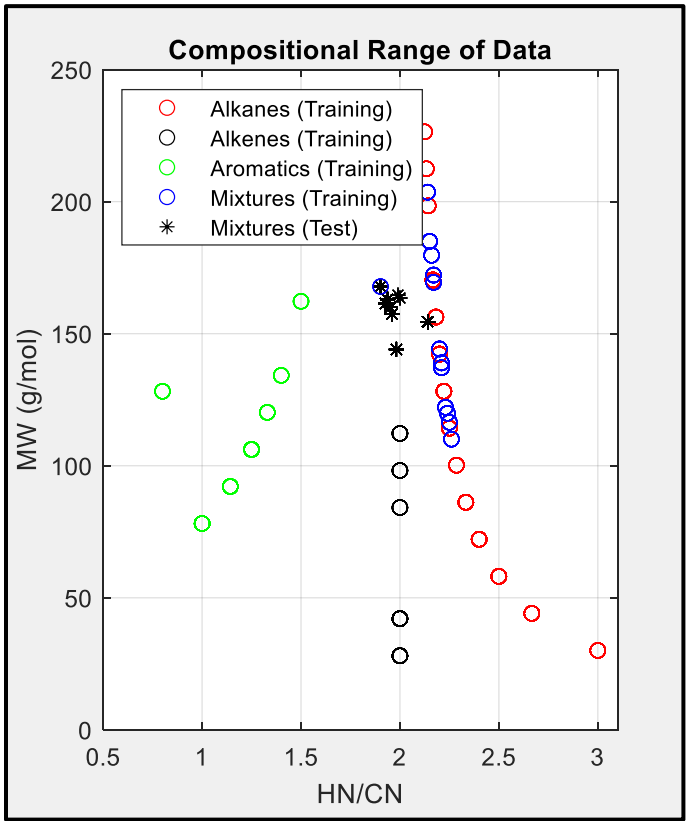

Figure 10: Compositional Range of Thermal Conductivity Training and Test Data

The training data used for the network was comprised of three broad categories of hydrocarbon liquids: pure hydrocarbons, two or three component hydrocarbon mixtures, and a jet fuel where thermal conductivities were measured over a range of pressures and temperatures with a total of 528 data points, as shown in **Table 5**.

Table 5: Training Data for Thermal Conductivity Model

Hydrocarbon / Mixture	MW or $\overline{MW}$ (g/mol)	HN/CN	Data Points	Min. Temp. (°C)	Max. Temp. (°C)	Min. Press. (MPa)	Max. Press. (MPa)	Ref.
Methane	16.04	4.000	10	-180	-130	0.1	10	[90]
Ethane	30.07	3.000	17	-160	30	0.1	10	[90]
Propane	44.1	2.667	23	-140	60	0.1	10	[90]
Butane	58.12	2.500	30	-130	90	0.1	10	[91]
Pentane	72.15	2.400	30	-120	80	0.1	10	[90]
Hexane	86.18	2.333	30	-90	110	0.1	10	[90]
Heptane	100.21	2.286	29	-80	100	0.1	10	[90]
Octane	114.23	2.250	30	-50	150	0.1	10	[90]
Nonane	128.2	2.222	32	-50	150	0.1	10	[90]
Decane	142.29	2.200	30	-20	160	0.1	10	[90]
Undecane	156.31	2.182	8	19.3	90.7	0.1013	0.1013	[92]
Dodecane	170.33	2.167	33	0	200	0.1	10	[90]
Tetradecane	198.39	2.143	5	11.1	89.5	0.1013	0.1013	[92]
Pentadecane	212.42	2.133	4	12.9	89.4	0.1013	0.1013	[92]
Hexadecane	226.41	2.125	4	22.6	89.4	0.1013	0.1013	[92]
Ethene	28.05	2.000	16	-145	-5	0.1	10	[90]
Propene	42.08	2.000	27	-150	70	0.1	10	[90]
Hexene	84.16	2.000	5	4.86	50.25	0.1013	0.1013	[93]
Heptene	98.19	2.000	7	5.5	58.64	0.1013	0.1013	[93]
Octene	112.24	2.000	10	5.74	60.1	0.1013	0.1013	[93]
Benzene	78.114	1.000	21	20	180	0.098	120	[94]
Toluene	92.14	1.143	14	-43.15	86.85	0.1	0.1	[95]
1-2-4-5 Tetramethyl-benzene	134.22	1.400	3	86.85	336.85	0.101	0.101	[96]
Ethylbenzene	106.17	1.250	14	5.42	60	0.1013	0.1013	[93]
Propylbenzene	120.19	1.330	5	11.15	47.85	0.1013	0.1013	[93]

Hexamethyl-benzene	162.27	1.500	3	86.85	206.85	0.101	0.101	[96]
Naphthalene	128.17	0.800	3	106.85	156.85	0.101	0.101	[96]
Binary and Ternary Mixtures of Alkanes	114.2-208.9	2.14-2.26	72	14.8	72.3	0.1013	0.1013	[92]
JP-5-12011	167.85	1.835	13	-20	100	.1013	.1013	present study

To evaluate the ability of the ANN to predict the values other than the training data, a set of test data was used which was composed of jet and rocket fuels which is summarized in **Table 6**. All training data was normalized prior to being employed in network training.

Table 6: Test Data for Thermal Conductivity Model

Hydrocarbon / Mixture	$\overline{MW}$ (g/mol)	HN/CN	Data Points	Min. Temp. (°C)	Max. Temp. (°C)	Min. Press. (MPa)	Max. Press. (MPa)	Ref.
F-24-13147	144.02	1.926	11	0	100	0.1013	0.1013	present study
JP-5-18307	161.45	1.844	13	-20	100	0.1013	0.1013	present study
JP-5-12553	162.96	1.873	13	-20	100	0.1013	0.1013	present study
JP-8-3773	160	1.950	30	29.2	276.9	0.781	60.41	[34]
S-8	154.5	2.140	91	30.07	230.6	0.095	69.449	[34]
Jet A-4658	157.5	1.960	66	29.22	228.84	0.175	40.506	[34]
RP-1 Surrogate	163.5	2.000	1	15.55	15.55	0.1013	0.1013	[36]
RP-2 Surrogate	164.6	1.990	1	15.55	15.55	0.1013	0.1013	[36]

4.2.2.3 Hidden Layer Sizing

Determining the number nodes in the input and output layers for this type of effort is trivial once the desired independent and dependent variable(s) are identified. In the case of the present study, knowing that $\ln(\lambda^*) = f(\overline{MW}, HN/CN, s^*)$ leads to three input nodes and one output node.

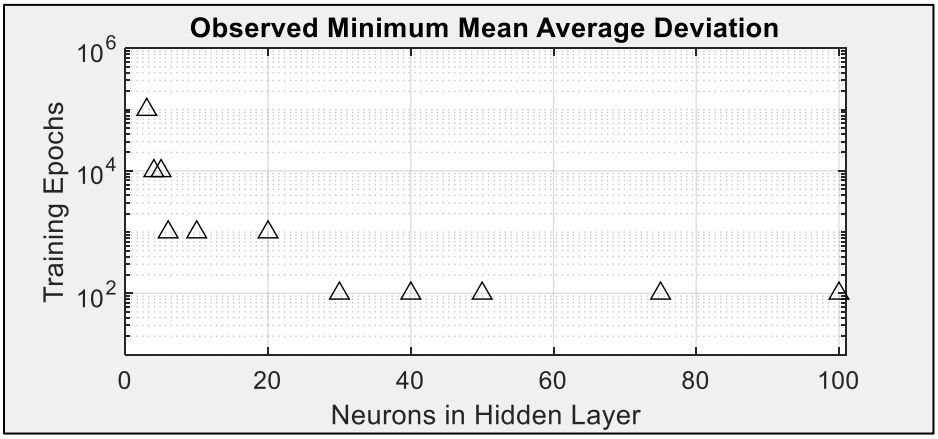

Figure 11: Observed Minimum Mean Average Deviation between model and Test set for thermal conductivity. 50 samples were recorded at each grid point with mean and standard deviation recorded for each location.

Unlike the simple exercise of determining the size of input and output layers, Faúndez et al. [73] point out that determining the number of nodes used in the hidden layer does not have a singular agreed upon approach identified within the literature. For the present study, the approach utilized by Faúndez et al. was expanded into a

grid search method where the mean and standard deviation of the average deviation between the model and the test set over 50 iterations was recorded versus the number of nodes in the hidden layer and number of epochs per training set. The set of hidden nodes investigated was 2, 3, 4, 5, 10, 20, 30, 40, 50, 75, and 100 while the set of epochs was $10, 10^2, 10^3, 10^4, 10^5$, and 10^6. The observed minimum mean of the average deviation for each number of hidden layer neurons considered is plotted in **Figure 11** where a stepwise Pareto front is observed. Additionally, it is worth noting that the behavior described in [73] was observed, where the mean of the average error started high, passed through a minimum, and then increased again when increasing the number of neurons from low to high and holding the number of epochs constant. This behavior also occurred when holding the number of neurons constant and increasing the number of epochs used in training.

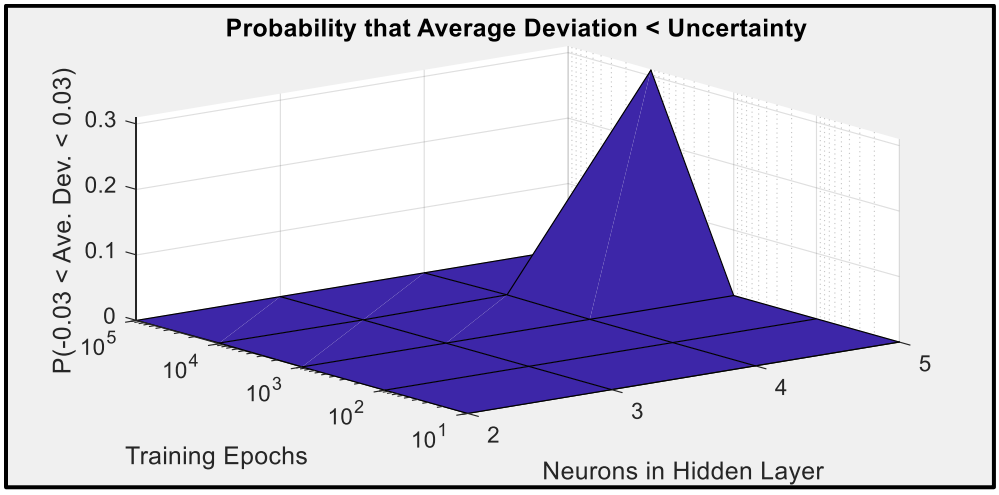

Figure 12: Probability of Model Configuration Containing Average Deviation Less than the Uncertainty of Thermal Conductivity Test Measurement

To avoid over-fitting, the set of possible network configurations observed on the Pareto front was narrowed down by following the guidance of [73] which lead to a limit for the number of neurons in a single hidden layer of between 70% of the number in network inputs and less than double the number of network inputs. For the present effort, this meant only considering the range of 2-5 neurons in the hidden layer.

At this point, a statistical approach was employed to select the final combination of neurons and training epochs. Assuming the means of the average deviation to be normally distributed, the proportion of the calculated distribution that falls within the uncertainty bands for the test measurement at each remaining grid point was calculated, using the typical uncertainty of 3% for thermal conductivity of liquids in the temperature and pressure ranges of interest. Results shown in **Figure 12** show that a clear maximum exists when using 5 hidden layer neurons and 10^5 training epochs.

With the network hyper-parameters identified, the training procedure was executed to completion multiple times with a final network being selected when the average deviation for test data was lower than 3%. The resulting weights and biases of the present study are given below in **Table 7**.

Table 7: Weights and biases for hybrid entropy scaling guided neural network model of thermal conductivity

	$\overline{MW}$ $(i=1)$	$\frac{HN}{CN}$ $(i=2)$	s^* $(i=3)$				
Layer 1 to 2				Layer 2 to 3		Biases	
$w_{i,1,1}$	-8.4513	-1.212	-3.1953	$w_{1,1,2}$	-0.1102	b_{12}	-4.5078
$w_{i,2,1}$	0.0638	0.2749	0.0246	$w_{2,1,2}$	-162.94	b_{22}	-2.625
$w_{i,3,1}$	7.8559	0.0263	0.3445	$w_{3,1,2}$	-137.069	b_{32}	-1.5293
$w_{i,4,1}$	7.93	0.0256	0.4095	$w_{4,1,2}$	136.8661	b_{42}	-1.4924
$w_{i,5,1}$	-0.6084	-0.4179	-3.9505	$w_{5,1,2}$	155.831	b_{52}	-6.8264
						b_{13}	-5.6351

4.3 Results

To evaluate the performance of the resulting model the average deviation, the absolute average deviation, and maximum deviation were calculated against the test data set of **Table 6**. **Figure 13** provides a quantitative comparison of the results against the Rokni et al. model applied on the same test set. Not only is the performance significantly improved, the average deviation (1%) and absolute average deviation (2.5%) are clearly both lower than the target of 3%. A qualitative view of the performance is given in the plots of **Figure 14 (a-b)** and **Figure 15** showing results for the full property suite samples and the entire training and test set respectively.

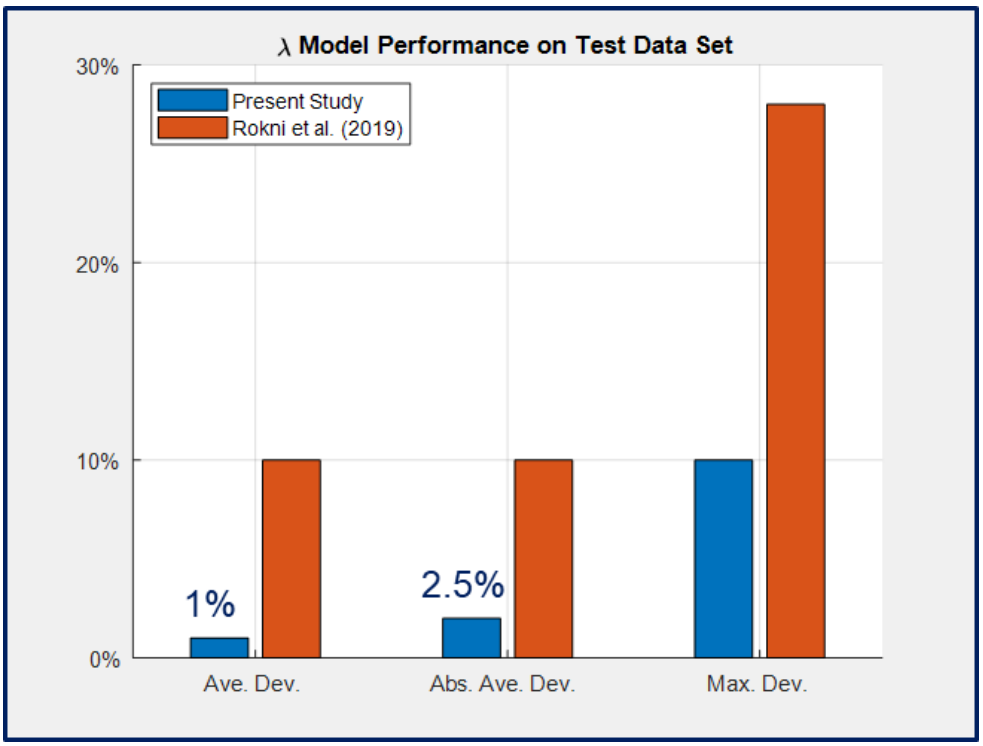

Figure 13: Thermal Conductivity Hybrid Model Performance

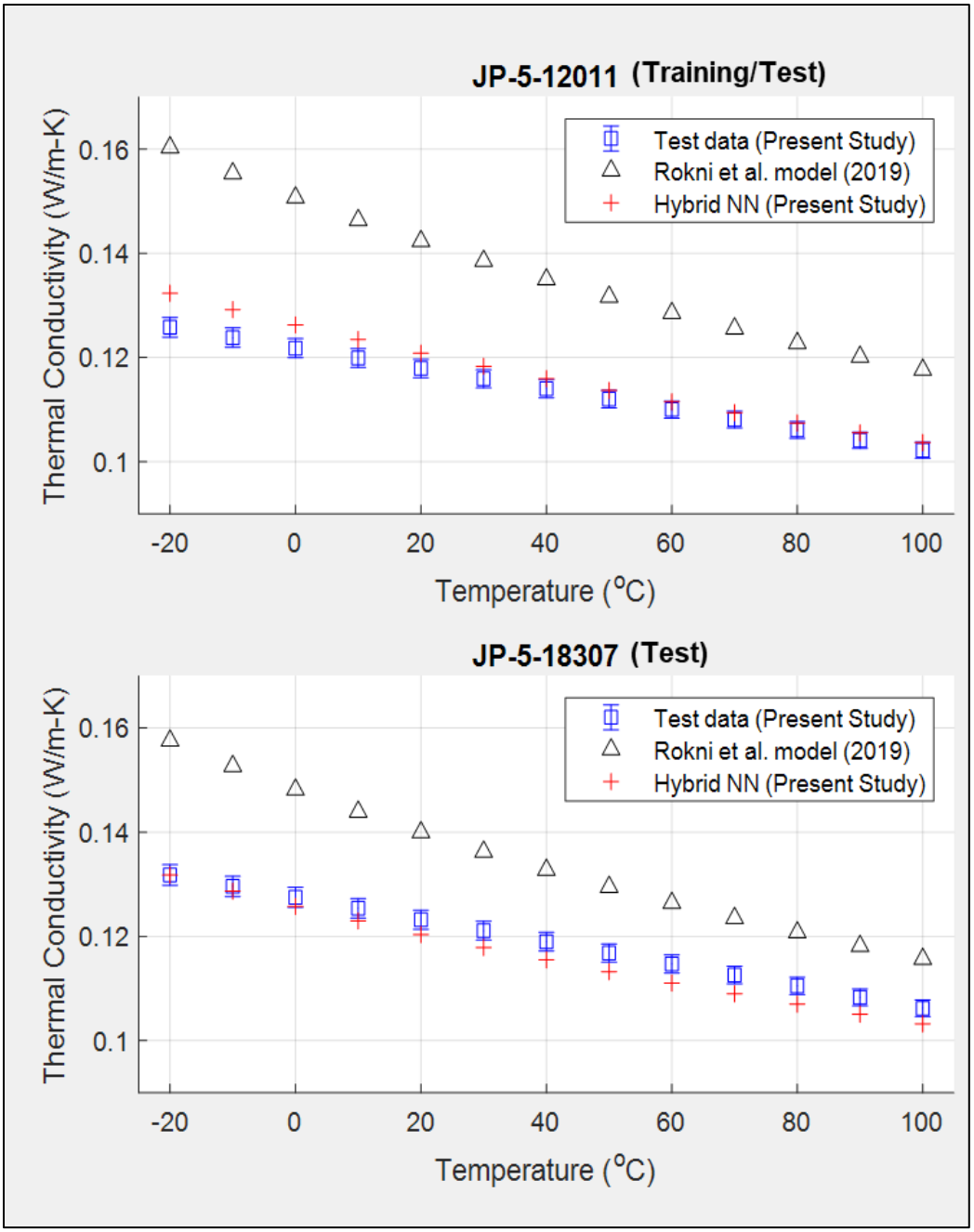

(a) Thermal Conductivity vs. temperature of JP-5 12011 and 18307

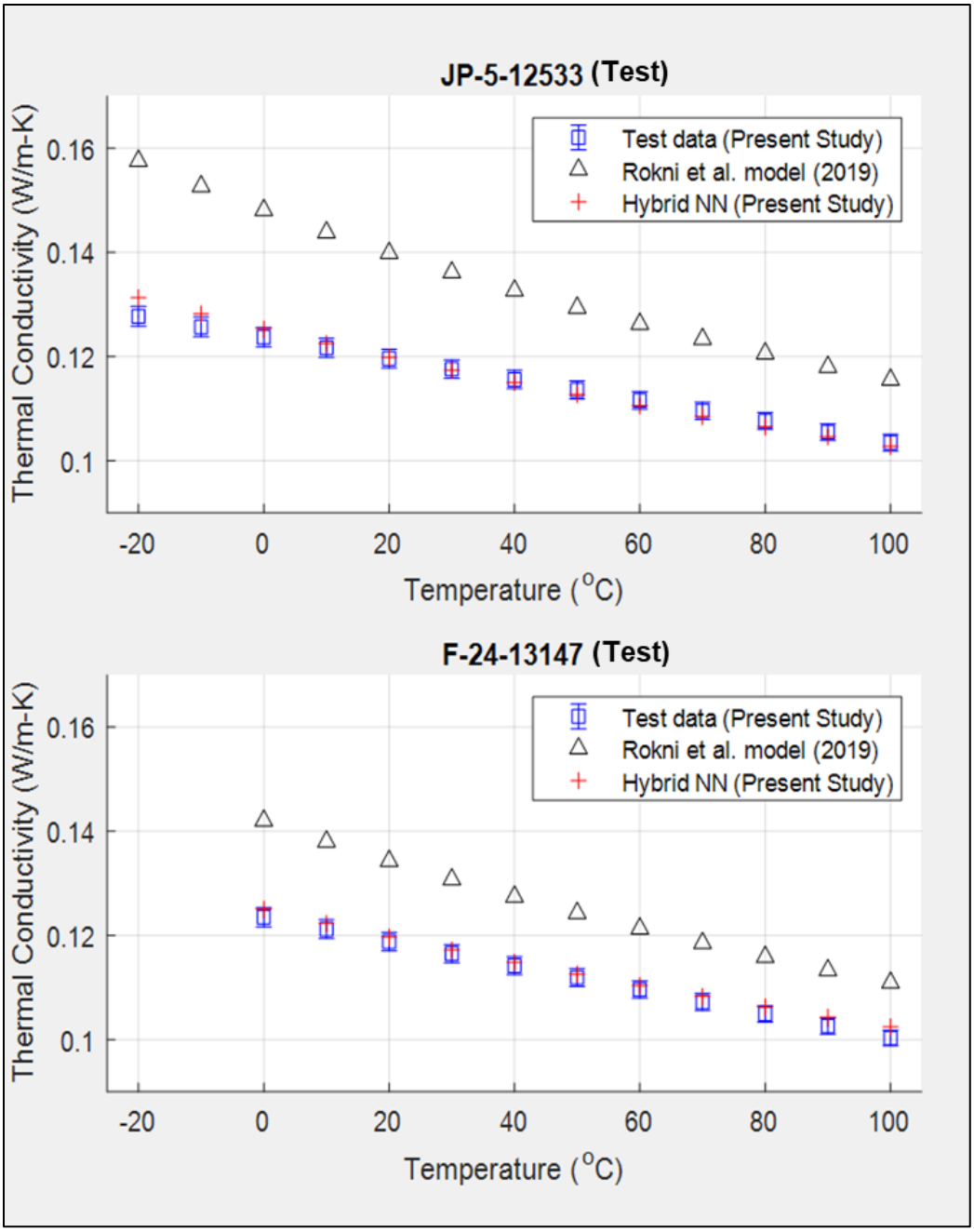

(b) Thermal Conductivity vs. temperature of JP-5 12533 and F-24 13147

Figure 14: Qualitative performance of hybrid model on full property suite samples

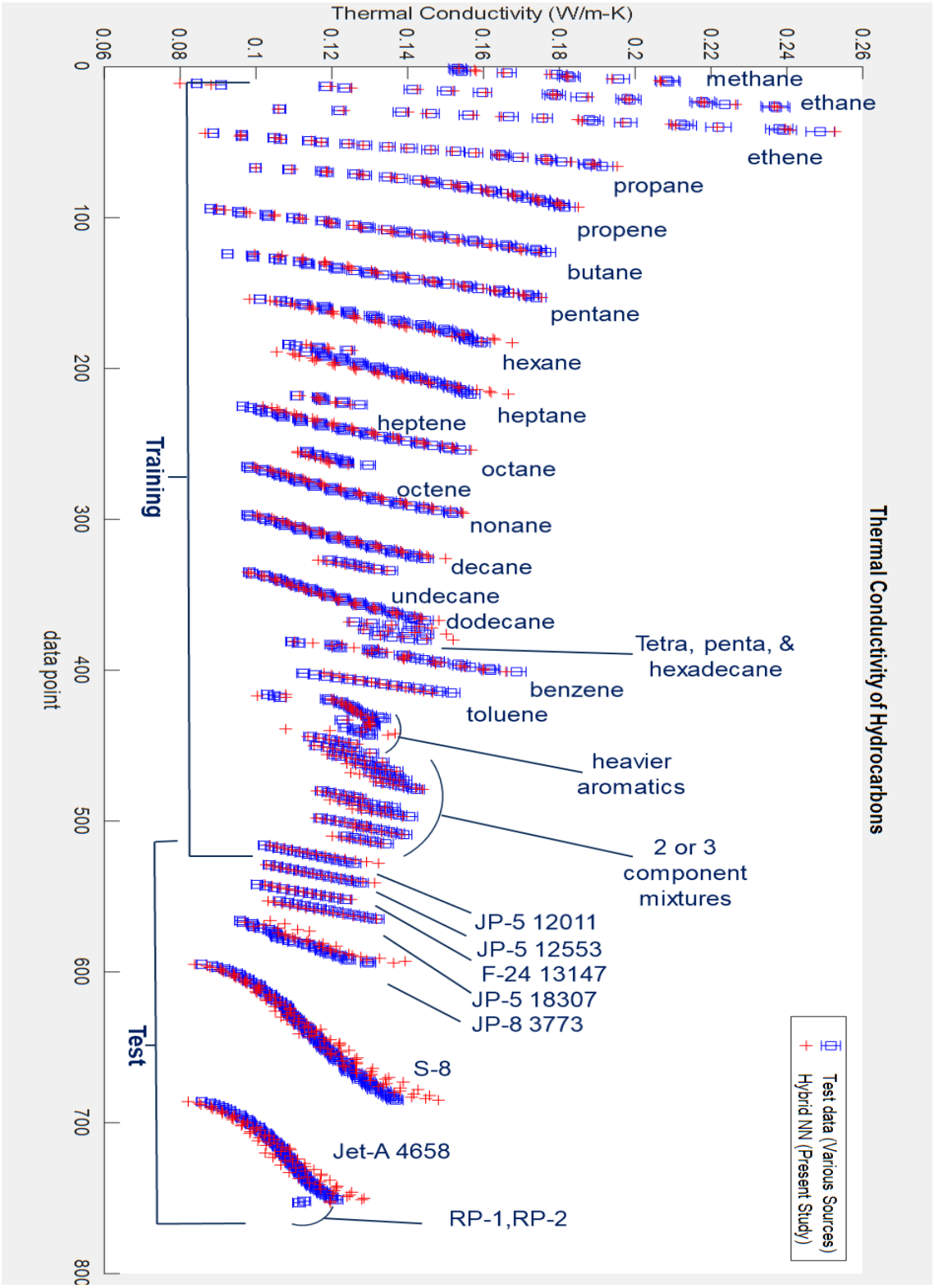

Figure 15: Qualitative view of hybrid model performance across training and test data

4.4 Stability

As a final consideration to examine the performance of the hybrid thermal conductivity model, the artificial neural network employed in the intermediate step of the model connecting the reduced residual entropy with the thermal conductivity was used to generate surfaces which provided the output $\ln(\lambda^*)$ as a function of the network input variables s^*, $\overline{MW}$, and $\frac{HN}{CN}$. The ranges of input variables used more than cover the compositional range of hydrocarbons used to develop the model (refer to **Figure 10**) as well as the reduced residual entropy values observed during training. The mesh size used to generate each surface is 40 by 40 regardless of the input parameters.

The observed surfaces provide insight into the non-linearity of the behavior yet are also well behaved over the regions of interest to provide confidence in generalization to other hydrocarbon mixtures, particularly those which fall within the bounds of the training set of pure components. The extreme behavior shown in the lower right plot of **Figure *16***, where a sharp increase in $\ln(\lambda^*)$ results within increasing $\frac{HN}{CN}$, is explained by that region not being physical for formation of stable hydrocarbon molecules. Given the quantitative and qualitative views of the model performance, this model should be sufficient to estimate the bounds of thermal conductivity using the compositional dataset, which will be presented in section **7.**

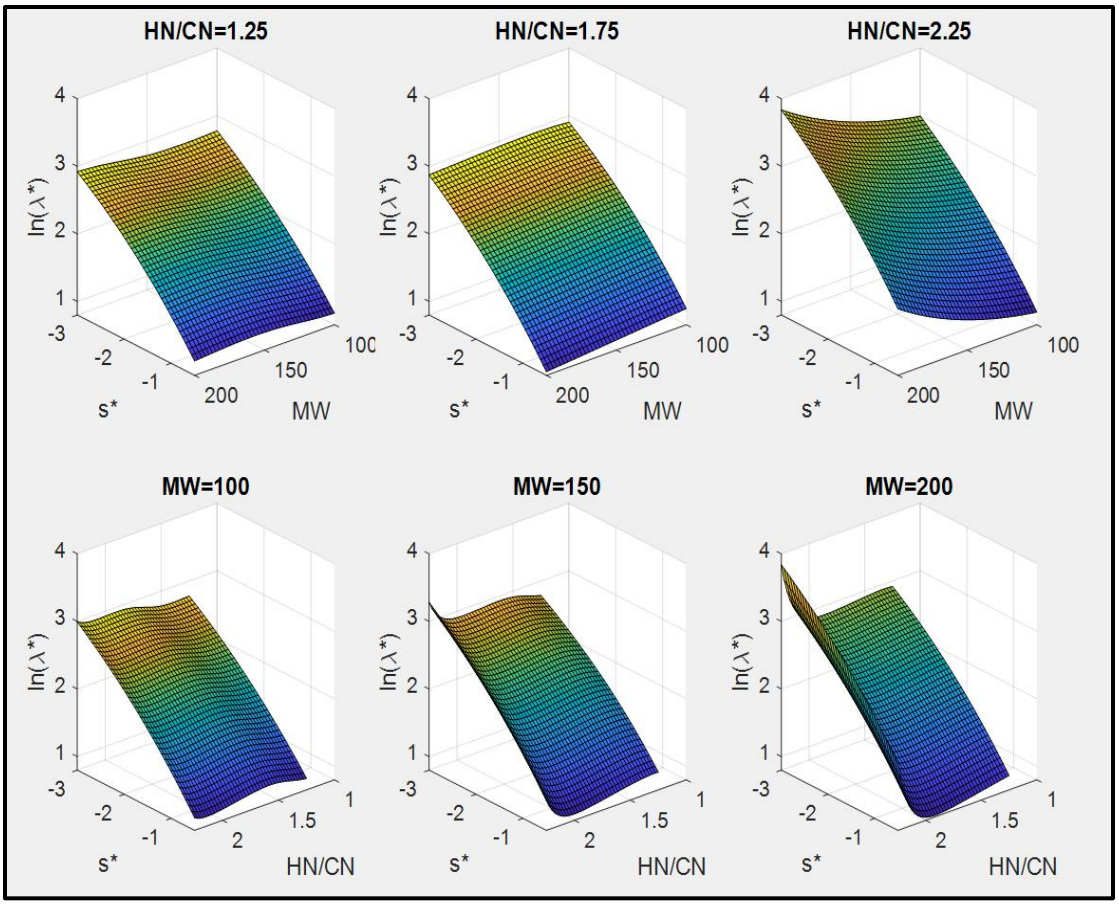

Figure 16: Artificial neural network for thermal conductivity stability assessment

5. Entropy Scaling Guided Neural Network Viscosity Model

As was the case for the thermal conductivity of aviation turbine fuel, the results of the literature review in section **2** suggested opportunity to improve the viscosity model of Rokni et al. 2019 [56] given that the error of the models was typically significantly higher than the uncertainty of the test data for viscosity of liquid hydrocarbons. The following sections describe the steps used to develop a novel predictive model which makes use of physical information about the system of interest to efficiently train and confidently deploy a hybrid entropy scaling guided artificial neural network for predicting the viscosity of well-defined liquid hydrocarbon mixtures. Overall, the approach is very similar to that used in the previous chapter and as such similar steps and arguments are presented.

5.1 Pseudo Component Entropy Scaling

The overall approach to the entropy scaling portion of the present work is well described by Rokni et al. 2019 [81] and is roughly similar to the process described by **Figure 17**. The fundamental concept in the entropy scaling process is that the natural logarithm of reduced transport properties of fluids tends to scale with the reduced residual entropy as originally described by Rosenfeld in 1977 [48]. The following section summarizes steps used in the present work to calculate the reduced dimensionless residual entropy s^* for the application in predicting viscosity. For the present work, the PC-SAFT EoS of [82] with correction described in [83] was employed using a Newton-Raphson iterative scheme with packing fraction as a the

independent variable and pressure as the dependent variable and using a forward difference scheme to calculate the derivatives used to determine subsequent guess values. As was done by in the thermal conductivity model, the complex composition of the fuel is represented as a homogenous substance of a single chain type hydrocarbon molecule with $m_{pseudo-comp.}$ segments per chain, segment diameter $\sigma_{pseudo-comp.}$, and potential well depth $(\varepsilon/k)_{pseudo-comp.}$ (equations 11-19). Just as in the thermal conductivity models, each of these pseudo component parameters is calculated by scaling between the extreme behaviors of the n-alkane and poly-nucleic-aromatic (PNA) bounds by utilizing the average molecular weight $(\overline{MW})$ of the hydrocarbon types and their respective concentrations, the degree of unsaturation (DoU) of the mixture, and the subsequent averaging parameter Z which provides a measure of the aromatic versus alkane content of the substance [81] (equations 20-23).

$$\ln(\eta^*) = \ln\left(\frac{\eta}{\eta_{ref}}\right) = f(s^*, composition) \tag{30}$$

$$\eta_{ref} = \frac{5}{16}\frac{\sqrt{\frac{\overline{MW}k_bT}{N_A\pi}}}{\Omega^{(2,2)*}\left(\sigma_{pseudo-comp.}\right)^2} \tag{31}$$

As prescribed by Rokni et al., the present study utilized the Chapman-Enskog relationship shown in equation (31) to calculate the reference viscosity (η_{ref}), with

collision integral ($\Omega^{(2,2)*}$) calculated using the method described by [84]. As discussed in the previous chapter, one the most critical parts of the entropy scaling process involves definition of the function $f(s^*, composition)$ on the right hand side of equation (2430), which enables quantitative description of the relationship between s^* and a transport property of interest and which varies based on substance [47]. For the present study, this piece of the pseudo component entropy scaling process was therefore accomplished by utilizing a machine learning method as described in the following sections.

5.2 Hybrid Artificial Neural Network

Determining an appropriate function to satisfy the relationship of equation (2430) with function inputs of s^* and compositional information of the substance of interest is a problem well posed for machine learning. Given a relatively long history and ease of implementation, a logical choice of machine learning techniques is the Artificial Neural Network. Neural networks can and have been used to model relationships between many types of complex behavior [87] as detailed further in the literature review.

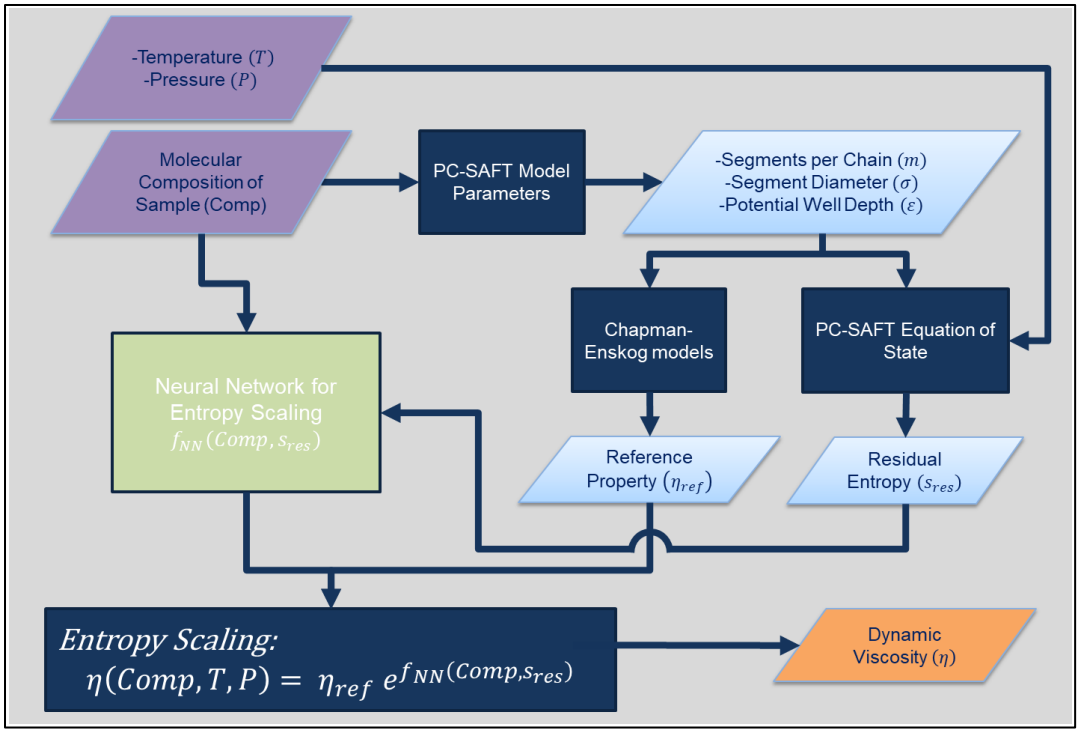

Figure 17: Entropy Scaling Guided Artificial Neural Network Viscosity Model Architecture

The following sections describe how the present work approached a novel implementation of a neural network in building a predictive model of aviation turbine fuel viscosity (η) where as shown in **Figure 17**, the network serves as an intermediate step between compositional description of a fuel and the predicted viscosity.

Along with the goal of creating a model that consistently predicts η with error on the order of the uncertainty in test data, a desire to describe a repeatable process for selection of neural network hyper parameters drove a careful treatment of network sizing and length of training which are further described below.

5.2.1 Network Architecture

The neural network used to calculate $\ln(\eta^*)$ is a fully connected feedforward neural network with three layers: input, hidden, and output. There are three nodes in the input layer $\left(\overline{MW}, \frac{HN}{CN}, s^*\right)$, 3 nodes in the hidden layer, and one single node in the output layer providing $\ln(\eta^*)$. Each node of the hidden layer utilizes a Sigmoid activation function $S(x)$ given by equation (26).

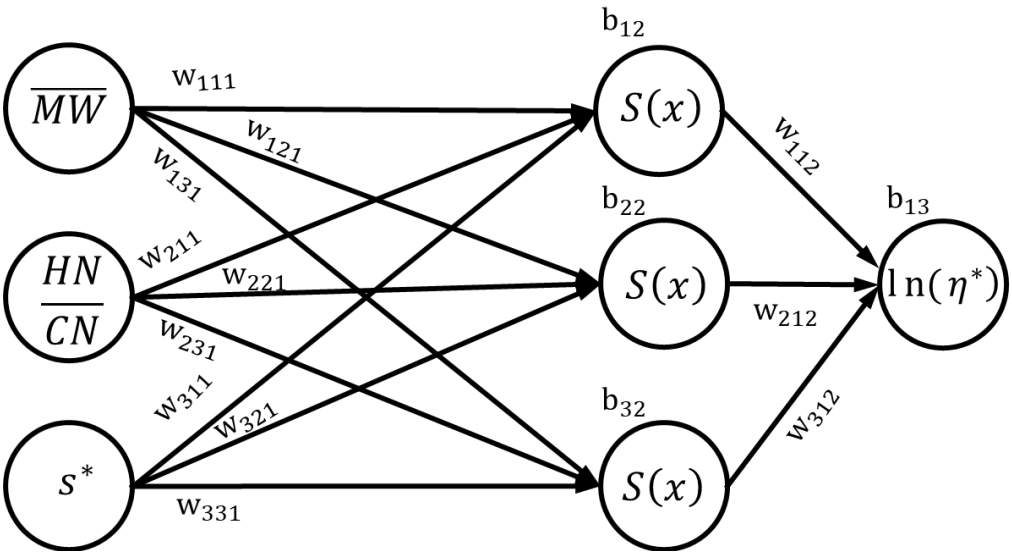

Figure 18: Neural Network Structure for Viscosity

The number of nodes in the hidden layer was determined utilizing a variation on the basic approach described by Faundez et al. [73] and is detailed in section **5.2.2.3**. As is standard for this type of network, the input (x_{jk}) to each node j and layer k after the input layer is the sum of the weighted outputs $(y_{i(k-1)})$from all of the nodes of the previous layer offset by the bias of that node as shown in equation (27) where $x_{i(k-1)}$ is the output of node i of the previous layer $(k-1)$, $w_{ij(k-1)}$is the weight applied to each x (there is a unique set for each node j of layer k), b_{jk} is the bias for the node of interest, and n is equal to the number of nodes in layer $k-1$. Applying this to a Sigmoid activation function gives the output of each node within the hidden layer as shown in equation (28).

Given the type of network used, the number of nodes, and a (3, 3, 1) architecture, the number if independent parameters in the network is therefore 16, with unique weights applied to each input variable before being passed to any of the nodes in the hidden layer (9), unique biases for each node in the hidden layer (3), unique weights applied to the output of each node in the hidden layer (3), and a single bias on the output node (1).

5.2.2 Training

To make any Artificial Neural Network (ANN) useful, the weights w_{ijk} and biases b_{jk} need to be adjusted during a training procedure until the outputs of the network provide an acceptable level of error when compared to a data set with known inputs and outputs. The sections which immediately follow outline a repeatable

process which can be employed to establish these weights and biases and to determine the number of neurons for a single hidden layer neural network.

5.2.2.1 Algorithm

For the present study, a supervised learning procedure was utilized where a specific set of training inputs was passed to the network and the outputs of the network were then quantitatively compared against the corresponding training data outputs by calculating the mean squared error $\left(MSE = \frac{1}{n}\sum_{i=1}^{n}\left(y_{i,ANN} - y_{i,train}\right)^2\right)$. When each data point (a given hydrocarbon or hydrocarbon mixture at a given temperature and pressure with a corresponding viscosity) had been passed to the network only one time in random order and the MSE calculated, a milestone referred to as an $epoch$ was met [88]. To facilitate a simple investigation into hyper-parameter selection, training was stopped once a pre-determined number of epochs was reached, as detailed in section **5.2.2.3**.

After randomly assigning initial values between -1 and 1, weights and biases were updated after each epoch using the Levenberg-Marquardt backpropagation algorithm as described in [89] and briefly outlined in the previous chapter. For the present application of training the viscosity model, μ_k of equation (29) was initialized at 0.001, and increased or decreased an order of magnitude as required based of the performance at the current iteration.

As described previously, the inputs to the ANN used from this training data were the $\overline{MW}$, HN/CN, and s^*. To calculate the MSE and update weights and biases

after each epoch, the outputs of the network were evaluated against their respective $\ln(\eta^*)$ values from the training set, which was calculated for each data point from the values for η found in the literature by utilizing the Chapman-Enskog relationship described by Rokni et al. [81]. This step enables the utilization of physical knowledge downstream of the ANN and was performed prior to the training procedure in the present study, which allowed for efficient computation of derivatives used in the Levenberg-Marquardt algorithm. However, it should be strongly noted, that utilization of physical information downstream of a neural network does not preclude this efficient implementation, particularly if analytical derivatives are employed when training using a backpropagation scheme.

5.2.2.2 Training Data

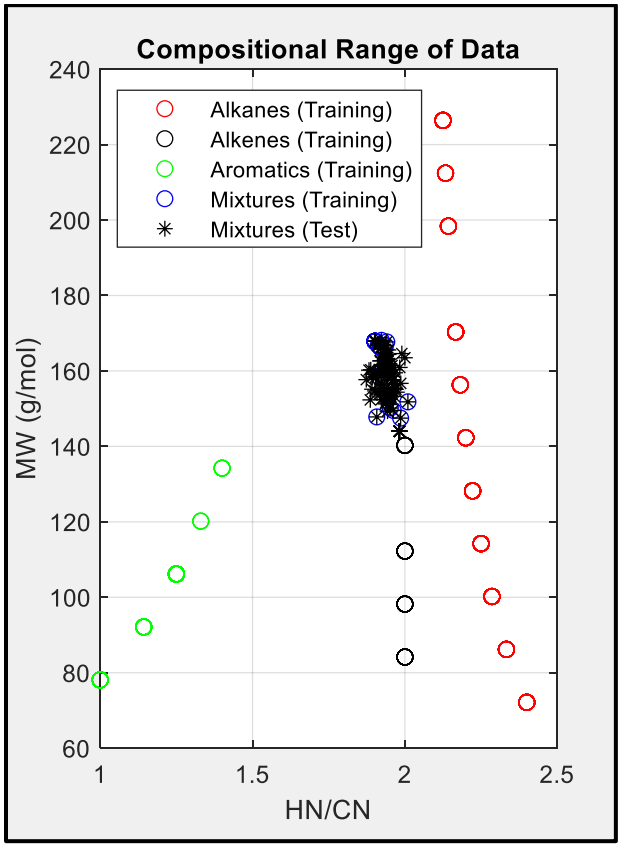

Figure 19: Compositional Range of Viscosity Training and Test Data

The training data used for the network was comprised of two broad categories of hydrocarbon liquids: pure hydrocarbons, and a jet fuel where viscosity were measured over a range of pressures and temperatures with a total of 494 data points, as shown in **Table 8**.

Table 8: Training Data for Viscosity Model

Hydrocarbon / Mixture	MW or $\overline{MW}$ (g/mol)	HN/CN	Data Points	Min. Temp. (°C)	Max. Temp. (°C)	Min. Press. (MPa)	Max. Press. (MPa)	Ref.
Pentane	72.15	2.400	30	-120	80	0.1	10	[90]
Hexane	86.18	2.333	30	-90	110	0.1	10	[90]
Heptane	100.21	2.286	29	-80	100	0.1	10	[90]
Octane	114.23	2.250	30	-50	150	0.1	10	[90]
Nonane	128.2	2.222	32	-50	150	0.1	10	[90]
Decane	142.29	2.200	30	-20	160	0.1	10	[90]
Undecane	156.31	2.182	17	10	90	0.1	0.1	[97]
Dodecane	170.33	2.167	33	0	200	0.1	10	[90]
Tetradecane	198.39	2.143	17	10	80	0.1	10	[98]
Pentadecane	212.42	2.133	15	20	85.1	0.1013	0.1013	[99]
Hexadecane	226.41	2.125	36	49.55	399.45	0.97	3.99	[100]
Hexene	84.16	2.000	23	17.5	100	0.101	14.7	[101]
Heptene	98.19	2.000	16	25	200.55	0.098	24.51	[102]
Octene	112.24	2.000	16	25	202.66	0.098	24.51	[103]
Decene	140.27	2.000	13	25	201.87	0.098	24.51	[103]
Benzene	78.114	1.000	23	25	120	0.1	20	[104] [105]
Toluene	92.14	1.143	24	24.31	151.52	0.1	10	[106]
Iso-butylbenzene	134.22	1.400	5	20	60	0.1	0.1	[107]
Ethylbenzene	106.17	1.250	52	-19.94	99.46	0.1	10	[108]
Iso-Propylbenzene	120.19	1.330	3	25	45	0.1	0.1	[109]
JP-5-12011	167.85	1.902	13	-20	100	.1013	0.1013	present study
F-24-12974	166.75	1.936	1	-20	-20	0.1	0.1	present study
F-24-13033	167.70	1.941	1	-20	-20	0.1	0.1	present study
F-24-13073	166.71	1.913	1	-20	-20	0.1	0.1	present study
F-24-13074	166.81	1.912	1	-20	-20	0.1	0.1	present study
Jet-A-11721	166.03	1.921	1	-20	-20	0.1	0.1	present study
Jet-A-11821	166.29	1.921	1	-20	-20	0.1	0.1	present study
Jet-A-12831	168.10	1.923	1	-20	-20	0.1	0.1	present study

To evaluate the ability of the ANN to predict the values other than the training data, a set of test data was used which was composed of jet fuels which is summarized in **Table 6**. All training data was normalized prior to being employed in network training.

Table 9: Test Data for Viscosity Model

Hydrocarbon / Mixture	$\boldsymbol{MW}$ or $\boldsymbol{\overline{MW}}$ $(\boldsymbol{g/mol})$	HN/CN	Data Points	Min. Temp. (°C)	Max. Temp. (°C)	Min. Press. (MPa)	Max. Press. (MPa)	Ref.
Jet A-4658	157.5	1.960	23	-10	100	0.1	0.1	[34]
Jet Fuel Specification test at −20°C	147.49-168.1	1.87-2.01	96	-20	-20	0.1	0.1	present study
JP-5-12011	167.85	1.902	13	-20	100	.1013	0.1013	present study
JP-5-12533	162.96	1.938	13	-20	100	0.1013	0.1013	present study
F-24-13147	144.02	1.982	13	-20	100	0.1013	0.1013	present study
JP-5-18307	161.45	1.927	13	-20	100	0.1013	0.1013	present study
RP-1 Surrogate	163.5	2.000	1	15.55	15.55	0.1013	0.1013	[36]
RP-2 Surrogate	164.6	1.990	1	15.55	15.55	0.1013	0.1013	[36]

5.2.2.3 Hidden Layer Sizing

Determining the number nodes in the input and output layers for this type of effort is trivial once the desired independent and dependent variable(s) are identified. In the case of the present study, knowing that $\ln(\eta^*) = f(\overline{MW}, HN/CN, s^*)$ leads to three input nodes and one output node.

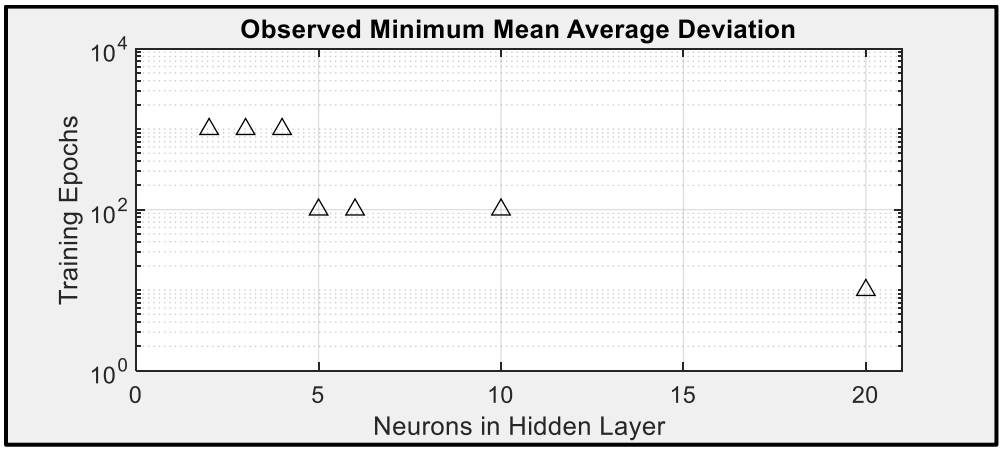

Figure 20: Observed Minimum Mean Average Deviation between model and Test set for Viscosity. 50 samples were recorded at each grid point with mean and standard deviation recorded for each location.

As utilized in the thermal conductivity model development, the approach utilized by Faúndez et al. was expanded into a grid search method where the mean and standard deviation of the average deviation between the model and the test set over 50 iterations was recorded versus the number of nodes in the hidden layer and number of epochs per training set. The set of hidden nodes investigated was 2, 3, 4, 5, 6, 10, and 20 while the set of epochs was $10, 10^2, 10^3, 10^4, 10^5$, and 10^6. The observed minimum mean of the average deviation for each number of hidden layer neurons considered is plotted in **Figure 20** where a stepwise Pareto front is observed. Additionally, it is worth noting that the behavior described in [73] was again observed, where the mean of the average error started high, passed through a minimum, and then increased again when increasing the number of neurons from low

to high and holding the number of epochs constant. This behavior also occurred when holding the number of neurons constant and increasing the number of epochs used in training.

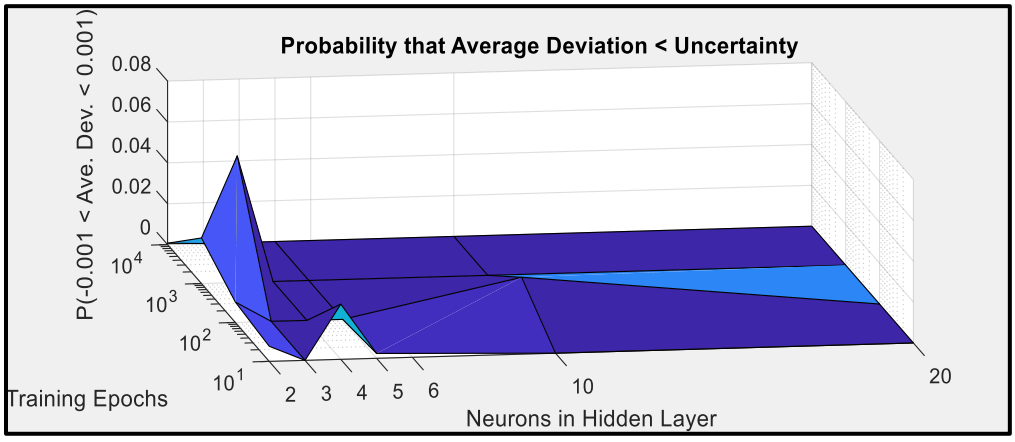

Figure 21: Probability of Model Configuration Containing Average Deviation Less than the Uncertainty of Viscosity Test Measurement

To avoid over-fitting, the set of possible network configurations observed on the Pareto front was narrowed down by following the guidance of [73] which lead to a limit for the number of neurons in a single hidden layer of between 70% of the number in network inputs and less than double the number of network inputs. For the present effort, this meant only considering the range of 2-5 neurons in the hidden layer.

At this point, a statistical approach was employed to select the final combination of neurons and training epochs. Assuming the means of the average deviation to be normally distributed, the proportion of the calculated distribution that

falls within the uncertainty bands for the test measurement at each remaining grid point was calculated, using the typical uncertainty of 0.1% for viscosity of liquids in the temperature and pressure ranges of interest. Results shown in **Figure 21** show that a clear maximum exists when using 3 hidden layer neurons and 10^3 training epochs.

With the network hyper-parameters identified, the training procedure was executed to completion multiple times with a final network being selected when the average deviation for test data was lower than 0.1%. The resulting weights and biases of the present study are given below in **Table 10.**

Table 10: Weights and biases for hybrid entropy scaling guided neural network model of viscosity

	$\overline{MW}$ $(i=1)$	$\frac{HN}{CN}$ $(i=2)$	s^* $(i=3)$				
Layer 1 to 2				Layer 2 to 3		Biases	
$w_{i,1,1}$	-0.1813	-0.0268	1.3703	$w_{1,1,2}$	-1.0934	b_{12}	-0.7430
$w_{i,2,1}$	0.752	-0.1182	-1.8793	$w_{2,1,2}$	2.0423	b_{22}	-1.2630
$w_{i,3,1}$	0.7578	-0.8993	-1.1936	$w_{3,1,2}$	-1.4295	b_{32}	-1.3045
						b_{13}	0.1001

5.3 Results

To evaluate the performance of the resulting model the average deviation, the absolute average deviation, and maximum deviation were calculated against the test data set of **Table 9**. **Figure 22** provides a quantitative comparison of the results against the Rokni et al. model applied on the same test set. Not only is the performance significantly improved, the average deviation is at the target of 0.1%. A qualitative view of the performance is given in the plots of **Figure 23 (a-b)** where results for the full property suite samples are plotted against the test data and Rokni et al. model predictions. It is worth noting that the bulk of the improvement in this model over the performance of the Rokni et al. model is in the low temperature regime. This applies to all of the full property suite samples and is particularly evident in **Figure 24** near the bottom of the plot (from the perspective of the page), where the 96 measured specification viscosity measurements collected for this study are shown.

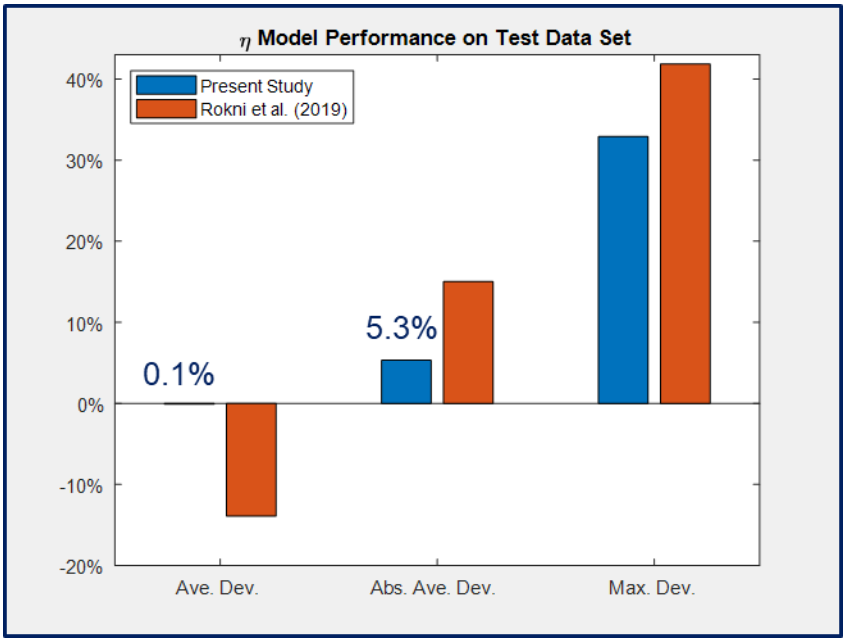

Figure 22: Viscosity Hybrid Model Performance

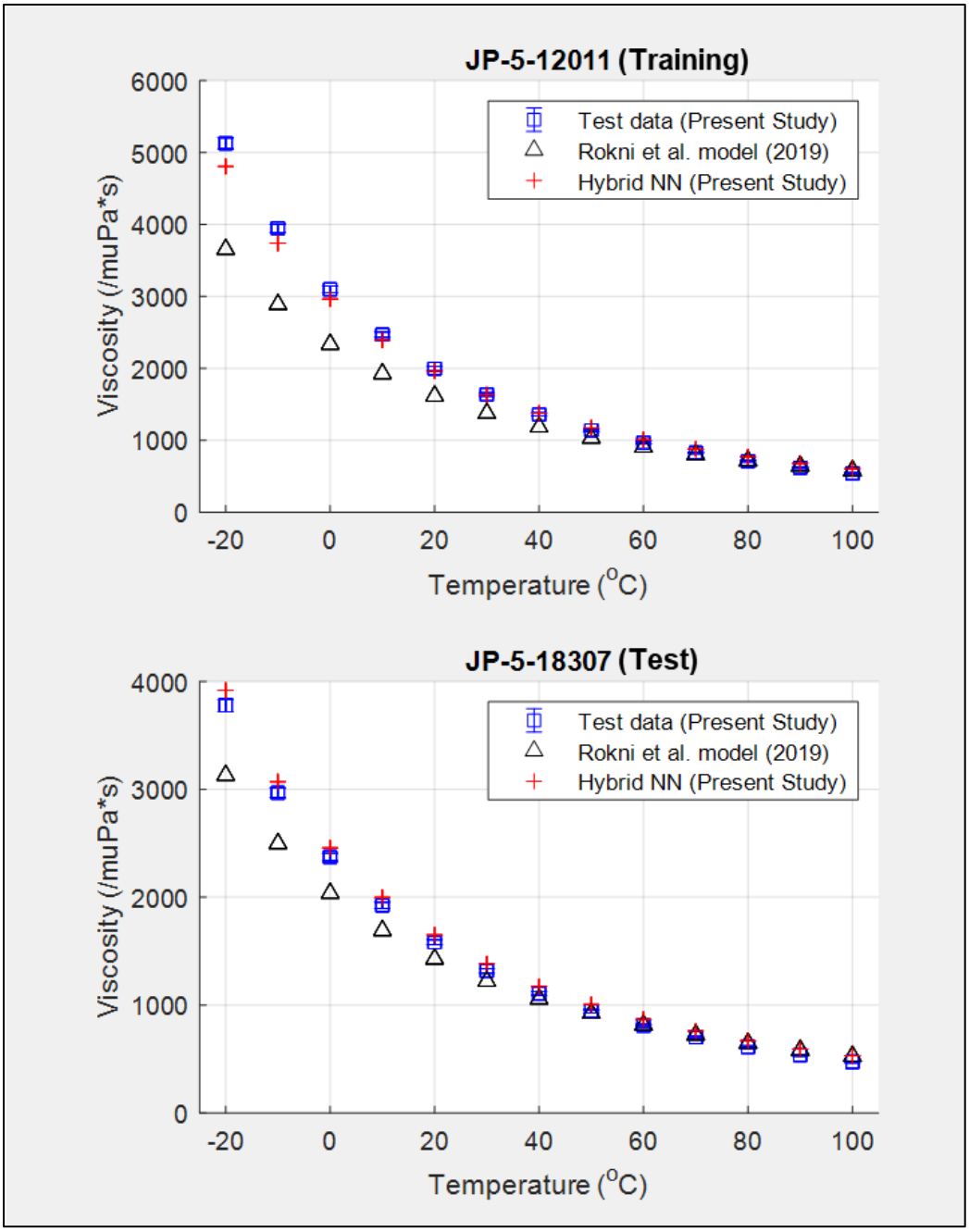

(a) Viscosity vs. temperature of JP-5 12011 and 18307

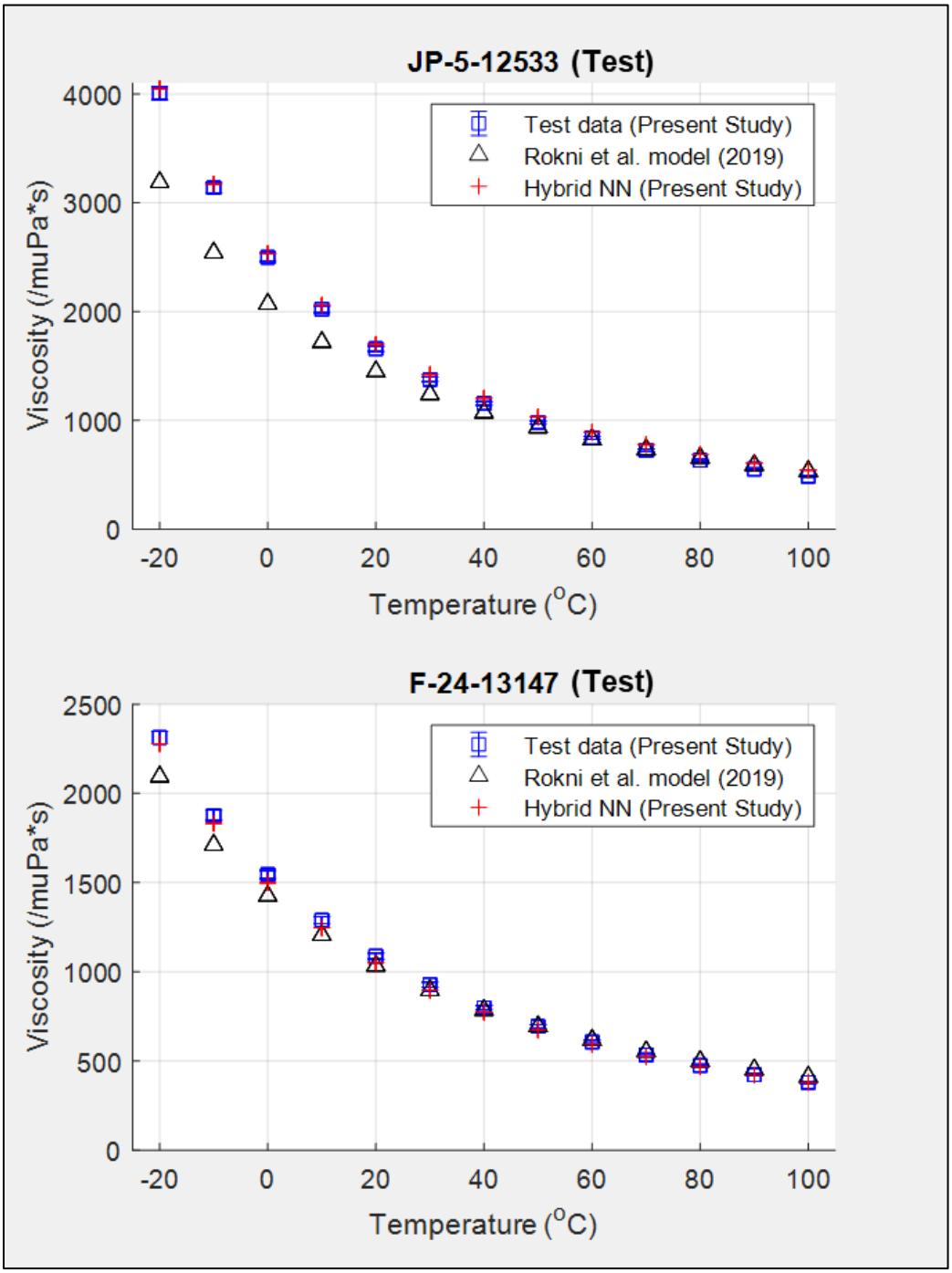

(b) Viscosity vs. temperature of JP-5 12533 and F-24 13147

Figure 23: Qualitative performance of hybrid viscosity model on full property suite samples

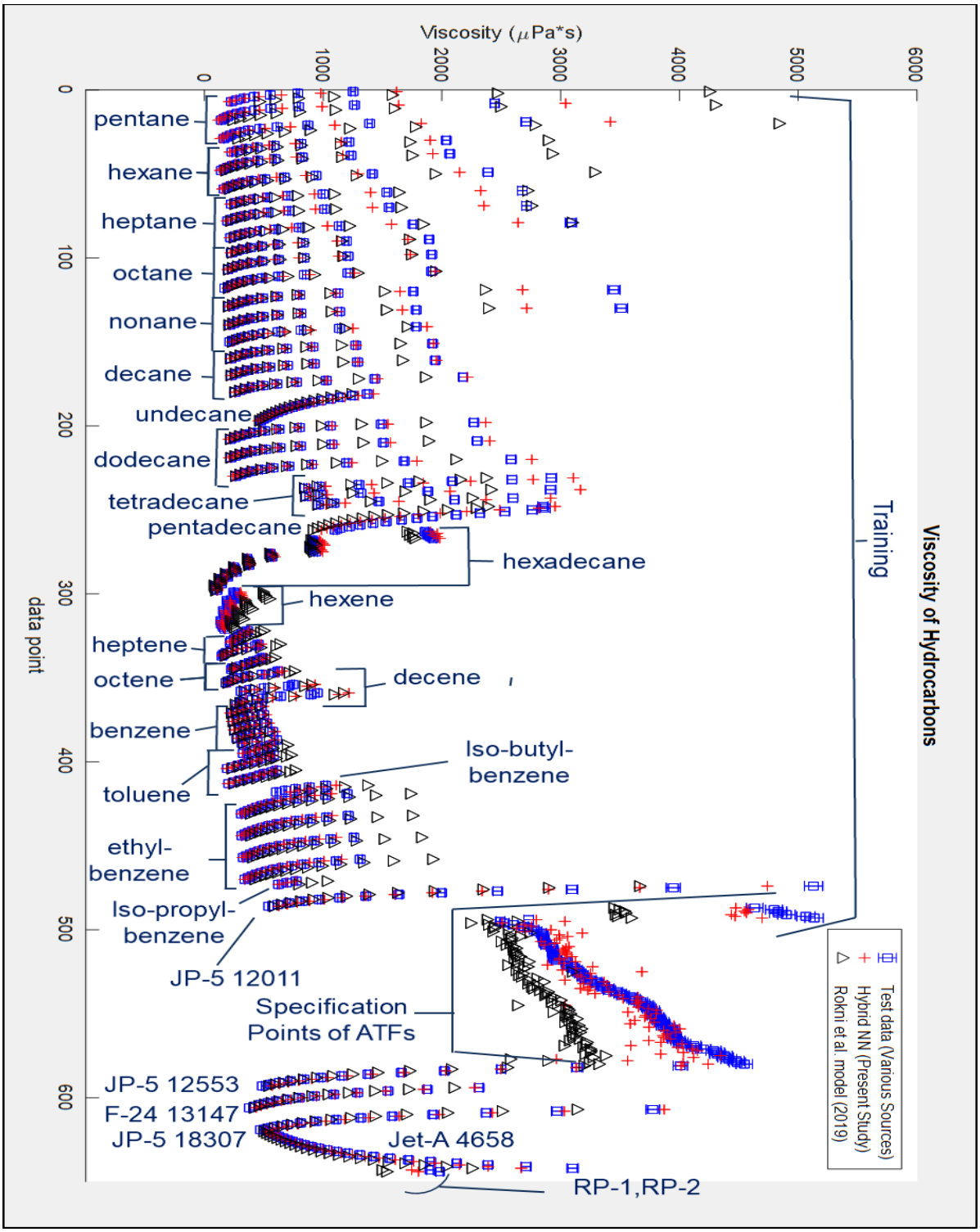

Figure 24: Qualitative view of hybrid model performance across training and test data

5.4 Stability

As a final consideration to examine the performance of the hybrid viscosity model, the artificial neural network employed in the intermediate step of the model connecting the reduced residual entropy with the viscosity was used to generate surfaces which provided the output $\ln(\eta^*)$ as a function of the network input variables s^*, $\overline{MW}$, and $\frac{HN}{CN}$ (**Figure 25**). The ranges of input variables used more than cover the compositional range of hydrocarbons used to develop the model (refer to **Figure 19**) as well as the reduced residual entropy values observed during training. The mesh size used to generate each surface is 40 by 40 regardless of the input parameters.

The observed surfaces provide insight into the non-linearity of the behavior yet are also well behaved over the regions of interest to provide confidence in generalization to other hydrocarbon mixtures, particularly those which fall within the bounds of the training set of pure components.

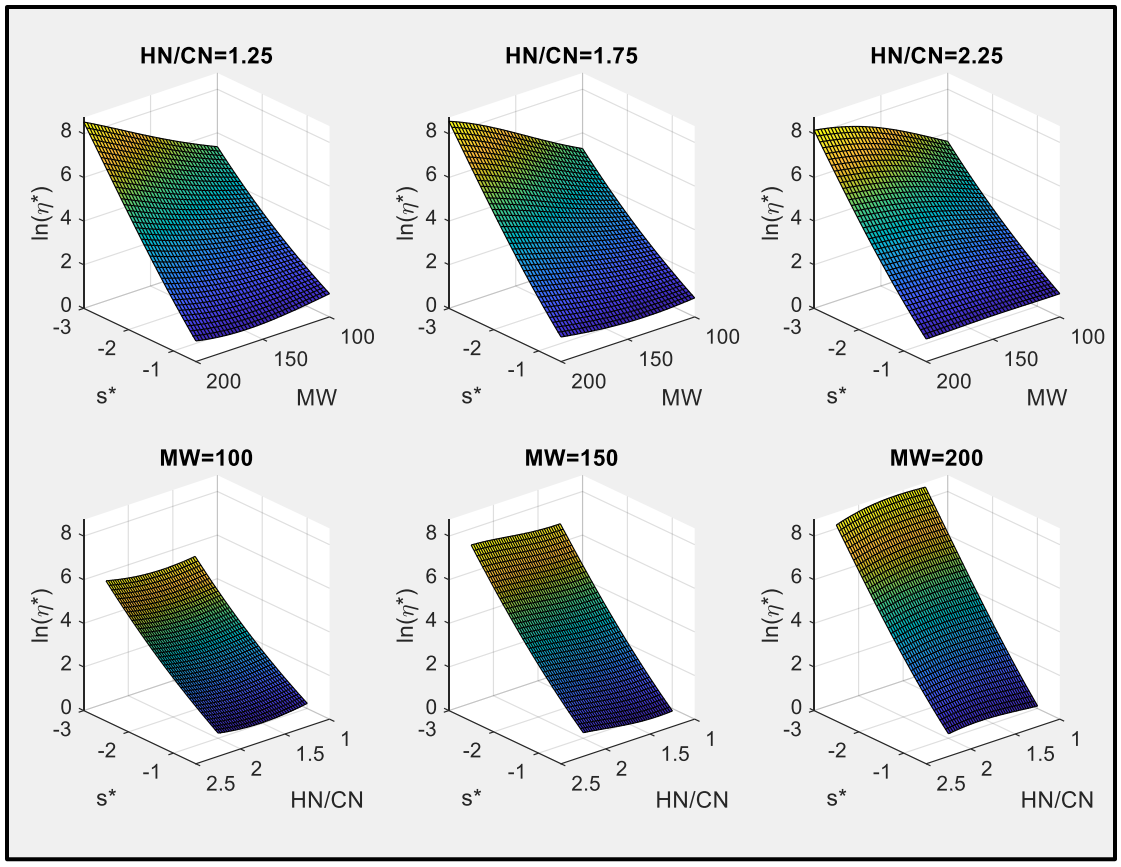

Figure 25: Artificial neural network for viscosity stability assessment

6. Specific Heat Model

The final model to be developed for this effort aimed to predict the constant pressure specific heats of molecularly well-defined liquid mixtures such as the samples of fuel collected for the present study. The model is a logical extension of the approach of Dadgostar and Shaw 2012 [54] where a similarity variable α (equation 32) was derived based on the connection between the high temperature heat capacities of solids composed of large molecules and their associated atomic vibrations [110]. The similarity variable makes use of the fundamental relationship between the number of atoms in a molecule (N) and the associated molar mass of the molecule (M) in grams per mole, which has the same form as the thermodynamic relationship between the number of vibrations per unit mass of a molecule: $3N/M$ [110].

$$\alpha = N/M \tag{32}$$

The present study explicitly extends the similarity parameter into a form suitable for mixtures by utilizing an approach roughly similar to what was used by Rokni et al. in the sense that a pseudo molecule with molar fraction (x_i) weighted similarity parameters as described by equation 33 could be used to express the atomic density needed for the Dadgostar and Shaw model.

$$\alpha_{mixture} = \sum_{i=1}^{n} \alpha_i x_i = \sum_{i=1}^{n} \frac{(HN_i + CN_i)}{MW_i} x_i = \sum_{i=1}^{n} \frac{(HN_i + CN_i)}{MW_i} w_i \frac{\overline{MW}}{MW_i} \quad (33)$$

Applying the expressions above to the full property suite samples using the data in **APPENDIX A: GCxGC COMPOSITION OF FULL PROPERTY SUITE SAMPLES** yields the results shown below in **Table 11**.

Table 11: Mixture similarity parameter (α) for the full property suite samples

	JP-5-12011	**JP-5-18307**	**JP-5-12553**	**F-24-13147**
$\alpha_{mixture}$	0.2075	0.2086	0.2095	0.2121

With this in hand, the model proceeds with the empirically fitted form and parameters of the already developed model show in equations 34 and 35 where c_p is provided in (kj/kg · K), temperature (T) is in Kelvin, and the simplification for a_1 described in [54] has been applied given that the temperature range of interest is higher than 200 K.

$$c_p = a_1 + (a_{21}\alpha + a_{22}\alpha^2)T + (a_{31}\alpha + a_{32}\alpha^2)T^2 \quad (34)$$

$$a_1 = (a_{11}\alpha + a_{12}\alpha^2)24.5 \quad (35)$$

Table 12: Specific heat model coefficients

Coefficients for c_p Model	
a_{11}	-0.3416
a_{12}	2.2671
a_{21}	0.1064
a_{22}	-0.3874
a_{31}	-9.8231E-5
a_{32}	4.182E-4

Application of the resulting calculated $\alpha_{mixture}$ values for the full property suite samples provides the results shown in **Figure 26 (a-b)** and the error analysis shown in **Figure 27**. The results indicate that both the average and absolute average model performance are providing reasonable estimates of the heat capacities of the fuels considered for the present study which are not quite within the typical uncertainty of 2% for liquid heat capacity measurements.

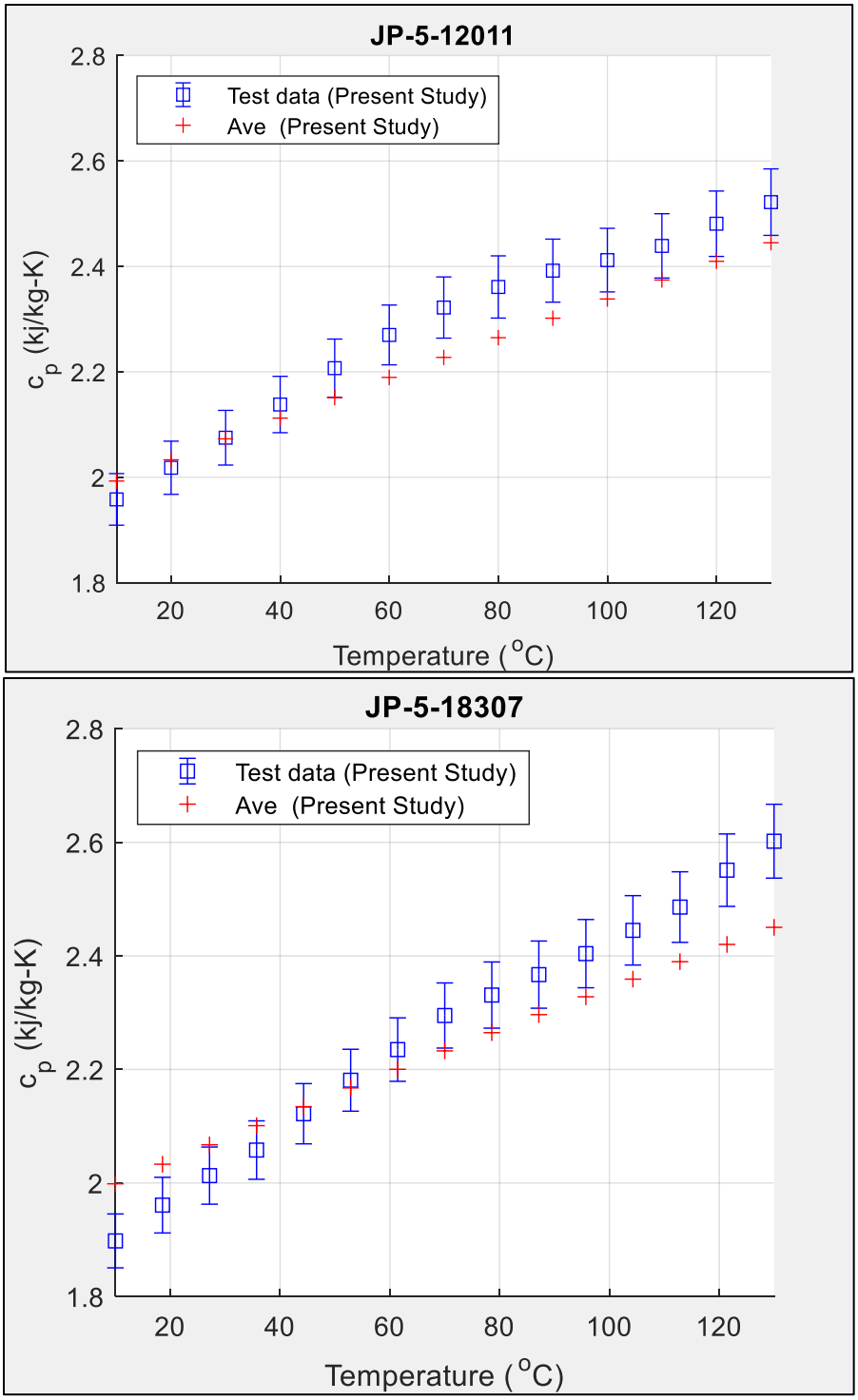

(a) Specific heat vs. temperature of JP-5 12011 and 18307

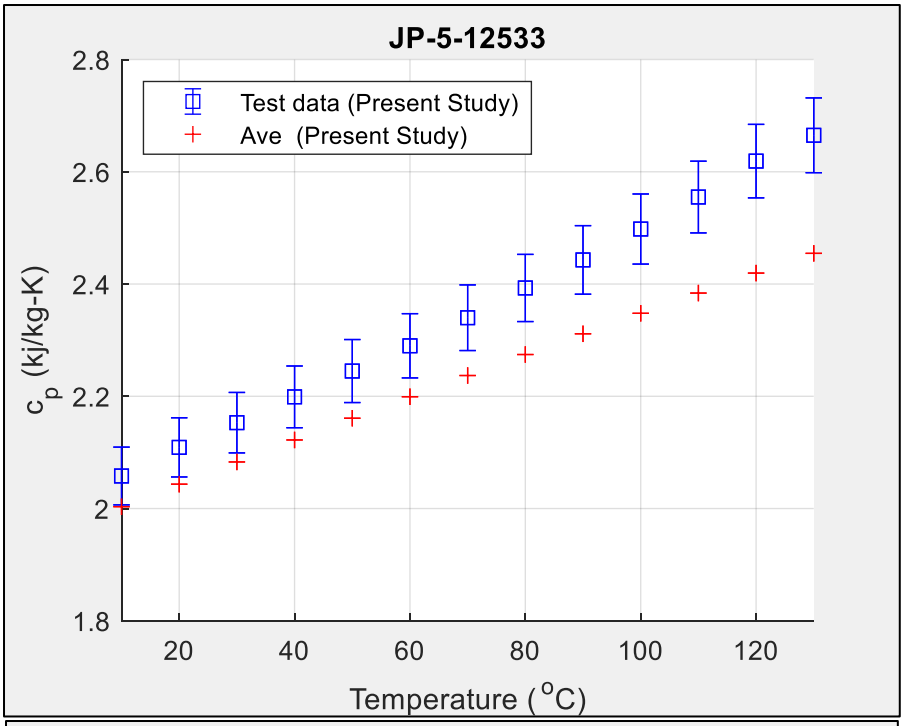

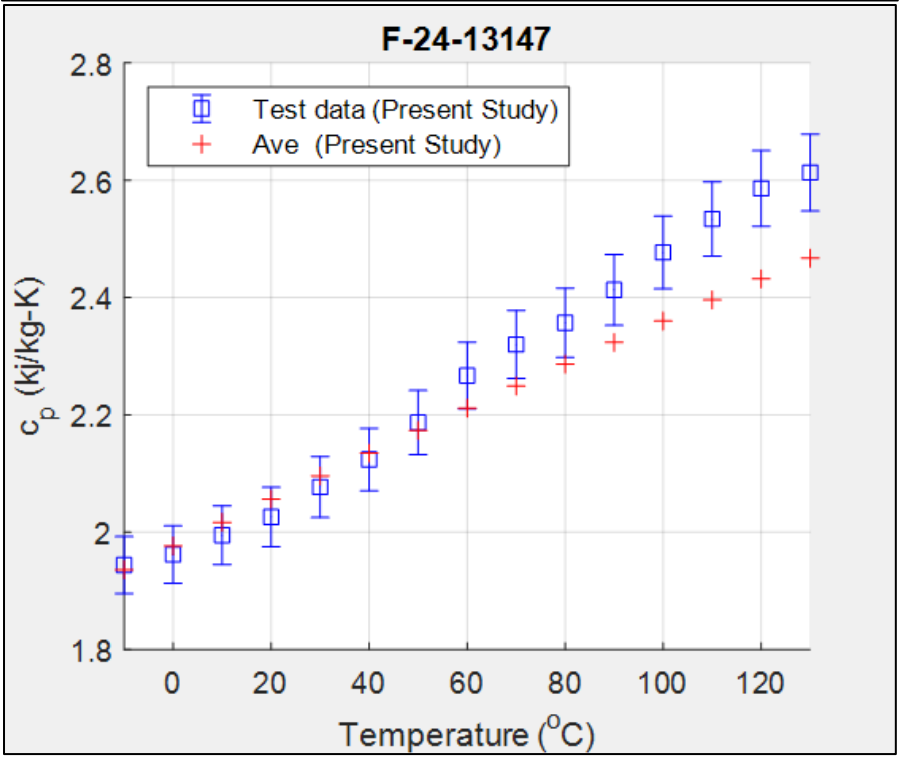

(b) Viscosity vs. temperature of JP-5 12533 and 13147

Figure 26: Modeled and measured specific heat of full property suite samples

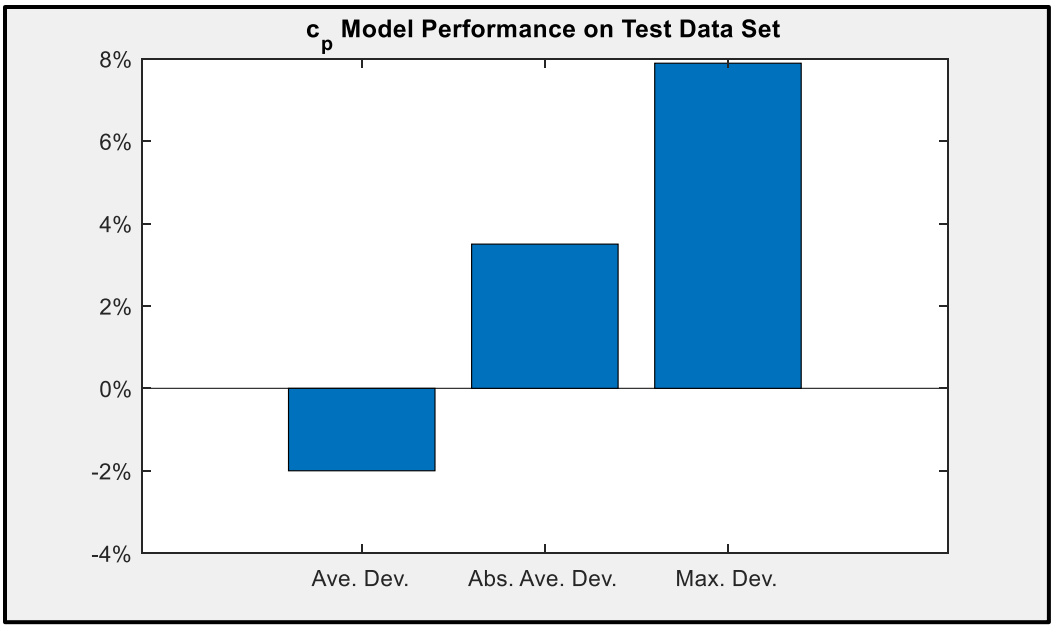

Figure 27: Average, absolute average, and maximum deviation between modeled and tested specific heat data

7. Predicted Ranges of Fuel Thermodynamic and Transport Properties

To complete the final objective of the present effort as outlined in section **2.4**, the compositional data collected in section **3** was supplied to the models of thermal conductivity (section **4**), viscosity (section **5**), and specific heat (section **6**) developed for this effort as well as the density model of Rokni et al. 2019. The resulting outputs of the respective models could then be used to develop estimates of the bounds of these respective properties across the typical primary military aviation fuel types and evaluated against the existing recommendations for these same properties. The following section provides the resulting range plots and recommendations on the bounds and expressions that can be used to represent the extreme cases. This section then concludes with an analysis considering the coupling between the properties.

7.1 Transport and Thermodynamic Properties of Aviation Turbine Fuel

The plots shown in **Figure 28** through **Figure 32** capture the output of the models cited above for the properties of interest as well as the data presented for various fuels from CRC 2014 [38]. The plot of density (**Figure 28**) captures the range of fuels of interest contained within the CRC data as JP-8 and Jet A are presented with values falling in between the JP-5 and Jet A-1 values show below. Given this, the present study shows a slightly different over central tendency across fuel types as well as a slightly different overall slope.

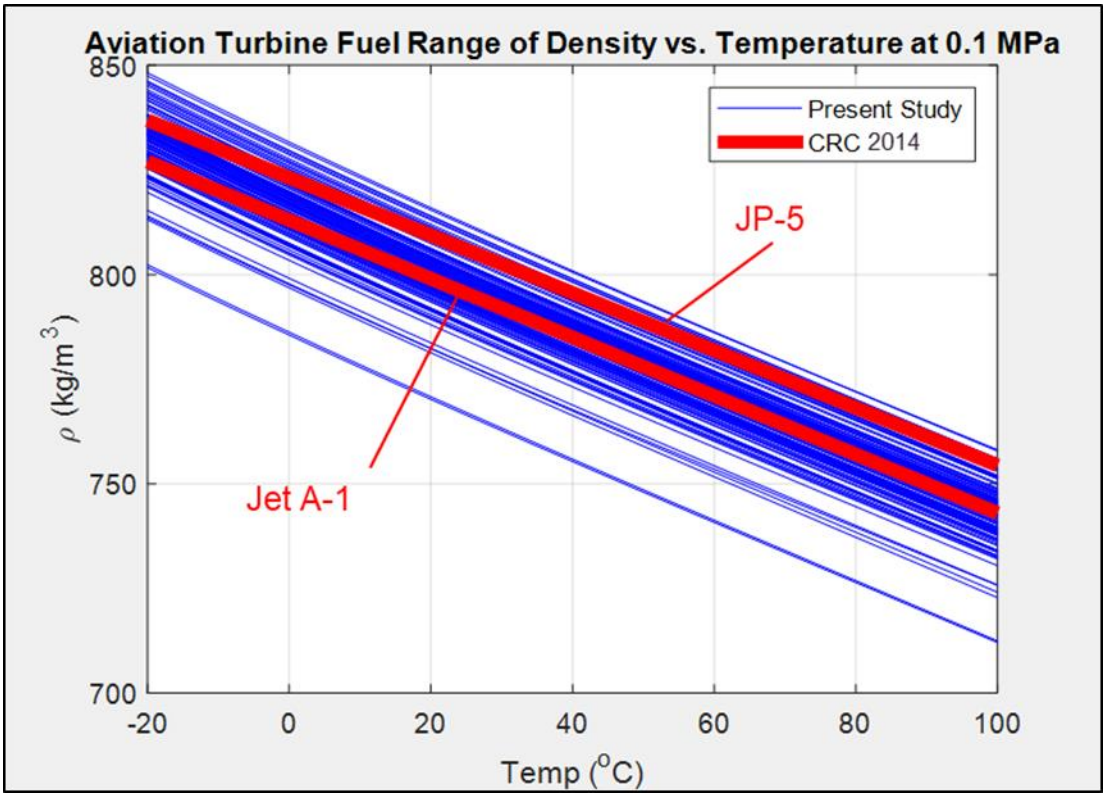

Figure 28: Predicted range of aviation turbine fuel density based on 100 sampled fuel compositions as inputs to the model of Rokni et al. 2019 *[55]*

Figure 29 presents the thermal conductivity of the present work along with the value prescribed by CRC 2014 which is recorded as representing the behavior across JP-4, JP-5, JP-7, JP-8, Jet A, Jet A-1 and Jet B fuel types. The output of the present effort clearly presents a differing view from the CRC data for both central tendency and slope as well as providing a much more detailed insight into potential variation across fuel samples.

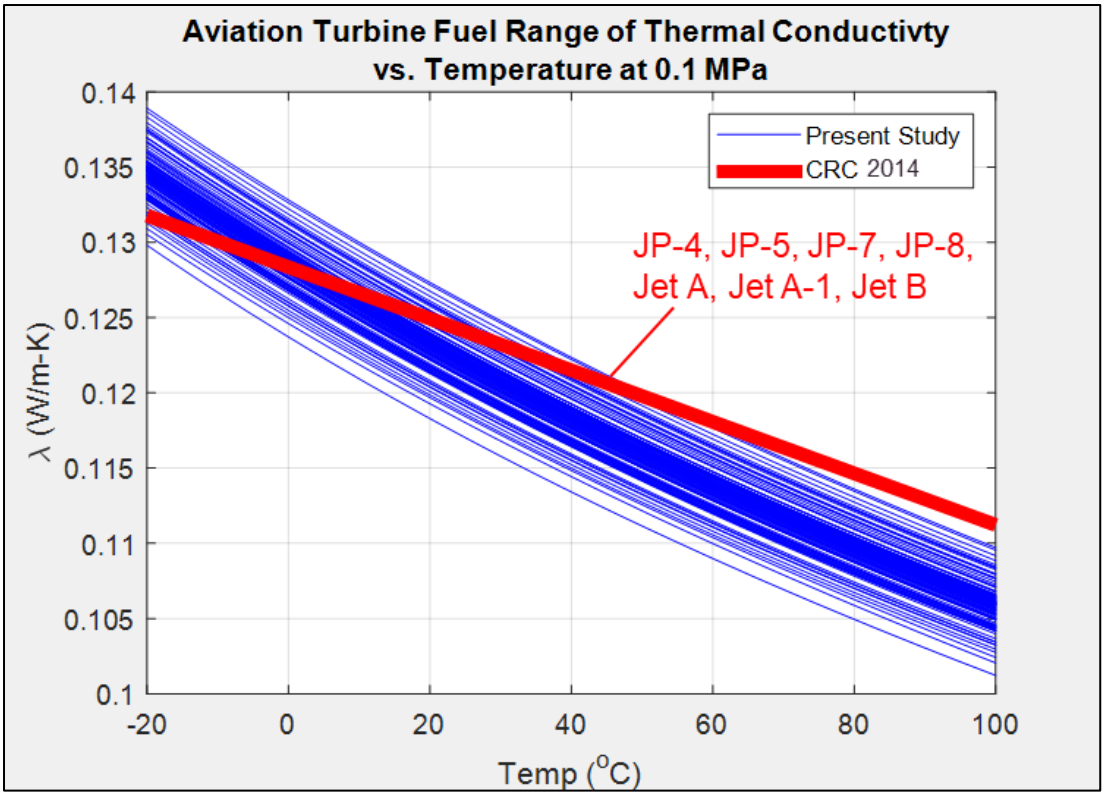

Figure 29: Predicted range of aviation turbine fuel thermal conductivity based on 100 sampled fuel compositions as inputs to the hybrid entropy scaling guided neural network model of the present study.

The viscosity model data is presented in **Figure 30** alongside the recommended value for JP-5 CRC 2014, which is derived from the density and kinematic viscosity values given in the text. As JP-5 is given with the highest density value (**Figure 28**) and the curve of kinematic viscosity in CRC is prescribed to represent JP-5, JP-8, and Jet A, it would represent the lower bound of viscosity prescribed by CRC. Given that this is at the upper range of the values of the present work, a new working range for these values should be considered.

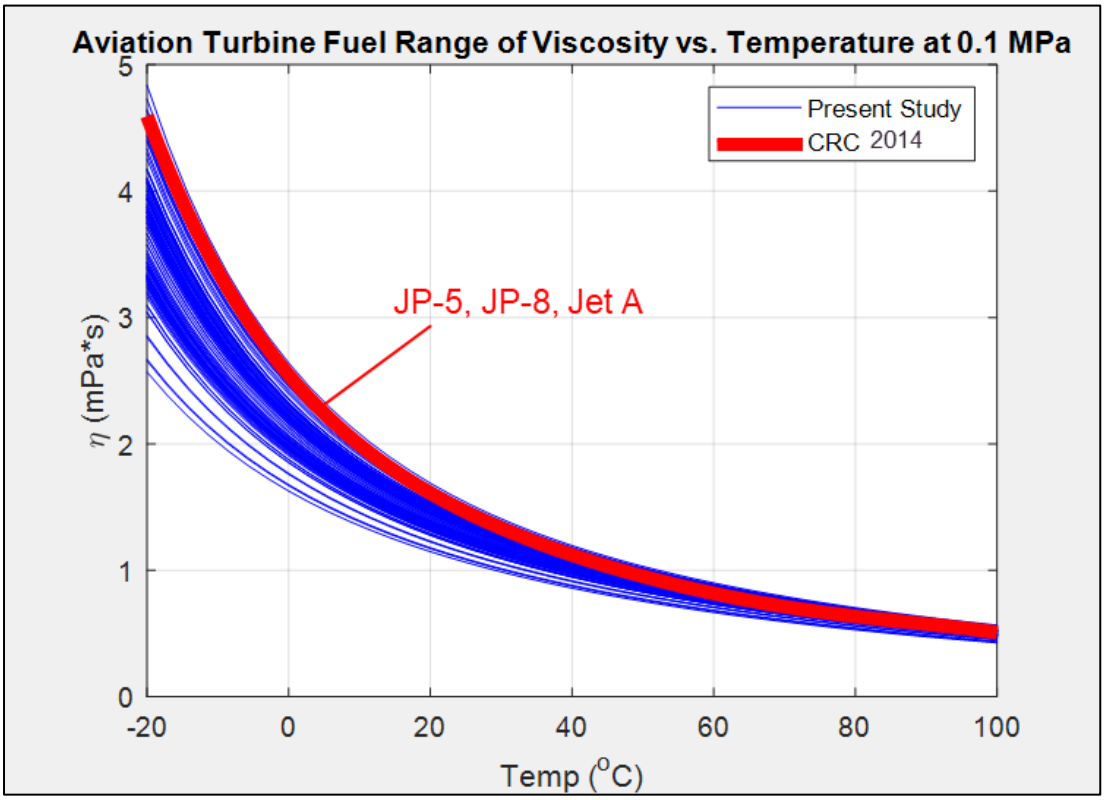

Figure 30: Predicted range of aviation turbine fuel viscosity based on 100 sampled fuel compositions as inputs to the hybrid entropy scaling guided neural network model of the present study.

Similarly, the specific heat values representing the bounds of the fuels of interest given by CRC 2014 are contrasted with those from the present study in **Figure 31**. Again, the values established in the present work cover a different range than the prescribe values of the literature with a slightly different slope as well.

Finally, the Prandtl numbers derived from the modeled data of the present work are given in **Figure 32**. The ranges observed, including a variation on the order of 50% near 20 ℃, coupled with the range of heat transfer modes within fighter aircraft fuel thermal management systems strongly suggest the potential for system

performance to be sensitive to the variation in fuel properties observed, particularly when low fuel temperatures are expected from either a cold day initial condition or high altitude flight.

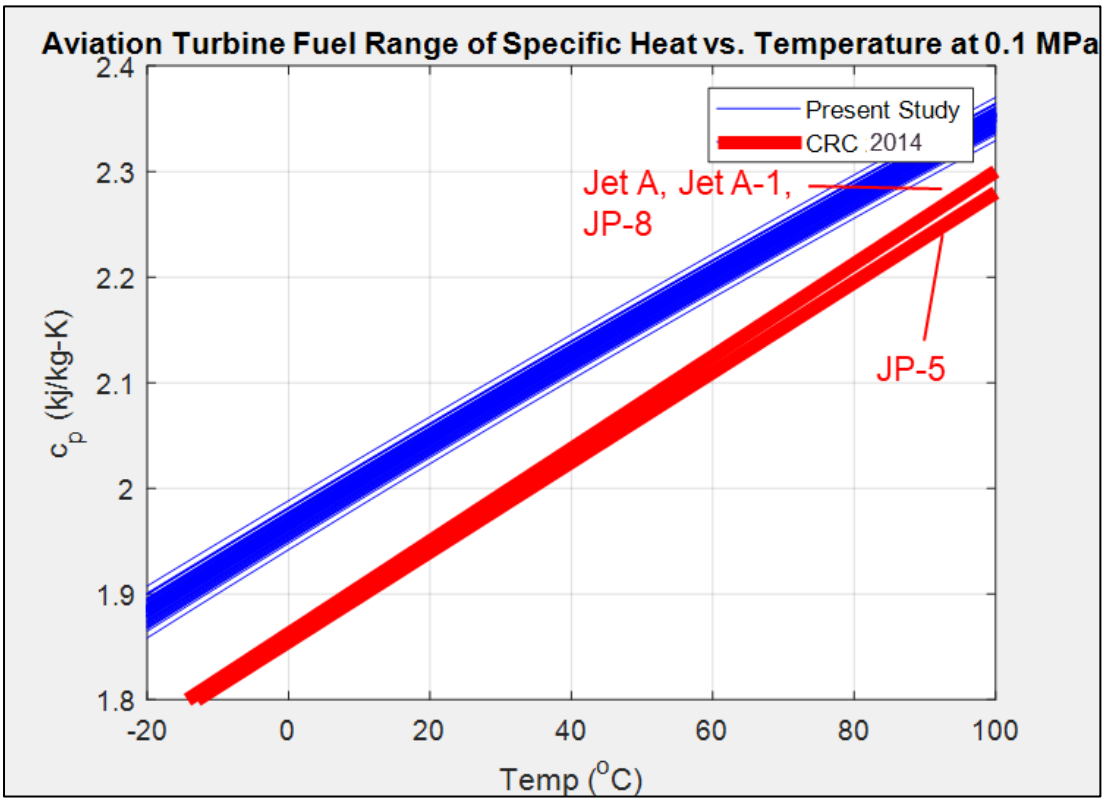

Figure 31: Predicted range of aviation turbine fuel specific heat based on 100 sampled fuel compositions as inputs to the model of the present study.

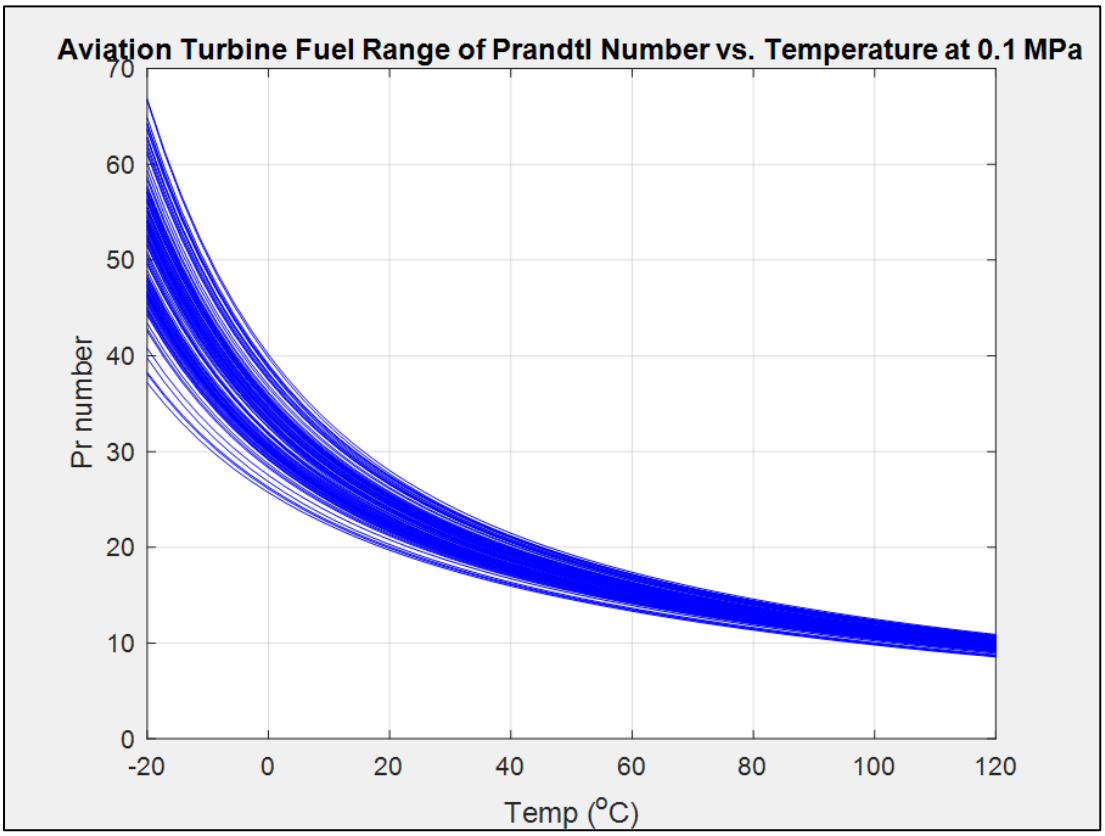

Figure 32: Predicted range of aviation turbine fuel Prandtl based on 100 sampled fuel compositions as derived from the models of the present study.

7.2 Analysis

To determine appropriate bounds for the ranges observed in the plots of the previous section, analysis of the data at various temperatures was performed. Prescribed fits for the bounds should be considered valid over the range of −40℃ to −100℃, as the effects of phase transformations should be considered outside of this regimes. Beginning with density, the distribution of the modeled data at the specification temperature of 15 ℃ was recorded and tested for normality. The Chi squared goodness of fit test that was employed failed to reject the hypothesis that the

data is normally distributed at the 95% confidence level with a p value of 0.2625 and hence the bounds can be established by computing a 99% confidence interval as shown in **Figure 33**. Given these results, observing a fuel near the limits of the specifications as provided in **Table 1** is improbable. However, it is worth noting that two fuels were observed lower that the bound of the 99% interval. Using the bounds established at 15℃ and 100℃ and assuming a linear relationship, the expressions in equations (36) and (37) were developed and are provided as the recommended bounds of density for use in aircraft thermal management analysis. The units for the expressions are ℃ and $\mathrm{kg/m^3}$.

$$\rho_{low} = -0.7204T + 793.8 \tag{36}$$

$$\rho_{high} = -0.7319T + 836.0 \tag{37}$$

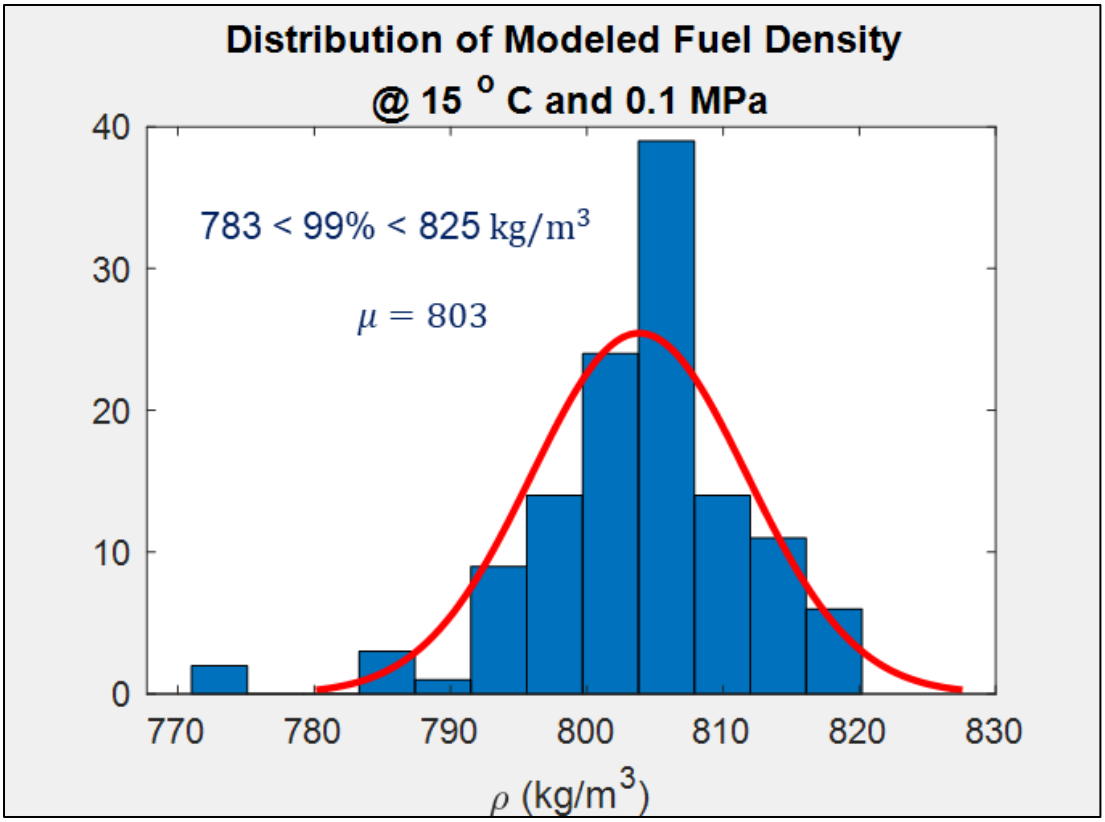

Figure 33: Distribution of modeled fuel density at specification temperature and predicted 99% confidence interval.

Following the same initial procedure, the distribution of modeled thermal conductivity values observed at 15℃ were tested for normality. The Chi squared goodness of fit test for normality failed to accept the hypothesis that the data is normally distributed at the 95% confidence level with a p value of 0.0087 and hence the observed bounds are provided in **Figure 34**. The resulting recommended expressions to represent the bounds of the data are provided below in equations (**38**) and (**39**) with T in ℃ and λ in $\mathrm{W/m \cdot K}$.

$$\lambda_{low} = (-2.6229E-4)T + 0.1229 \quad (38)$$

$$\lambda_{high} = (-2.2235E-4)T + 0.1319 \quad (39)$$

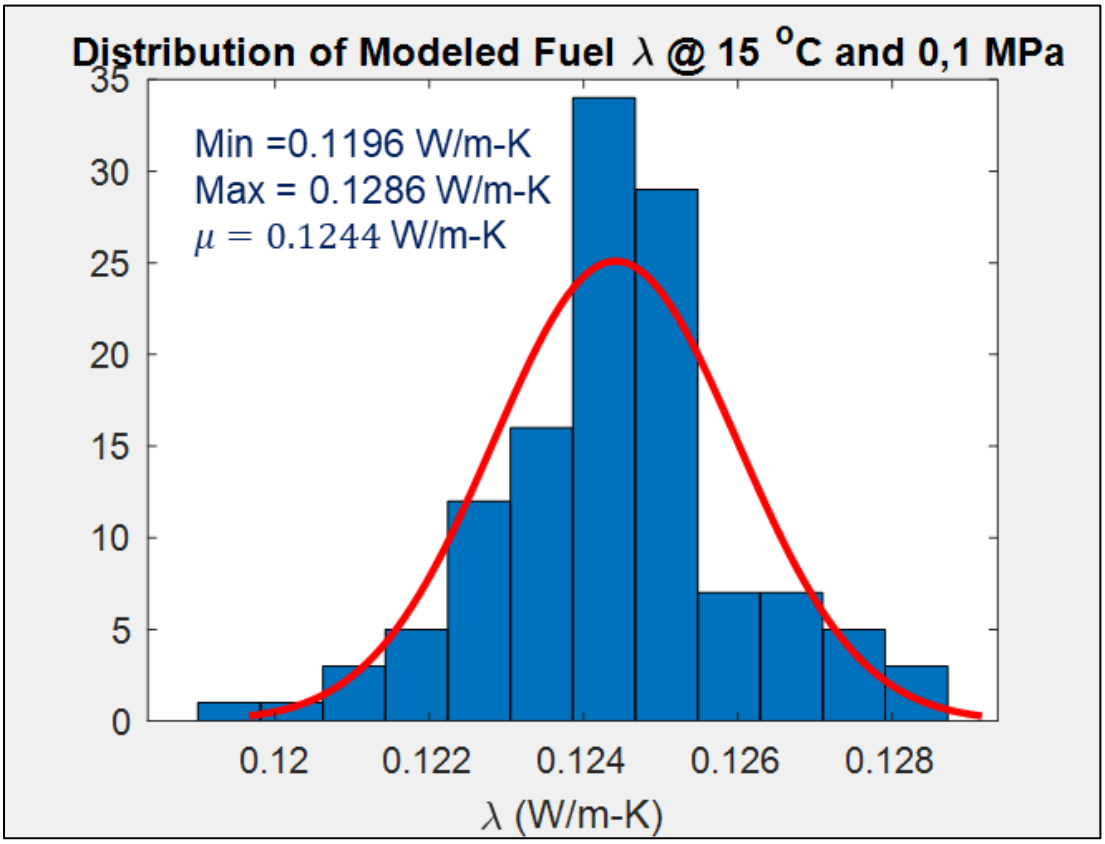

Figure 34: Distribution of modeled thermal conductivity at 15℃ and extreme behavior.

The distribution of modeled viscosity values observed at the specification temperature of −20 ℃ was also tested for also normality. The Chi squared goodness of fit test for normality failed to accept the hypothesis that the data is normally distributed at the 95% confidence level with a p value of 2.7E-5 and hence the observed bounds are provided in **Figure 35.** Fifth order polynomial fits which very closely match the observed curves in the figure were developed to represent

recommended bounds of the modeled values and are provided below with T in ℃ and η in mPa · s.

$$\eta_{low}(T) = (-2.0937\text{E}-10)T^5 + (6.2077E-8)T^4 - (7.5549\text{E}-6)T^3 + (5.4745E-4)T^2 - 0.0324T + 1.6252 \quad (40)$$

$$\eta_{high}(T) = (-5.3484\text{E}-10)T^5 + (1.5881E-7)T^4 - (1.9162\text{E}-5)T^3 + (1.3276E-3)T^2 - (6.6863E-2)T + 2.5452 \quad (41)$$

These expressions should be used with great care as the behavior of these polynomials outside of the temperature range of -20 ℃ to 100 ℃ will not match the physical nature of the fuels and other models should be employed.

The distribution of modeled specific heat values observed at 100 ℃ is shown in **Figure 36**. The Chi squared goodness of fit test for normality failed to reject the hypothesis that the data is normally distributed at the 95% confidence level with a p value of 0.0692 and hence the predicted 99% bounds are provided. Using the same procedure at 15 ℃, the associated 99% bounds and the assumption of linear behavior over the temperature range of interest, the expressions shown below were developed where T is in ℃ and c_p in kj/kg · K.

$$c_{p_{low}} = (3.88E-3)T + 1.942 \quad (42)$$

$$c_{p_{high}} = (3.80E-3)T + 1.980 \quad (43)$$

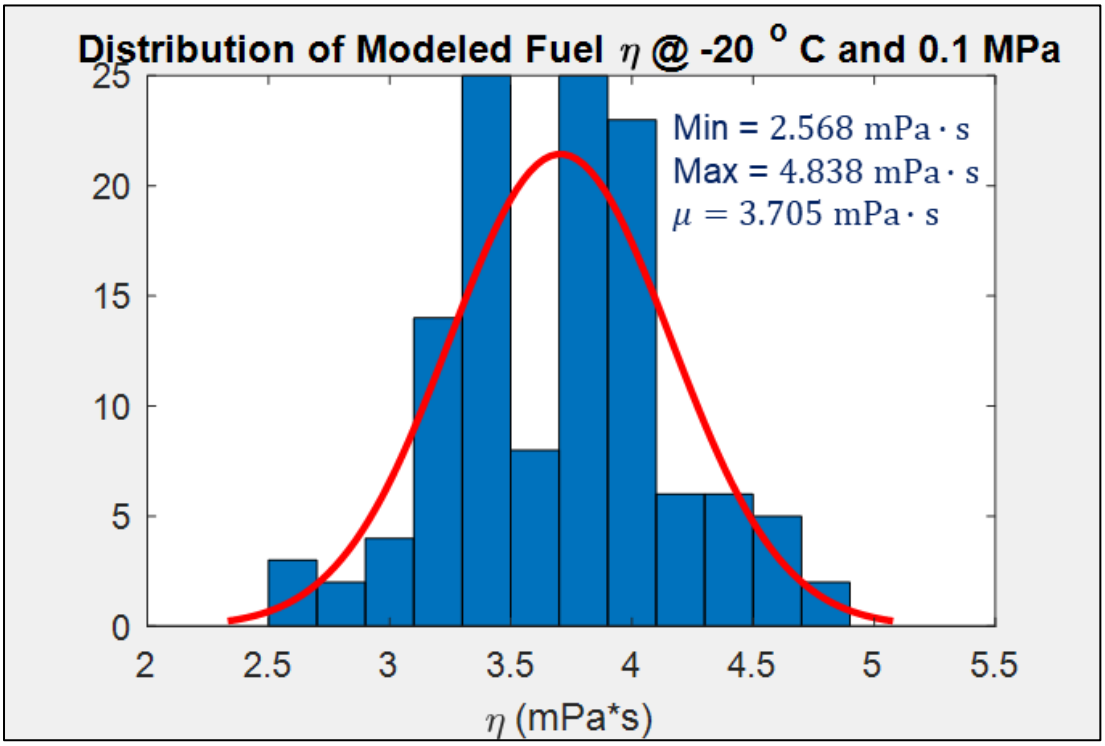

Figure 35: Distribution of modeled viscosity at -20 ℃ and extreme behavior.

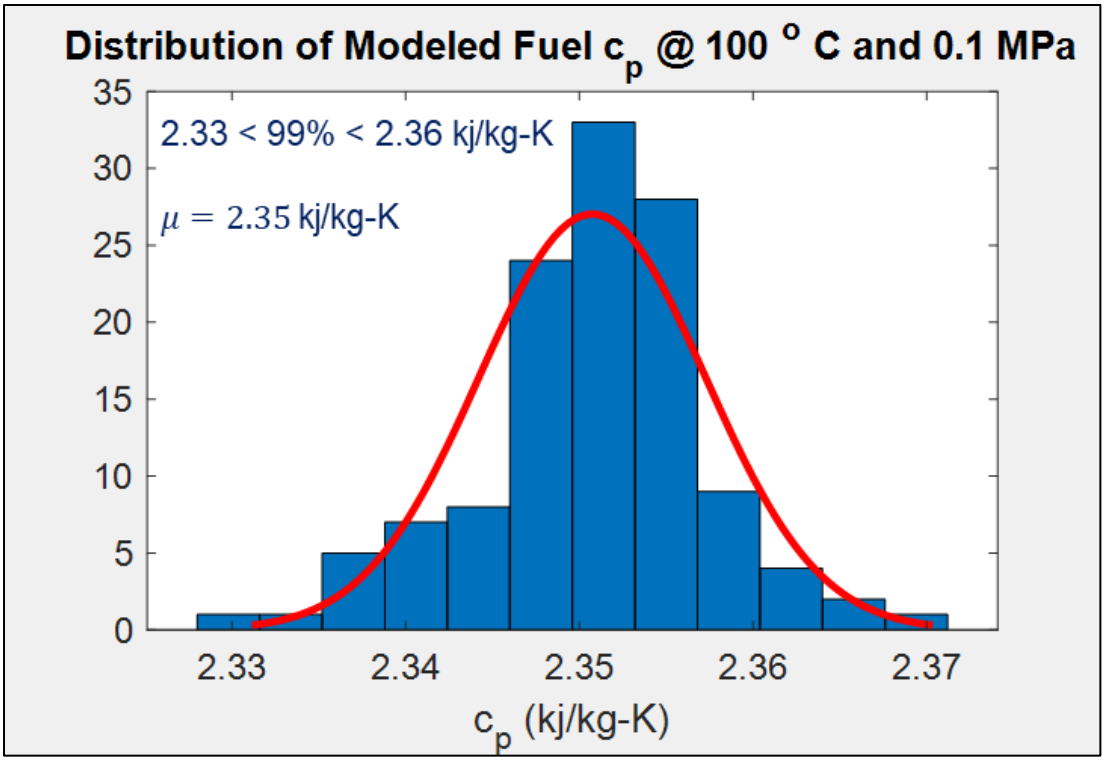

Figure 36: Distribution of modeled specific heat at 100 ℃ and extreme behavior.

To determine the appropriate way to apply these fits, a final bit of analysis was performed to determine the correlation between the properties at −20 ℃. **Figure 37 (a-f)** provides the resulting scatter plots along with the coefficients of determination for the six possible combinations of the properties of interest. Results indicate that there is not a strong reason to treat the properties as dependent on one another and that, where appropriate, 2k factorial analysis or similar may be employed to understand the resulting sensitivity to these property ranges.

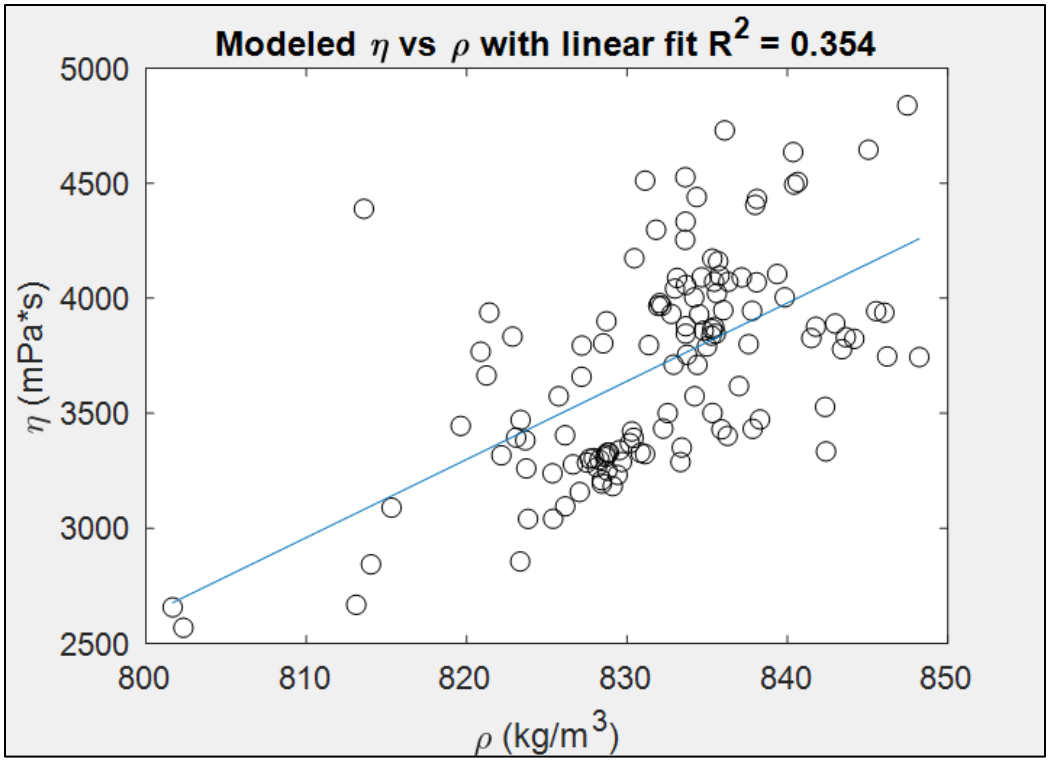

(a) Viscosity vs. density

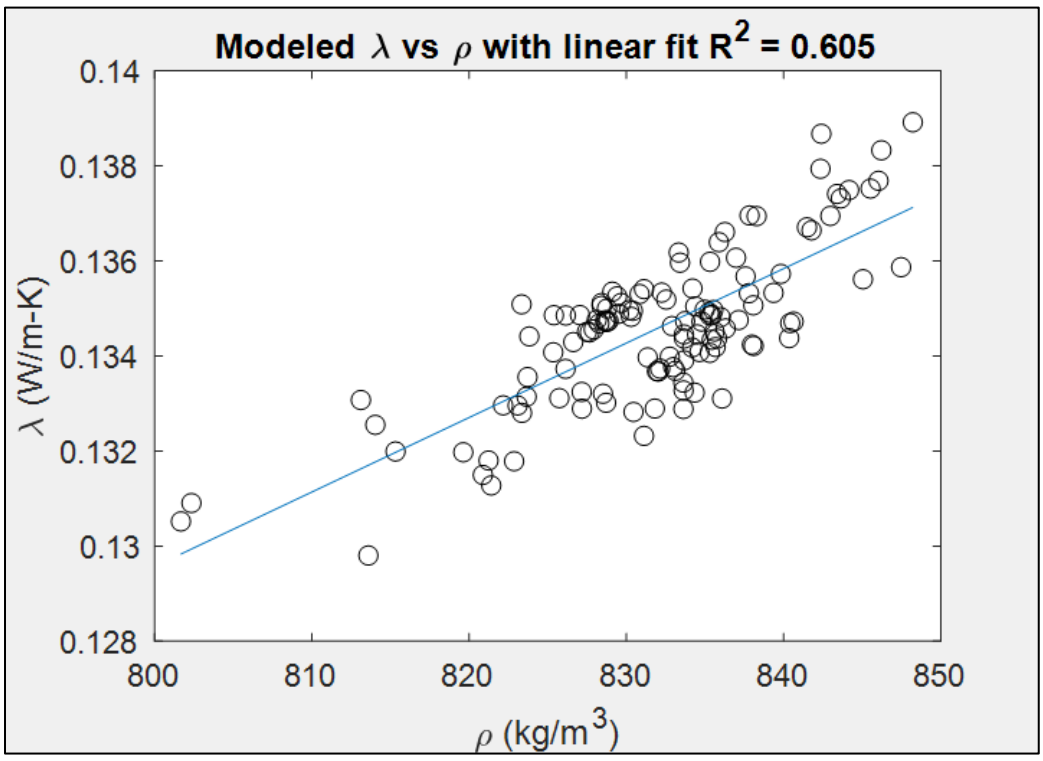

(b) Thermal Conductivity vs. density

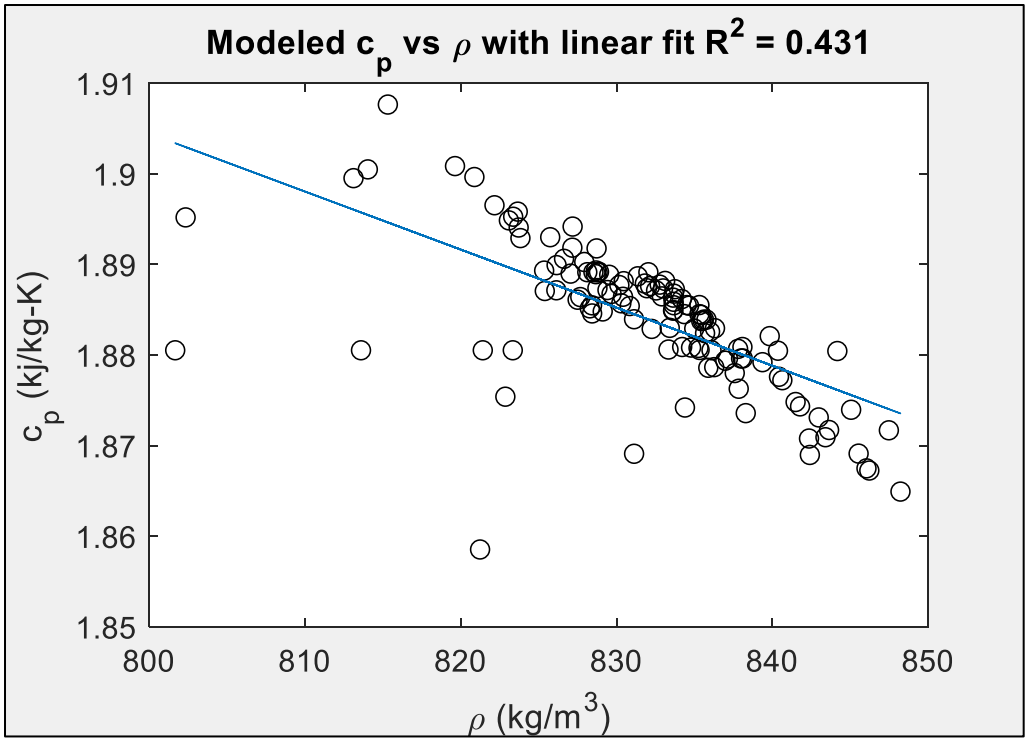

(c) Specific heat vs. density

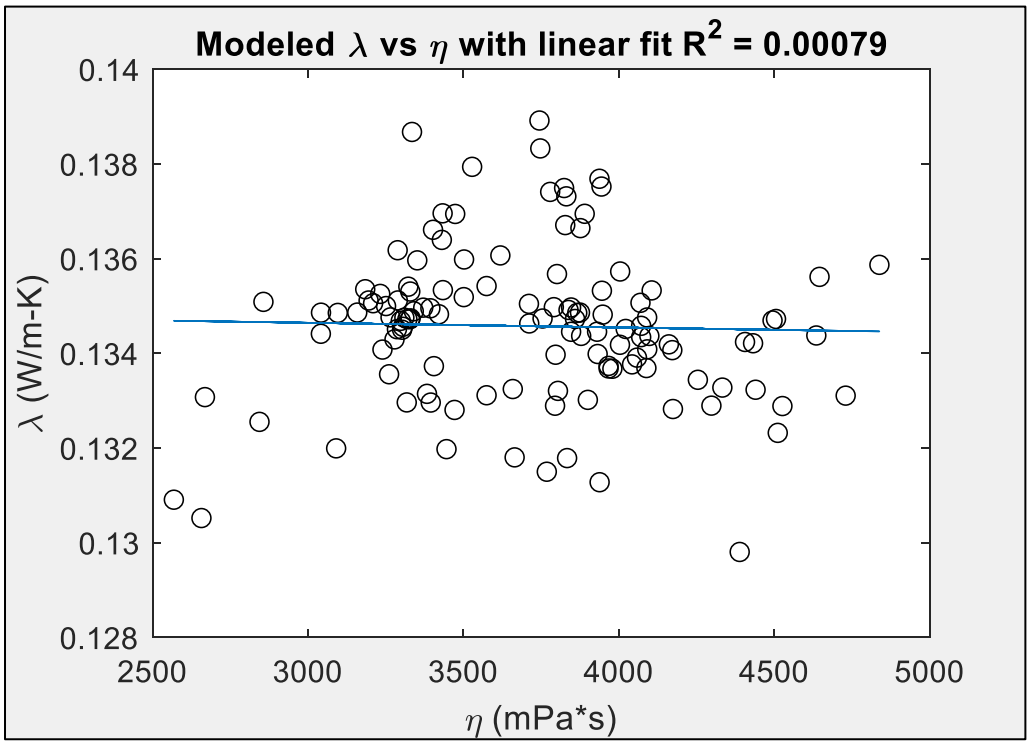

(d) Thermal Conductivity vs. viscosity

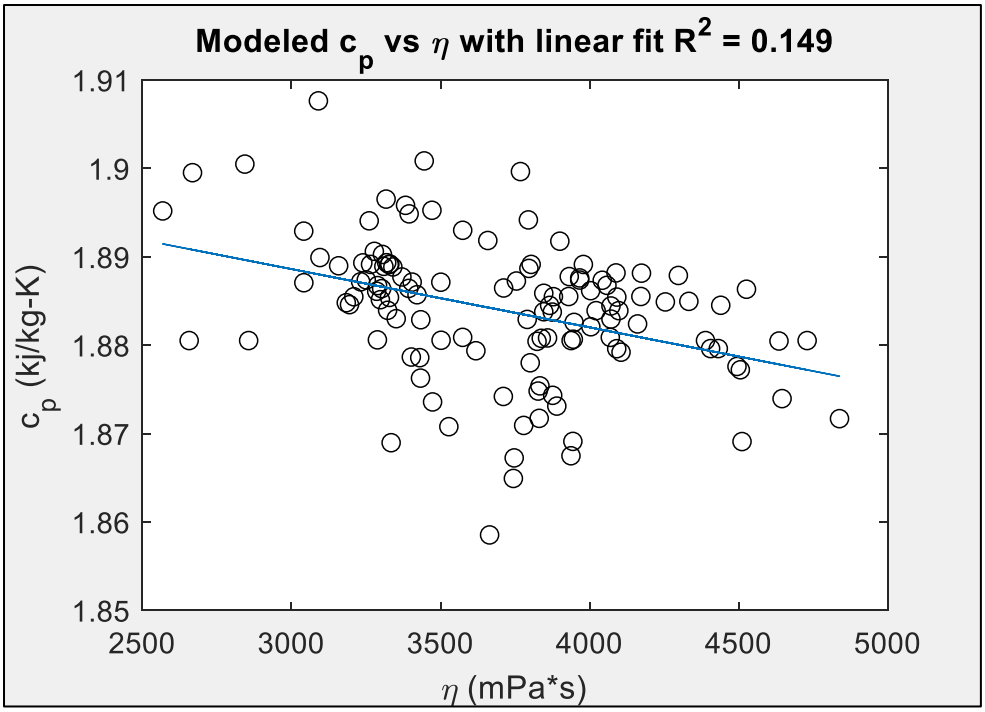

(e) Specific heat vs. viscosity

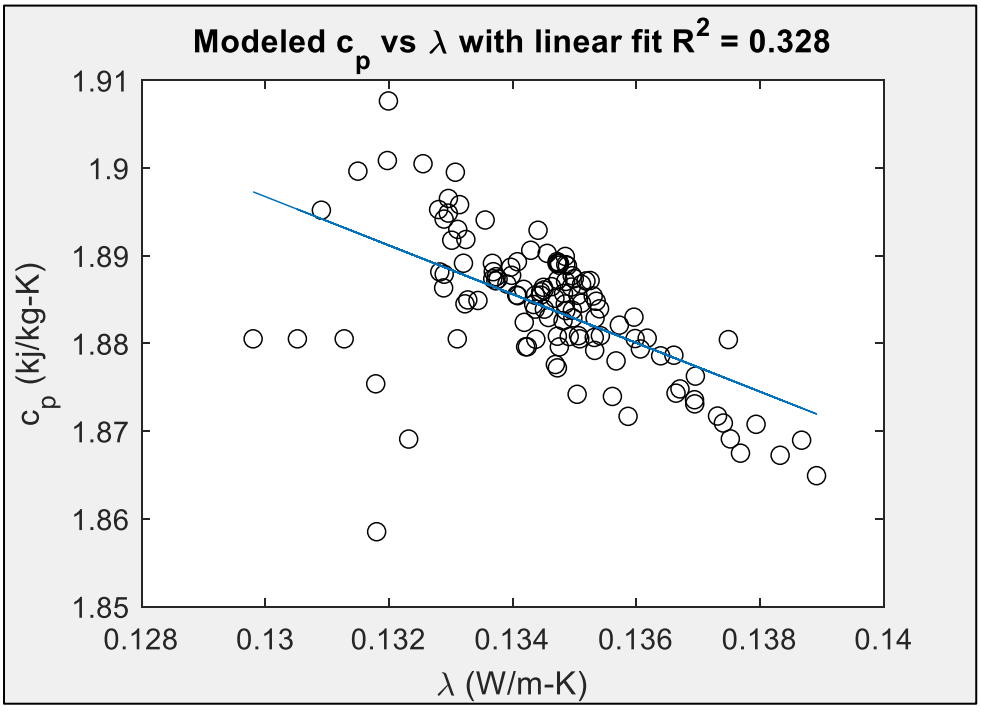

(f) Specific heat vs. thermal conductivity

Figure 37: Correlation between distributions of modeled density, thermal conductivity, viscosity, and specific heat.

8. Conclusion

Beginning with recognition of the trends of increased thermal loading and interactions between fighter aircraft subsystems driving fundamental research within the broad discipline of aircraft thermal management, the present work then connected the established reliance of these thermal management systems on aviation turbine fuel and its respective transport and thermodynamic properties relevant to performance as a heat sink: density, thermal conductivity, viscosity, specific heat, and Prandtl number. Adding the understanding of aviation turbine fuel as broad class of substances of varying composition rather than a singular well defined entity, the work then underscored the interest in connecting the variation in fuel properties with the performance of aircraft thermal management systems which could not be accomplished without understanding a the range of variation of these properties. This is therefore the fundamental question addressed by present effort: defining a practical and informed understanding of the ranges of aviation turbine fuel thermodynamic and transport properties relevant to aircraft thermal management.

The literature reviewed to address the topic spanned (1) works directly concerned with testing the composition and properties of various samples of aviation turbine fuel, (2) works which aimed to utilize physical understanding of relationships between molecular constituents and properties to develop predictive models of behavior, and (3) works which utilized novel computational methods broadly termed as “machine learning” methods which utilized measured fluid property and

compositional data as inputs to black box models which had parameters that were optimized against other measured data. Upon completion of this review, the approach to addressing the research topic was established which required (1) the addition of fuel property and compositional test data, (2) the development of methods to predict the properties of interest using compositional information (data which is easier and cheaper to obtain).

In particular, the methods developed by Rokni et al. 2019 were identified as providing a strong foundational point for computational methods but lacked the overall accuracy required to give confidence in the final result. To overcome this hurdle, the use of a novel machine learning architecture was developed and employed which applied physical models both upstream and downstream of an artificial neural network. This concept was applied to develop models for both viscosity and thermal conductivity of aviation turbine fuels. Additionally, a specific heat model for well-defined hydrocarbon mixtures was developed using a simple modification of the work of Dadgostar and Shaw 2012. All of these models were then compared against data found in the literature as well as that collected for the present study, finding average deviations on the order of (specific heat) or with the limits of (viscosity, thermal conductivity) uncertainty of the test data.

Finally, the 100 GC x GC hydrocarbon compositional samples of aviation turbine fuel collected for the study were entered into the models of thermal conductivity, viscosity, and specific heat develop in the present work and the density model of Rokni et al. 2019 to establish practical bounds of these properties for aviation turbine fuels typically used for aircraft of these type. Analysis of the

resulting distributions against published recommended values for these properties revealed significantly more variation than currently prescribed values as well as somewhat differing values and trends for central tendency. Additional investigation showed little correlation between the properties of interest, drawing the conclusion that the expressions developed to represent the bounds of the properties of interest could be employed independently in future efforts. Finally, the range of Prandtl numbers predicted in over reasonable temperature ranges suggests that for the large variation in heat transfer modes observed within a typical aircraft fuels system, the overall thermal management system performance is expected to be sensitive to the variation in transport and thermodynamic properties of aviation turbine fuel, which could impact the outcomes of missions across flight envelopes.

8.1 Academic Contributions

The present work made contributions to the existing body of knowledge for aircraft thermal management, aviation turbine fuel properties and composition, and predictive modeling of complex mixtures of molecular fluids.

By elucidating the range of aviation turbine fuel properties relevant to aircraft thermal management, higher fidelity studies may be conducted, including a quantification of uncertainty that includes the influence of fuel property variation. Given the arguments of **1.11.1Motivation**, there are many different regimes and time scales of flow and heat transfer within an aircraft fuel system that are expected to be sensitive to the variation of property ranges presented.

With regard to aviation fuel properties and composition, the present effort expanded the existing literature dataset which was comprised of only two fuels (Jet-A-4658 and JP-8-3773) with known hydrocarbon composition and $\rho(T)$, $\eta(T)$, $\lambda(T)$, $c_P(T)$ by adding 4 additional fuels (three JP-5 and one F-24). Each of the fuels tested showed differing compositions and properties from the previous two fuels as well as different central tendency of properties from that expected in the literature. This experimental data should be of interest to future work in fuel property modeling, including specification properties relating to combustion behavior.

In developing a novel approach to predicting transport properties of well-defined molecular fluids, a hybrid physics guided machine learning method was employed for fluid property prediction for the first time within peer-reviewed literature. Along with the novel approach to combined physics based and machine learning architectures, the present effort also established repeatable methods for hyper-parameter optimization within machine learning architectures which were not discussed in the relevant literature explored as part of this effort. These machine learning methods should lay the foundation for more consistent and wide-spread adoption of hybrid machine learning modeling.

Finally, during my time as a PhD student under Dr. Bao Yang, my ability to contribute to the accepted body of knowledge was demonstrated in the form of multiple publications in peer-reviewed literature relevant to the thermal fluids discipline as both a co-author (2-3) and a lead author (1):

(1) W. A. Malatesta and B. Yang, "Aviation Turbine Fuel Thermal Conductivity: A Predictive Approach Using Entropy Scaling-Guided Machine Learning with Experimental Validation," *ACS Omega*, **2021** [111]

(2) B. Zhao, W. Yang, C. Zheng, Y. Pei, W. A. Malatesta, X. Liu and B. Yang, "Experimental Study on Heat Transfer Enhancement by Using Textile Flap Oscillation," *Heat Transfer Engineering*, **2021** [112]

(3) M. Glebocki, W. A. Malatesta, K. McCarthy, N. Jain, "Exergy-based Analysis and Optimization of Complex Aircraft Thermal Management Systems," accepted for: *AIAA SciTech Forum*, San Diego CA, **2022** [113]

8.2 Future Work

Aside from the work directly relevant to aircraft thermal management, including expansions on the works reviewed in section **1.2 Active Research** using approaches similar to Rodriguez et al. 2019 [114], additional areas of logical expansion on the present effort include:

- Expanding the compositional range of the viscosity and thermal conductivity models to verify performance against other hydrocarbon mixtures and potentially include polar molecules such as described by Niklas et al. 2019 [115]

- Conducting a detailed uncertainty analysis on the viscosity, thermal conductivity, and specific heat models with regard to the compositional inputs of hydrocarbons bins citing the variability described in Metz et al. 2019 [74]

- Conducting sensitivity analysis on models of combustion behavior such as employed by Ulcay et al 2019 [116], where several of the properties of interest within the present work are utilized to predict minimum hot surface ignition temperature (MHSIT)

- Application of the overall approach to novel machine learning architectures and selection of hyper-parameters to further refine the predictive capability of models of physical systems in general

APPENDIX A: GCxGC COMPOSITION OF FULL PROPERTY SUITE SAMPLES

Hydrocarbon Type	Atoms/Molecule		MW (g/mol)	Mass %			
	H	C		JP-5-12011	JP-5-18307	JP-5-12553	F-24-13147
n-paraffin C7	16	7	100.20	0.01	0.02	0.00	0.21
n-paraffin C8	18	8	114.23	0.12	0.15	0.00	0.74
n-paraffin C9	20	9	128.26	0.58	0.79	0.02	3.25
n-paraffin C10	22	10	142.28	1.67	3.13	3.60	6.94
n-paraffin C11	24	11	156.31	3.01	7.84	5.39	5.98
n-paraffin C12	26	12	170.34	3.42	6.25	4.39	2.63
n-paraffin C13	28	13	184.36	3.14	3.80	3.44	0.60
n-paraffin C14	30	14	198.39	2.24	1.69	1.97	0.13
n-paraffin C15	32	15	212.42	1.02	0.58	0.51	0.04
n-paraffin C16	34	16	226.44	0.13	0.19	0.06	0.02
n-paraffin C17	36	17	240.47	0.01	0.07	0.01	0.01
n-paraffin C18	38	18	254.50	0.00	0.02	0.01	0.00
n-paraffin C19	40	19	268.52	0.00	0.01	0.00	0.00
n-paraffin C20	42	20	282.55	0.00	0.01	0.00	0.00
n-paraffin C21	44	21	296.58	0.00	0.01	0.00	0.00
n-paraffin C22	46	22	310.60	0.00	0.01	0.00	0.00
n-paraffin C23	48	23	324.63	0.00	0.00	0.00	0.00
n-paraffin C24	50	24	338.66	0.00	0.00	0.00	0.00
n-paraffin C25	52	25	352.68	0.00	0.00	0.00	0.00

n-paraffin C26	54	26	366.71	0.00	0.00	0.00	0.00
n-paraffin C27	56	27	380.74	0.00	0.00	0.00	0.00
n-paraffin C28	58	28	394.76	0.00	0.00	0.00	0.00
n-paraffin C29	60	29	408.79	0.00	0.00	0.00	0.00
n-paraffin C30	62	30	422.82	0.00	0.00	0.00	0.00
i-paraffin C7	16	7	100.20	0.03	0.01	0.05	0.20
i-paraffin C8	18	8	114.23	0.08	0.09	0.05	0.57
i-paraffin C9	20	9	128.26	0.44	0.50	0.50	2.30
i-paraffin C10	22	10	142.28	1.48	2.03	2.67	7.19
i-paraffin C11	24	11	156.31	2.78	5.90	5.64	8.02
i-paraffin C12	26	12	170.34	3.75	7.32	5.47	4.99
i-paraffin C13	28	13	184.36	4.57	5.99	5.31	2.39
i-paraffin C14	30	14	198.39	4.17	3.65	4.11	0.61
i-paraffin C15	32	15	212.42	3.11	1.77	2.24	0.08
i-paraffin C16	34	16	226.44	1.39	0.60	0.62	0.02
i-paraffin C17	36	17	240.47	0.07	0.08	0.00	0.00
i-paraffin C18	38	18	254.50	0.01	0.03	0.00	0.00
i-paraffin C19	40	19	268.52	0.00	0.01	0.00	0.00
i-paraffin C20	42	20	282.55	0.00	0.00	0.00	0.00
i-paraffin C21	44	21	296.58	0.00	0.00	0.00	0.00
i-paraffin C22	46	22	310.60	0.00	0.00	0.00	0.00
i-paraffin C23	48	23	324.63	0.00	0.00	0.00	0.00
i-paraffin C24-C31	57	27.5	387.75	0.00	0.00	0.00	0.00
monocyclo-paraffin C6 - C7	13	6.5	91.17	0.02	0.00	0.00	0.26
monocyclo-paraffin C8	16	8	112.21	0.28	0.19	0.00	2.21
monocyclo-paraffin C9	18	9	126.24	1.07	0.69	0.74	5.43
monocyclo-paraffin C10	20	10	140.27	2.41	2.29	4.07	9.35
monocyclo-paraffin C11	22	11	154.29	3.99	4.72	5.54	7.82
monocyclo-paraffin C12	24	12	168.32	5.79	4.93	5.77	4.50

monocyclo-paraffin C13	26	13	182.35	5.63	3.40	4.50	1.47
monocyclo-paraffin C14	28	14	196.37	4.24	1.76	2.74	0.02
monocyclo-paraffin C15	30	15	210.40	2.43	0.73	1.02	0.00
monocyclo-paraffin C16	32	16	224.43	0.46	0.03	0.04	0.00
monocyclo-paraffin C17	34	17	238.45	0.00	0.00	0.00	0.00
monocyclo-paraffin C18	36	18	252.48	0.00	0.00	0.00	0.00
monocyclo-paraffin C19	38	19	266.51	0.00	0.00	0.00	0.00
monocyclo-paraffin C20	40	20	280.53	0.00	0.00	0.00	0.00
monocyclo-paraffin C21	42	21	294.56	0.00	0.00	0.00	0.00
monocyclo-paraffin C22-C26	48	24	336.64	0.00	0.00	0.00	0.00
dicyclo-paraffin C8	14	8	110.20	0.01	0.01	0.00	0.04
dicyclo-paraffin C9	16	9	124.22	0.25	0.10	0.13	0.97
dicyclo-paraffin C10	18	10	138.25	1.38	0.92	1.78	3.49
dicyclo-paraffin C11	20	11	152.28	2.77	2.06	2.96	3.23
dicyclo-paraffin C12	22	12	166.30	3.64	1.70	2.74	1.24
dicyclo-paraffin C13	24	13	180.33	4.86	1.43	2.65	0.18
dicyclo-paraffin C14	26	14	194.36	2.53	0.41	1.08	0.00
dicyclo-paraffin C15	28	15	208.38	0.54	0.01	0.00	0.00
dicyclo-paraffin C16	30	16	222.41	0.00	0.00	0.00	0.00
dicyclo-paraffin C17	32	17	236.44	0.00	0.00	0.00	0.00

dicyclo-paraffin C18	34	18	250.46	0.00	0.00	0.00	0.00
dicyclo-paraffin C19-25	42	22	306.57	0.00	0.00	0.00	0.00
tricyclo-paraffin C10	16	10	136.23	0.01	0.00	0.02	0.02
tricyclo-paraffin C11	18	11	150.26	0.04	0.02	0.04	0.05
tricyclo-paraffin C12	20	12	164.29	0.12	0.02	0.06	0.00
tricyclo-paraffin C13	22	13	178.31	0.46	0.04	0.01	0.00
tricyclo-paraffin C14	24	14	192.34	0.30	0.00	0.00	0.00
tricyclo-paraffin C15	26	15	206.37	0.05	0.00	0.00	0.00
tricyclo-paraffin C16	28	16	220.39	0.00	0.00	0.00	0.00
tricyclo-paraffin C17	30	17	234.42	0.00	0.00	0.00	0.00
tricyclo-paraffin C18	32	18	248.45	0.00	0.00	0.00	0.00
tricyclo-paraffin C19	34	19	262.47	0.00	0.00	0.00	0.00
tricyclo-paraffin C20	36	20	276.50	0.00	0.00	0.00	0.00
C00-benzene C6	6	6	78.11	0.00	0.00	0.00	0.01
C01-toluene C7	8	7	92.14	0.02	0.03	0.00	0.18
C02-benzene C8	10	8	106.17	0.32	0.37	0.05	1.24
C03-benzene C9	12	9	120.19	1.28	1.87	1.80	4.15
C04-benzene C10	14	10	134.22	1.90	4.11	3.32	3.28
C05-benzene C11	16	11	148.25	2.00	4.00	2.76	1.73
C06-benzene C12	18	12	162.27	1.97	2.66	2.06	0.61
C07-benzene C13	20	13	176.30	1.37	1.12	1.14	0.01

C08-benzene C14	22	14	190.33	0.97	0.49	0.60	0.00
C09-benzene C15	24	15	204.35	0.29	0.10	0.00	0.00
C10-benzene C16	26	16	218.38	0.00	0.01	0.00	0.00
C11-benzene C17	28	17	232.41	0.00	0.00	0.00	0.00
C12-benzene C18	30	18	246.43	0.00	0.00	0.00	0.00
C13-benzene C19	32	19	260.46	0.00	0.00	0.00	0.00
C14-benzene C20 to C18-benzene C24	38	22	302.54	0.00	0.00	0.00	0.00
cycloaromatic C9	10	9	118.18	0.03	0.04	0.06	0.04
cycloaromatic C10	12	10	132.20	0.78	1.09	0.60	0.53
cycloaromatic C11	14	11	146.23	2.17	1.89	1.74	0.57
cycloaromatic C12	16	12	160.26	2.40	1.31	1.60	0.15
cycloaromatic C13	18	13	174.28	1.54	0.58	0.95	0.00
cycloaromatic C14	20	14	188.31	0.54	0.17	0.21	0.00
cycloaromatic C15	22	15	202.34	0.03	0.00	0.00	0.00
cycloaromatic C16	24	16	216.36	0.01	0.00	0.00	0.00
cycloaromatic C17-21	26	17	230.39	0.00	0.00	0.00	0.00
Diaromatics C10	8	10	128.17	0.10	0.27	0.11	0.10
Diaromatics C11	10	11	142.20	0.44	0.73	0.38	0.13
Diaromatics C12	12	12	156.22	0.76	0.79	0.52	0.04
Diaromatics C13	14	13	170.25	0.25	0.30	0.12	0.00

Diaromatics C14	16	14	184.28	0.03	0.05	0.02	0.00
Diaromatics C15	18	15	198.30	0.00	0.00	0.00	0.00
Diaromatics C16	20	16	212.33	0.00	0.00	0.00	0.00
Diaromatics C17 - C20	25	18.5	247.40	0.02	0.01	0.00	0.00
triaromatics C14-C18	14	16	206.28	0.06	0.00	0.00	0.00
Light Hydrocarbon Compounds	14	6	86.18	0.18	0.00	0.00	0.03

APPENDIX B: DENSTIY, VISCOSITY, SPECIFIC HEAT, AND THERMAL CONDUCTIVITY OF FULL PROPERTY SUITE SAMPLES AT 0.1 MPa

Fuel Sample	Temp. (°C)	ρ (kg/m^3)	η ($\mu Pa \cdot s$)	c_p (kj/kg · K)	λ (W/m · K)
JP-5-12011	-20	845.8	5128.943	-	0.1258
	-10	838.6	3948.32	-	0.1238
	0	831.3	3096.055	-	0.1218
	10	824.0	2468.106	1.958	0.1199
	20	816.7	1996.831	2.018	0.1179
	30	809.5	1637.199	2.075	0.1159
	40	802.2	1358.584	2.138	0.1140
	50	794.9	1139.745	2.207	0.1120
	60	787.7	965.6821	2.270	0.1100
	70	780.4	825.6312	2.322	0.1081
	80	773.1	711.7477	2.361	0.1061
	90	765.9	618.2354	2.392	0.1041
	100	758.6	540.7559	2.412	0.1022
	110	-	-	2.439	-
	120	-	-	2.481	-
	130	-	-	2.522	-
JP-5-18307	-20	826.8	3777.104	-	0.1318
	-10	819.4	2967.802	1.898	0.1296
	0	812.0	2371.694	1.961	0.1275
	10	804.6	1924.188	2.013	0.1254
	20	797.3	1582.432	2.058	0.1232
	30	789.9	1317.36	2.122	0.1211
	40	782.5	1108.851	2.181	0.1190
	50	775.1	942.7203	2.235	0.1168
	60	767.8	808.7943	2.295	0.1147
	70	760.4	699.6644	2.331	0.1126
	80	753.0	609.8574	2.367	0.1105
	90	745.7	535.2761	2.404	0.1083
	100	738.3	472.8161	2.445	0.1062
	110	-	-	2.486	-
	120	-	-	2.551	-
	130	-	-	2.602	-

JP-5-12553	-20	830.5	4007.17	-	-
	-10	823.1	3137.563	-	-
	0	815.8	2499.247	2.058	0.1249
	10	808.4	2021.591	2.109	0.1228
	20	801.1	1657.898	2.153	0.1207
	30	793.7	1376.597	2.199	0.1186
	40	786.4	1155.901	2.245	0.1165
	50	779.0	980.4901	2.290	0.1144
	60	771.7	839.4085	2.340	0.1123
	70	764.3	724.6974	2.393	0.1102
	80	757.0	630.4908	2.443	0.1080
	90	749.6	552.4076	2.498	0.1059
	100	742.3	487.135	2.555	0.1038
	110	-	-	2.619	-
	120	-	-	2.665	-
	130	-	-	2.058	-
F-24-13147	-20	811.6	2312.538	1.982075	-
	-10	804.0	1876.732	1.982075	-
	0	796.4	1545.32	1.982075	0.1235
	10	788.8	1289.034	1.982075	0.1212
	20	781.2	1087.827	1.982075	0.1188
	30	773.6	927.6835	1.982075	0.1165
	40	766.0	798.6278	1.982075	0.1142
	50	758.5	693.4384	1.982075	0.1119
	60	750.9	606.807	1.982075	0.1096
	70	743.3	534.7767	1.982075	0.1072
	80	735.7	474.3591	1.982075	0.1049
	90	728.1	423.2703	1.982075	0.1026
	100	720.5	379.7454	1.982075	0.1003
	110	-	-	2.619	-
	120	-	-	2.665	-
	130	-	-	2.058	-

APPENDIX C: COMPOSITIONAL RANGE DATASET

Fuel Sample	$\overline{MW}$ (g/mol)	HN/CN	$\alpha_{mixture}$	Temp. (°C)	Pressure (MPa)	η $(\mu Pa \cdot s)$
F-24-12360	159.5112	1.96798	0.211941	-20	0.1	4477
F-24-12843	162.6971	1.920615	0.208815	-20	0.1	4488
F-24-12910	153.3323	1.941556	0.20999	-20	0.1	2492.4
F-24-12946	163.6345	1.928736	0.209217	-20	0.1	4390.2
F-24-12953	164.8819	1.936792	0.209649	-20	0.1	4547.2
F-24-12974	166.7527	1.935841	0.209603	-20	0.1	4634.1
F-24-12977	162.9175	1.933022	0.209357	-20	0.1	4035
F-24-12979	164.3824	1.946798	0.210241	-20	0.1	4287.7
F-24-12981	165.7217	1.93637	0.209687	-20	0.1	4379.4
F-24-12983	161.0806	1.937946	0.209504	-20	0.1	3783.5
F-24-12985	147.4938	1.986035	0.212383	-20	0.1	2528
F-24-12987	155.3964	1.967853	0.211415	-20	0.1	3188
F-24-12989	155.1287	1.970597	0.211524	-20	0.1	3184
F-24-12991	160.2045	1.882206	0.206255	-20	0.1	4013.1
F-24-12993	155.0994	1.943411	0.210074	-20	0.1	3308.7
F-24-12995	163.7958	1.93801	0.20969	-20	0.1	4201.6
F-24-12997	156.4818	1.968816	0.21143	-20	0.1	3096.6
F-24-12999	163.0985	1.946735	0.21012	-20	0.1	3939.6
F-24-13001	154.3632	1.973401	0.211594	-20	0.1	2923
F-24-13003	159.1725	1.914698	0.208161	-20	0.1	3735.2
F-24-13005	162.686	1.942307	0.209776	-20	0.1	3944.5
F-24-13007	161.9926	1.940147	0.209752	-20	0.1	3944.5
F-24-13009	156.8479	1.918796	0.208407	-20	0.1	3470.1
F-24-13011	161.9499	1.949449	0.210259	-20	0.1	3939.6
F-24-13013	159.8705	1.92322	0.208762	-20	0.1	3811.7
F-24-13015	159.8305	1.89944	0.207264	-20	0.1	3821.1
F-24-13017	158.5379	1.957941	0.210833	-20	0.1	3524.4
F-24-13019	160.3108	1.965649	0.211174	-20	0.1	3591
F-24-13021	159.7507	1.903201	0.207577	-20	0.1	3902.4
F-24-13023	161.4176	1.957636	0.210849	-20	0.1	3854.4
F-24-13025	156.5235	1.924006	0.20864	-20	0.1	3296.4
F-24-13027	161.2968	1.945301	0.210027	-20	0.1	3774.1
F-24-13029	159.7884	1.947899	0.210193	-20	0.1	3693.8
F-24-13031	158.5143	1.940913	0.209772	-20	0.1	3613.5
F-24-13033	167.702	1.940641	0.209923	-20	0.1	4796.7
F-24-13035	161.7899	1.944544	0.210006	-20	0.1	3949.4

F-24-13037	162.6556	1.918296	0.208599	-20	0.1	4314.2
F-24-13039	159.3055	1.930048	0.209243	-20	0.1	3627
F-24-13041	162.5813	1.943763	0.209882	-20	0.1	3864
F-24-13043	162.0549	1.933237	0.209333	-20	0.1	3959.2
F-24-13046	152.3271	1.886508	0.206617	-20	0.1	3252
F-24-13057	155.1469	1.89212	0.207	-20	0.1	3500.2
F-24-13061	155.6813	1.943057	0.209626	-20	0.1	3360
F-24-13064	152.656	1.949846	0.210474	-20	0.1	4416.5
F-24-13073	166.712	1.913285	0.208399	-20	0.1	4832.1
F-24-13074	166.8062	1.912287	0.208343	-20	0.1	4832.1
F-24-13079	161.8156	1.94388	0.209999	-20	0.1	3954.3
F-24-13277	160.3116	1.888065	0.206611	-20	0.1	4320.77
F24-13333	158.3376	1.903412	0.20812	-20	0.1	4120
F-24-13901	160.3104	1.930711	0.209107	-20	0.1	3747.458
F-24-13904	159.056	1.896386	0.207183	-20	0.1	3147.61
F-24-13905	154.7429	1.930973	0.209223	-20	0.1	2837.669
F-24-13907	157.6932	1.873396	0.205853	-20	0.1	3861.585
F-24-13908	154.157	1.908585	0.207907	-20	0.1	3398.974
Jet A-10325	158.9772	1.943976	0.20971	-20	0.1	3778.8
Jet A-11721	166.0303	1.920663	0.208785	-20	0.1	4902
Jet A-11769	154.7017	1.901997	0.207579	-20	0.1	3409.7
Jet A-11821	166.2856	1.920798	0.208779	-20	0.1	5065.4
Jet A-12784	160.1832	1.924082	0.208942	-20	0.1	3988.6
Jet A-12831	168.1024	1.922963	0.208799	-20	0.1	5134.5
Jet A-13065	165.5622	1.945786	0.210187	-20	0.1	3078
Jet A-13067	158.4168	1.892769	0.206957	-20	0.1	3830.5
Jet A-13208	153.186	1.937848	0.20979	-20	0.1	3055.2
Jet A-13224	151.5164	1.936487	0.209627	-20	0.1	3055.2
Jet A-13385	153.097	1.940913	0.209964	-20	0.1	3135.6
Jet A-1-13047	160.2139	1.934946	0.20934	-20	0.1	3788.2
Jet A-1-13048	162.6507	1.934599	0.209571	-20	0.1	4125.9
Jet A-1-13071	153.8519	1.916965	0.208241	-20	0.1	3047.6
Jet A-1-13077	151.9976	1.943333	0.209898	-20	0.1	2775.5
Jet A-1-13906	153.3363	1.940376	0.209653	-20	0.1	3725.244
JP-8-10264	151.8109	2.009855	0.213372	-20	0.1	2730
JP-8-13045	152.8602	1.941888	0.209767	-20	0.1	2945.2
JP-8-13049	160.9295	1.983139	0.212416	-20	0.1	3675.4
JP-8-13050	149.5451	1.961638	0.210696	-20	0.1	2600.4
JP-8-13051	153.3407	1.953038	0.21037	-20	0.1	2934.1
JP-8-13052	150.1625	1.952141	0.210206	-20	0.1	2689.4
JP-8-13053	152.6903	1.949548	0.210141	-20	0.1	2858.4

JP-8-13054	153.5805	1.949851	0.210172	-20	0.1	2937.8
JP-8-13055	149.329	1.943027	0.21002	-20	0.1	2800
JP-8-13056	153.5995	1.949774	0.210194	-20	0.1	2930.4
JP-8-13058	151.2531	1.93616	0.209482	-20	0.1	2876.4
JP-8-13059	147.8133	1.907789	0.2076	-20	0.1	2723.4
JP-8-13060	156.7048	1.986441	0.212467	-20	0.1	3164
JP-8-13062	151.0978	1.948978	0.210147	-20	0.1	2858.4
JP-8-13063	152.4265	1.922546	0.208622	-20	0.1	2963.7
JP-8-13066	155.3928	1.922679	0.208649	-20	0.1	3212
JP-8-13068	153.235	1.965157	0.211139	-20	0.1	2851.2
JP-8-13069	153.0915	1.954049	0.210491	-20	0.1	2854.8
JP-8-13070	153.6704	1.948647	0.210109	-20	0.1	2937.8
JP-8-13072	154.368	1.941027	0.209824	-20	0.1	3112.2
JP-8-13075	154.0513	1.945439	0.209941	-20	0.1	2941.5
JP-8-13076	153.4628	1.950291	0.210192	-20	0.1	2934.1
JP-8-13078	157.5899	1.961824	0.21111	-20	0.1	3347.4
JP-8-13215	152.3769	1.944959	0.209994	-20	0.1	2865.6
JP-8-13332	158.9301	1.922921	0.207269	-20	0.1	2613.6
JP-8-13902	153.3861	1.932083	0.209086	-20	0.1	2854.43

References

[1] Office of Naval Research, "Naval Air Warfare and Weapons," U. S. Navy, Arlington, VA, 2017.

[2] Congressional Resaerch Service, "Air Force Next Generation Air Dominance Program: An Introduction," Congressional Resaerch Service, Washington, D. C., 2020.

[3] A. Kusko, "Thermal consideration of generators in high-speed aircraft," *Transactions of the American Institute of Electrical Engineers, Part II: Applications and Industry,* vol. 76, no. 4, pp. 205-208, 1957.

[4] B. J. German, "Tank Heating Model for Aircraft Fuel Thermal System with Recirculation," *J. of Propulsion and Power,* vol. 28, no. 1, pp. 204-210, 2012.

[5] M. F. Ahlers, Aircraft thermal management : systems architectures, SAE International, 2016.

[6] M. W. Oppenheimer, D. O. Sigthorsson and D. B. Doman, "Control of Fuel Thermal Management," in *AIAA SciTech Forum,* San Diego, 2019.

[7] F. T. C. Yuen, J. J. Liang, N. G. Young, S. Oskooei, S. Sreekanth and O. L. Gulder, "Novel Experimental Approach to Studying the Thermal Stability and Coking Propensity of Jet Fuel," *Energy & Fuels,* vol. 31, no. 4, pp. 3585-3591, 2017.

[8] R. Langton, C. Clark, M. Hewitt and L. Richards, Aircraft Fuel Systems, John Wiley & Sons, 2009.

[9] United States Department of Defense, "PERFORMANCE SPECIFICATION COOLANT FLUID, HYDROLYTICALLY STABLE, DIELECTRIC," United States Department of Defense, Washington, D. C., 2015.

[10] U. S. A. Force, F-16A/B Flight Manual Blocks 10 and 15, Hill AFB: United States Air Force, 2003.

[11] U. S. D. o. t. Navy, Naval Air Training and Operating Procedures Standardization Navy Model F/A-18 E/F, Patuxent River, 2017.

[12] W. E. Harrison, K. Binns, S. D. Anderson and R. W. Morris, "High Heat Sink Fuels for Improved Aircraft THermal Management," *SAE Transactions,* vol. 102, pp. 709-718, 1993.

[13] Y. Ho, T. Lin, B. P. Hill and G. B. Tibbs, "Thermal Benefits of Advanced Integrated Fuel System Using JP-8+100 Fuel," in *World Aviation Congress & Exposition AIAA*, Reston, VA, 1997.

[14] S. P. Heneghan, S. Zabarnick, D. R. Ballal and W. E. Harrison, "JP-8+100—The Development of High Thermal Stability Jet Fuel," in *AIAA 34th Aerospace Sciences Meeting and Exhibit AIAA*, Reston, VA, 1996.

[15] D. J. Luning Prak, P. J. Luning Prak, P. Trulove and J. S. Cowart, "Formulation of Surrogate Fuel Mixtures Based on Physical and Chemical

Analysis of Hydrodepolymerized Cellulosic Diesel Fuel," *Energy and Fuels*, vol. 30, no. 9, pp. 7331-7341, 2016.

[16] United States Department of Defense, *MIL-DTL-5624W Detail Specification: Turbine Fuel, Aviation, Grades JP-4 and JP-5*, Washington D. C.: United States Government, 2016.

[17] United States Department of Defense, *MIL-DTL-83133J Detail Specification: Turbine FUel, Aviation, Kerosene Type, JP-8(NATO F-34), NATO F-35, and JP-8+100 (NATO F-37)*, Washington D. C.: United States Government, 2015.

[18] North Atlantic Treaty Organization (NATO), "ALFP-3747 GUIDE SPECIFICATIONS (MINIMUM QUALITY STANDARDS) FOR AVIATION TURBINE FUELS (F-24, F-27, F-34, F-35, F-37, F-40 AND F-44)," North Atlantic Treaty Organization (NATO), Brussels, 2017.

[19] American Society for Testing and Materials (ASTM), "D1655 Standard Specification for Aviation Turbine Fuels," ASTM International, West Conshohocken, PA, 2020.

[20] E. Walters and S. Iden, "INVENT Modeling, Simulation, Analysis and Optimization," in *48th AIAA Aerospace Sciences Meeting*, Orlando Florida, 2010.

[21] R. A. Roberts, S. M. Eastbourn and A. C. Maser, "Generic Aircraft Thermal Tip-to-Tail Modeling and Simulation," in *47th AIAA/ASME/SAE/ASEE Joint Propulsion Conference & Exhibit*, San Diego, CA, 2011.

[22] M. W. Oppenheimer, D. O. Sigthorsson and D. B. Doman, "Extending Aircraft Thermal Endurance by Fuel Pump Sizing," in *AIAA Guidance, Navigation, and Control Conference* , Kissimmee, Florida, 2018.

[23] A. Donovan, Vehicle Level Transient Aircraft Thermal Management Modeling and Simulation, Dayton, OH: Wright State University, 2016.

[24] H. C. Pangborn, J. Hey, T. Deppen, A. Alleyne and T. Fisher, "Hardware-in-the-loop Validation of Advanced Fuel Thermal Management Control," *Journal of THermophysics and Heat Transfer*, vol. 31, no. 4, pp. 901-909, 2017.

[25] D. B. Doman, "Fuel Flow Topology and Control for Extending Aircraft Thermal Endurance," *J. of Thermophysics and Heat Transfer*, vol. 32, no. 1, pp. 35-50, 2018.

[26] J. N, Thermodynamics-based optimization and control of integrated energy systems, Urbana-Champaign, IL: University of Illinois at Urbana-Champaign, 2013.

[27] P. D. Pearce, S. Seto, P. Dom, C. Moses and R. Alvarez, "JP-8+100 Engine Demonstration," Air Force Research Laboratory, Dayton, OH, 2002.

[28] K. L. Berrier, C. E. Freye, M. C. Billingsly and R. E. Synovec, "Predictive Modeling of Aerospace Fuel Properties Using Comprehensive Two-Dimensional Gas Chromatography with Time-Of-Flight Mass Spectrometry

and Partial Least Squares Analysis," *Energy&Fuels*, vol. 34, pp. 4084-4094, 2020.

[29] K. McCarthy, "Probabilistic Design of Fuel Thermal Management Systems," United States Small Business Association, 2017.

[30] J. E. Hesselgreaves, Compact Heat Exchangers - Selection, Design, and Operation, Oxford, UK: Elsevier, 2001.

[31] T. Bergman, A. Lavine, F. Incropera and D. Dewitt, Fundamentals of Heat and Mass Transfer, John Wiley & Sons, 2011.

[32] T. Bruno, A. Laesecke, S. Outcalt, H.-D. Seelig and B. Smith, "Properties of a 50/50 Mixture of Jet-A + S-8," National Institute of Standards Interagency/Internal Report (NISTIR), Washington D. C., 2007.

[33] M. L. Huber, E. W. Lemmon and T. J. Bruno, "Surrogate Mixture Models for the Thermophysical Properties of Aviation Fuel Jet-A," *Energy & Fuels*, vol. 24, p. 35653571, 2010.

[34] T. Bruno, M. Huber, A. Laesecke, E. Lemmon, M. McLinden, S. Outcalt, R. Perkins, B. Smith and J. Widegren, "Thermodynamic, Transport, and Chemical Properties of "Reference" JP-8," National Institute of Standards Interagency/Internal Report (NISTIR), Washington D. C., 2010.

[35] W. Affens, J. Hall, S. Holt and R. Hazlett, "Effect of composition on freezing points of model hydrocarbon fuels," *Fuel*, vol. 63, no. 4, pp. 543-547, 1984.

[36] M. L. Huber, E. W. Lemmon, L. S. Ott and T. J. Bruno, "Preliminary Surrogate Mixture Models for the Thermophysical Properties of Rocket Propellants RP-1 and RP-2," *Energy & Fuels*, vol. 23, pp. 3083-3088, 2009.

[37] S. Outcalt, A. Laesecke and M. B. Freund, "Density and Speed of Sound Measurements of Jet A and S-8 Aviation Turbine Fuels," *Energy & Fuels*, vol. 23, pp. 1626-1633, 2009.

[38] Coordniated Research Council, "World Fuel Sampling Program, CRC Report 663," Alpharetta, Georgia, 2014.

[39] S. Outcalt, A. Laesecke and K. Brumback, "Comparison of Jet Fuels by Measurements of Density and Speed of Sound of a Flightline JP-8," *Energy & Fuels*, vol. 24, p. 5573–5578, 2010.

[40] S. L. Outcalt and T. J. Fortin, "Density and Speed of Sound Measurements of Two Synthetic Aviation Turbine Fuels," *Journal of Chemical and Engineering Data*, vol. 56, p. 3201–3207, 2011.

[41] S. L. Outcalt and T. J. Fortin, "Density and Speed of Sound Measurements of Four Bioderived Aviation Fuels," *Journal of Chemical and Engineering Data*, vol. 57, p. 2869−2877, 2012.

[42] T. J. Bruno and E. Baibourine, "Comparison of Biomass-Derived Turbine Fuels with the Composition-Explicit Distillation Curve Method," *Energy and Fuels*, vol. 25, no. 4, p. 1847–1858, 2011.

[43] S. L. Outcalt, "Compressed-liquid Density Measurements of Three Alternative Turbine Fuels," *Fuel*, vol. 124, pp. 1-6, 2014.

[44] R. V. Gough and T. J. Bruno, "Composition-Explicit Distillation Curves of Alternative Turbine Fuels," *Enegy and Fuels,* vol. 27, no. 1, pp. 294-302, 2013.

[45] S. Sonawane, U. Bhandarkar, B. Puranik and S. Kumar, "Convective Heat Transfer Characterization of Aviation Turbine Fuel-Metal Oxide Nanofluids," *J. Thermophysics and Heat Transfer,* vol. 26, no. 4, pp. 619-628, 2012.

[46] R. Coetzer, T. Joubert, C. Viljoen, R. Nel and C. Strydon, "Response Surface Models for Synthetic Jet Fuel Properties," *Applied Petrochemical Research,* vol. 8, pp. 39-53, 2018.

[47] O. Lötgering-Lin and J. Gross, "Group Contribution Method for Viscosities Based on Entropy Scaling Using the Perturbed-Chain Polar Statistical Associating Fluid Theory," *Industrial and Engineering Chemistry Research,* vol. 54, pp. 7942-7952, 2015.

[48] Y. Rosenfeld, "Relation Between the Transport Coefficients and the Internal Entropy of Simple Systems," *Physical Review,* vol. 15, no. 6, pp. 2545-2549, 1977.

[49] O. Lötgering-Lin, M. Fischer, M. Hopp and J. Gross, "Pure Substance and Mixture Viscosities Based on Entropy Scaling and an Analytic Equation of State," *Industrial and Chemical Engineering Research,* vol. 57, p. 4095−4114, 2018.

[50] A. Vasquez and J. Briano, "Thermal Conductivity of Hydrocarbon Mixtures: A Perturbation," *Ind. Eng. Chem. Res.,* vol. 32, no. 1, pp. 194-199, 1993.

[51] M. Hopp and J. Gross, "Thermal Conductivity of Real Substances from Excess Entropy Scaling Using PCP-SAFT," *Industrial and Chemical Engineering Research,* vol. 56, p. 4527−4538, 2017.

[52] M. Hopp and J. Gross, "Thermal Conductivity from Entropy Scaling: A Group-Contribution Method," *Industrial & Engineering Chemistry Research,* vol. 58, pp. 20441-20449, 2019.

[53] R. Naef, "Calculation of the Isobaric Heat Capacities of the Liquid and Solid Phase of Organic Compounds at and around 298.15 K Based on Their “True” Molecular Volume," *Molecules,* vol. 25, no. 5, 2019.

[54] N. Dadgostar and J. Shaw, "A Predictive Correlation for the Constant-pressure Specific Heat Capacity of Pure and Ill-defined Liquid Hydrocarbons," *Fluid Phase Equilibria,* vol. 313, p. 211– 226, 2012.

[55] H. B. Rokni, J. D. Moore, A. Gupta, M. A. McHugh and M. Gavaises, "Purely Predictive Method for Density, Compressibility, and Expansivity for Hydrocarbon Mixtures and Diesel and Jet Fuels up to High Temperatures and Pressures," *Fuel,* vol. 236, pp. 1377-1390, 2019.

[56] H. B. Rokni, J. D. Moore, A. Gupta, M. A. McHugh and M. Gavaises, "Entropy Scaling Based Viscosity Predictions for Hydrocarbon Mixtures and Diesel Fuels up to Extreme Conditions," *Fuel,* vol. 241, pp. 1203-1213, 2019.

[57] H. B. Rokni, J. D. Moore, A. Gupta, M. Hugh, R. Mallepally and M. Gavaises, "General method for prediction of thermal conductivity for well-characterized hydrocarbon mixtures and fuels up to extreme conditions using entropy scaling," *Fuel,* vol. 245, pp. 594-604, 2019.

[58] J. C. Dyre, "Perspective: Excess-entropy Scaling," *Journal of Chemical Physics,* vol. 149, no. 21, 2018.

[59] N. I. o. S. a. T. (NIST), "Machine Learning Fluid Equations of State," National Institute of Standards and Technology (NIST), 2020. [Online]. Available: https://www.nist.gov/programs-projects/machine-learning-fluid-equations-state.

[60] A. Piccione, J. W. Berkery, S. A. Sabbagh and Y. Andreopoulos, "Physics-guided Machine Learning Approaches to Predict the Ideal Stability Properties of Fusion Plasmas," *Nuclear Fusion,* vol. 60, p. 14, 2020.

[61] L. Joss and E. A. Müller, "Machine Learning for Fluid Property Correlations: Classroom Examples with MATLAB," *Journal of Chemical Education,* vol. 96, pp. 697-703, 2019.

[62] S. Atashrouz, G. Pazuki and S. Kakhki, "A GMDH-type Neural Network for Prediction of Water Activity in Glycol and Poly(ethylene glycol) Solutions," *Journal of Molecular Liquids,* vol. 202, pp. 95-100, 2016.

[63] M. Lashkarbolooki, A. Hezave and S. Ayatollahi, "Artificial Neural Network as an Applicable Tool to Predict the Binary Heat Capacity of Mixtures Containing Ionic Liquids," *Fluid Phase Equilibria,* vol. 324, pp. 102-107, 2012.

[64] A. Dargahi-Zarandi, A. Hemmati-Sarapardeh, S. Hajirezaie, B. Dabir and S. Atashrouz, "Modeling Gas/Vapor Viscosity of Hydrocarbon Fluids Using a Hybrid GMDH-type Neural Network System," *Journal of Molecular Liquids,* vol. 236, pp. 162-171, 2017.

[65] I. Wole-Osho, E. Okonkwo, H. Adun, D. Kavaz and S. Abbasoglu, "An Intelligent Approach to Predicting the Effect of Nanoparticle Mixture Ratio, Concentration and Temperature on Thermal Conductivity of Hybrid Nanofluids," *Journal of Thermal Analysis and Calorimetry,* 2020.

[66] V. Goussard, F. Duprat, J. Ploix, G. Drefuys, V. Nardello-Rataj and J. Aubry, "A New Machine-Learning Tool for Fast Estimation of Liquid Viscosity. Application to Cosmetic Oils," *Journal of Chemical Information and Modeling,* vol. 60, no. 4, pp. 2012-2023, 2020.

[67] Y. Liu, W. Hong and B. Cao, "Machine Learning for Predicting Thermodynamic Properties of Pure Fluids and Their Mixtures," *Energy,* vol. 188, 2019.

[68] Z. Gong, W. Yanze, L. Wu and H. Sun, "Predicting Thermodynamic Properties of Alkanes by High-Throughput Force Field Simulation and Machine Learning," *Journal of Chemical Information and Modeling,* vol. 58, pp. 2502-2516, 2018.

[69] G. Craven, N. Lubbers, K. Barros and S. Tretiak, "Machine Learning Approaches for Structural and Thermodynamic Properties of a Lennard-Jones Fluid," *Journal of Chemical Physics,* vol. 153, no. 10, 2020.

[70] A. Sözen, Arcaklioğlu, T. Menli˙k and M. Özalpc, "Determination of Thermodynamic Properties of an Alternative Refrigerant (R407c) Using Artificial Neural Network," *Expert Systems with Applications,* vol. 36, no. 3, pp. 4346-4356, 2009.

[71] D. Saldana, L. Starck, P. Mougin and B. Roussea, "Prediction of Flash Points for Fuel Mixtures Using Machine Learning and a Novel Equation," *Energy & Fuels,* vol. 27, no. 7, p. 3811–3820, 2013.

[72] Z. Jiao, S. Yuan, Z. Zhang and Q. Wang, "Machine Learning Prediction of Hydrocarbon Mixture Lower Flammability Limits Using Quantitative Structure-Property Relationship Models," *Process Safety Progress,* vol. 39, no. 2, 2020.

[73] C. A. Faundez, R. A. Campusano and J. O. Valderrama, "Misleading results on the use of artificial neural networks for correlating and predicting properties of fluids. A case on the solubility of refrigerant," *Journal of Molecular Liquids,* vol. 298, 2020.

[74] A. Metz, T. Loegel, P. Wrzesinski, D. Baniszewski, M. Esposito, L. Shafer, D. Truong, G. Simms, M. Peretich, A. McDaniel and R. Kamin, "GCXGC Hydrocarbon Method Alignment Across Multiple DoD Facilities," in *International Association for Stability, Handling, and Use of Liquid Fuels*, Long Beach, CA, 2019.

[75] ASTM International, "Standard Test Method for Dynamic Viscosity and Density of Liquids by Stabinger Viscometer," ASTM International, West Conshohocken, PA, 2014.

[76] ASTM International, "Standard Method for Determining Specific Heat Capacity by Differential Scanning Calorimetry," ASTM International, West Conshohocken, PA, 2018.

[77] S. Rudtsch, "Uncertainty of Heat Capacity Measurements with Differential Scanning Calorimeters," *Thermochimica Acta,* vol. 382, no. 1-2, pp. 17-25, 2002.

[78] ASTM International, "Standard Test Method for Thermal Conductivity, Thermal Diffusivity, and Volumetric Heat Capacity of Engine Coolants and Related Fluids by Transient Hot Wire Liquid Thermal Conductivity Method," ASTM International, West Conshohocken, PA, 2019.

[79] U. Hammerschmidt and W. Sabuga, "Transient Hot Wire (THW) Method: Uncertainty Assessment," *International Journal of Thermophysics,* vol. 21, no. 6, 2000.

[80] C. Poole, Gas Chromatography, Oxford, UK: Elsevier, 2012.

[81] H. B. Rokni, J. D. Moore, A. Gupta, M. A. McHugh, R. R. Mallepally and M. Gavaises, "General Method for Prediction of Thermal Conductivity for Well-

Characterized Hydrocarbon Mixtures and Fuels up to Extreme Conditions Using Entropy Scaling," *Fuel,* vol. 245, pp. 594-604, 2019.

[82] J. Gross and G. Sadowski, "Perturbed-Chain SAFT: An Equation of State Based on a Perturbation Theory for Chain Molecules," *Industrial & Engineering Chemistry Research,* vol. 40, no. 4, pp. 1244-1260, 2001.

[83] W. Cañas-Marín, D. González and B. Hoyos, "Comment on "Perturbed-Chain SAFT: An Equation of State Based on a Perturbation Theory for Chain Molecules"," *Industrial and Chemical Engineering Research,* vol. 58, p. 5743−5743, 2019.

[84] P. Neufeld, A. R. Janzen and R. A. Aziz, "Empirical Equations to Calculate 16 of the Transport Collision Integrals Ω(l, s)* for the Lennard-Jones (12–6) Potential," *J. Chemical Physics,* vol. 57, no. 3, pp. 1100-1101, 1972.

[85] L. Novak, "Self-Diffusion Coefficient and Viscosity in Fluids," *International Journal of Chemical Reactor Engineering,* vol. 9, no. 1, 2011.

[86] I. Bell, "Probing the Link Between Residual Entropy and Viscosity of Molecular Fluids and Model Potentials," *Proceedings of the National Academy of Sciences of the United States of America,* vol. 116, no. 10, pp. 4070-4079, 2019.

[87] S. J. Kwon, Artificial Neural Networks, New York: Nova Science Publishers, 2011.

[88] L. Google, "Machine Learning Glossary," Google, 2020. [Online]. Available: https://developers.google.com/machine-learning/glossary/. [Accessed 2020].

[89] M. Hagan, H. Demuth and M. H. Beale, Neural Network Design, Boston, MA: PWS Publishing, 1996.

[90] NIST, "NIST Standard Reference Database Number 69," 2020. [Online]. Available: https://doi.org/10.18434/T4D303. [Accessed 2019-2020].

[91] R. A. Perkins, M. L. Ramires, C. A. Nieto de Castro and L. Cusco, "Measurement and Correlation of the Thermal Conductivity of Butane from 135 K to 600 K at Pressures to 70 Mpa," *J. Chemical Engineering & Data,* vol. 47, pp. 1263-1271, 2002.

[92] Y. Wada, Y. Nagasaka and A. Hagashima, "Measurements and Correlation of the Thermal Conductivity of Liquid n-Paraffin Hydrocarbons and Their Binary and Ternary Mixtures," *International Journal of Thermophysics,* vol. 6, pp. 251-265, 1985.

[93] H. Watanabe and H. Kato, "Thermal Conductivity and Thermal Diffusivity of Twenty-Nine Liquids: Alkenes, Cyclic (Alkanes, Alkenes, Alkadienes, Aromatics), an d Deuterated Hydrocarbons," *J. Chemical Engineering & Data,* vol. 49, no. 4, pp. 809-825, 2004.

[94] Dortmund Data Bank, "Thermal Conductivity of Benzene," [Online]. Available: Dortmund Data Bank. [Accessed 2020].

[95] C. A. L. S. F. Y. Nieto de Castro, A. Nagashime, R. D. Trengrove and W. A. Wakeham, "Standard Reference Data for the Thermal Conductivity of Liquids," *Journal of Physical and Chemical Reference Data,* vol. 15, no. 3, pp. 1073-1081, 1986.

[96] G. Latini, G. Di Nicola and M. Pierantozzi, "A Critical Survey of Thermal Conductivity Literature Data for Organic Compounds at Atmospheric Pressure and an Equation for Aromatic Compounds," *Energy Procedia,* vol. 45, pp. 616-625, 2014.

[97] G. A. Iglesias-Silva, A. Guzmán-López, G. Pérez-Durán and M. Ramos-Estrada, "Densities and Viscosities for Binary Liquid Mixtures of n-Undecane + 1-Propanol, + 1-Butanol, + 1-Pentanol, and + 1-Hexanol from 283.15 to 363.15 K at 0.1 MPa," *Journal of Chemical and Engineering Data,* vol. 61, no. 8, pp. 2682-2699, 2016.

[98] T. V. M. Santos, M. F. V. Pereira, H. M. N. T. Avelino, F. J. P. Caetano and J. M. N. A. Fareleira, "Viscosity and Density Measurements on Liquid n-Tetradecane at Moderately High Pressures," *Fluid Phase Equilibria,* vol. 453, pp. 46-57, 2017.

[99] F. Esmaeilzadeh, A. S. Teja and A. Bakhtyari, "The Thermal Conductivity, Viscosity, and Cloud Points of Bentonite Nanofluids with n-Pentadecane as the Base Fluid," *Journal of Molecular Liquids,* vol. 300, 2020.

[100] Y. Sanchez-Vicente, I. Emerson, R. Glover, O. Herbage, R. S. Martin and J. P. M. Trusler, "Viscosities of Liquid Hexadecane at Temperatures between 323 K and 673 K and Pressures up to 4 MPa Measured Using a Dual-Capillary Viscometer," *Journal of Chemical and Engineering Data,* vol. 64, no. 2, pp. 706-712, 2019.

[101] Dortmund Data Bank, "Dynamic Viscosity of 1-Hexene," [Online]. Available: http://www.ddbst.com/en/EED/PCP/VIS_C100.php. [Accessed 2020].

[102] D. I. Sagdeev, M. G. Fomina, G. K. Mukhamedzyanov and I. M. Abdulagatov, "Experimental Study and Correlation Models of the Density and Viscosity of 1-Hexene and 1-Heptene at Temperatures from (298 to 473) K and Pressures up to 245 MPa," *Journal of Chemical & Engineering Data,* vol. 59, p. 1105−1119, 2014.

[103] D. I. Sagdeev, M. G. Fomina, G. K. Mukhamedzyanov and I. M. Abdulagatov, "Experimental Study of the Density and Viscosity of 1-Octene and 1-Decene at High Temperatures and High Pressures," *High Temperatures-High Pressures,* vol. 42, no. 6, pp. 509-536, 2013.

[104] M. A. Hernández-Galván, F. García-Sánchez and R. Macías-Salinas, "Liquid Viscosities of Benzene, n-Tetradecane, and Benzene + n-Tetradecane from 313 to 393 K and Pressures up to 60 MPa: Experiment and Modeling," *FLuid Phase Equilibria,* vol. 262, no. 1-2, pp. 51-60, 2007.

[105] F. J. Vieira dos Santos and C. A. Nieto de Castro, "Viscosity of Benzene and Toluene Under High Pressure," *Internation Journal of Thermophysics,* vol. 18, no. 2, 1997.

[106] A. H. Krall, J. V. Sengers and J. Kestin, "Viscosity of Liquid Toluene at Temperatures from 25 to 150 °C and at Pressures up to 30 MPa," *Journal of Chemical and Engineering Data,* vol. 37, no. 3, 1992.

[107] D. Luning Prak, J. Cowart and G. Simms, "Physical Properties of Binary Mixtures of n-Dodecane and Various Ten-Carbon Aromatic Compounds (2-Methyl-1-phenylpropane, 2-Methyl-2-phenylpropane, 2-Phenylbutane, and 1,3-Diethylbenzene): Densities, Viscosities, Speeds of Sound, Bulk Moduli, Surface Tens," *Journal of Chemical & Engineering Data,* vol. 65, no. 8, pp. 3941-3954, 2020.

[108] X. Meng, X. Gu, J. Wu and V. Vesovic, "Viscosity Measurements of ortho-Xylene, meta-Xylene, para-Xylene and Ethylbenzene," *Journal of Chemical Thermodynamics,* vol. 95, pp. 116-123, 2016.

[109] D. Dragoescu, F. Sirbu, A. Shchamialiou and T. Kasanshin, "Thermophysical Properties of n-hexadecane + Some Alkylbenzenes Binary Mixtures at Temperatures from 298.15 K to 318.15 K and Atmospheric Pressure," *Journal of Molecular Liquids,* vol. 237, pp. 208-215, 2017.

[110] V. Lastovka, N. Sallamie and J. Shaw, "A Similarity Variable for Estimating the Heat Capacity of Solid Organic Compounds," *Fluid Phase Equilibria,* vol. 268, pp. 51-60, 2008.

[111] W. A. Malatesta and B. Yang, "Aviation Turbine Fuel Thermal Conductivity: A Predictive Approach Using Entropy Scaling-Guided Machine Learning with Experimental Validation," *ACS Omega,* no. https://doi.org/10.1021/acsomega.1c02934, 2021.

[112] B. Zhao, W. Yang, C. Zheng, Y. Pei, A. Malatesta, X. Liu and B. Yang, "Experimental Study on Heat Transfer Enhancement by Using Textile Flap Oscillation," *Heat Transfer Engineering,* vol. https://doi.org/10.1080/01457632.2021.1887638, 2021.

[113] M. Glebocki, W. A. Malatesta, K. McCarthy and N. Jain, "Exergy-based Analysis and Optimization of Complex Aircraft Thermal Management Systems (accepted)," in *AIAA SciTech Forum,* San Diego, CA, 2022.

[114] C. Rodriguez, P. Koukouvinis and M. Gavaises, "Simulation of Supercritical Diesel Jets Using the PC-SAFT EoS," *The Journal of Supercritical Fluids,* vol. 145, pp. 48-65, 2019.

[115] N. Haarman, S. Enders and G. Sadowski, "Heterosegmental Modeling of Long-Chain Molecules and Related Mixtures using PC-SAFT: 1. Polar Compounds," *Industrial and Chemical Engineering Research,* vol. 58, pp. 2551-2574, 2019.

[116] M. Ulcay, L. Dillard and J. Gore, "Empirical Modeling of Minimum Hot Surface Ignition Temperature (MHSIT) for Aviation Fluids," in *AIAA Propulsion and Energy Forum*, Indianapolis, IN, 2019.